CHALMERS

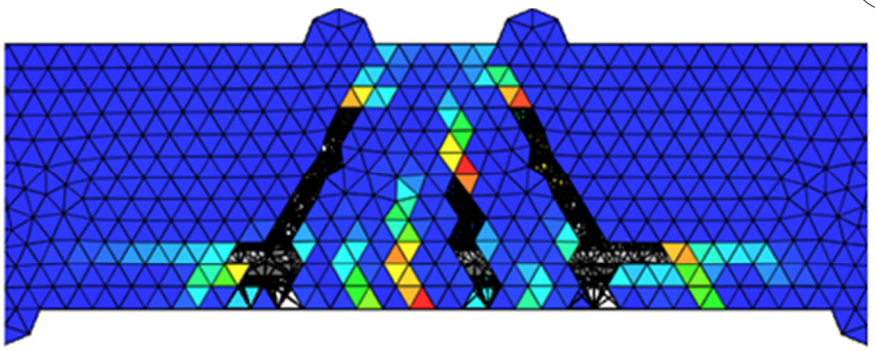

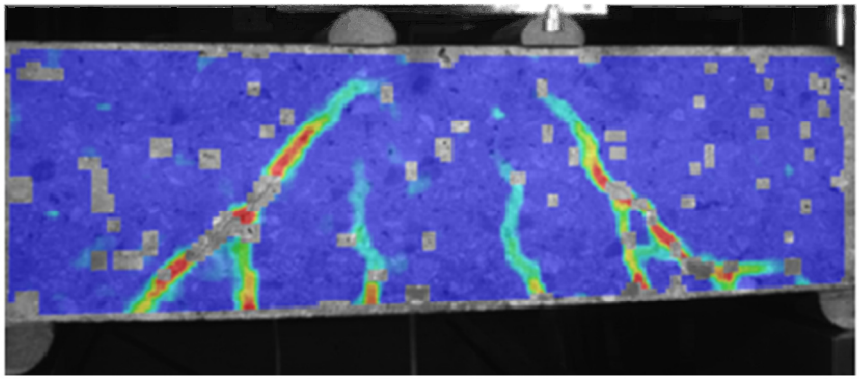

# Detailed Study of the Cracking Process at Shear Failure through FE Analysis of Beam Experiments

*Master of Science Thesis in the Master's Programme Structural Engineering and Building Performance Design*

HAO DU
NING CHEN

Department of Civil and Environmental Engineering
*Division of Structural Engineering*
*Concrete Structures*
CHALMERS UNIVERSITY OF TECHNOLOGY
Göteborg, Sweden 2012
Master's Thesis 2012:70

MASTER'S THESIS 2012:70

# Detailed Study of the Cracking Process at Shear Failure through FE Analysis of Beam Experiments

*Master of Science Thesis in the Master's Programme Structural Engineering and Building Performance Design*

HAO DU

NING CHEN

Department of Civil and Environmental Engineering
*Division of Structural Engineering*
CHALMERS UNIVERSITY OF TECHNOLOGY
Göteborg, Sweden 2012

Detailed Study of the Cracking Process at Shear Failure through FE Analysis of Beam Experiments

*Master of Science Thesis in the Master's Programme Structural Engineering and Building Performance Design*

HAO DU
NING CHEN



Examensarbete / Institutionen för bygg- och miljöteknik,
Chalmers tekniska högskola 2012:70

Department of Civil and Environmental Engineering
Division of Structural Engineering
Chalmers University of Technology
SE-412 96 Göteborg
Sweden
Telephone: + 46 (0)31-772 1000

Cover:

Crack pattern comparison between analysis based on Model Lundgren and experiment. See Figure 6.5.

Chalmers Reproservice
Göteborg, Sweden

Detailed Study of the Cracking Process at Shear Failure through FE Analysis of Beam Experiments

*Master of Science Thesis in the Master's Programme Structural Engineering and Building Performance Design*

HAO DU
NING CHEN
Department of Civil and Environmental Engineering
Division of Structural Engineering
Chalmers University of Technology

ABSTRACT

Shear strength of reinforced concrete beams has been extensively studied over the last decades. Nowadays, it is hard to say that there is a general design method for shear strength capacity of RC beams which can predict the failure load with a high degree of accuracy. In addition, many factors that influence the required minimum amount of shear reinforcement are not yet known. Thus, more research efforts need to be put into this area.

In this master's project, 3D finite element models were used to examine the experimental results which had been obtained by means of DIC (Digital Image Correlation) and AE (Acoustic Emission). A four-point shear test has been performed on a beam made by high strength concrete with crushed aggregates. FE analyses were based on smeared crack approach (rotating crack model) considering concrete-reinforcement relationship with perfect bond and bond-slip model, respectively. The aim was to investigate the factors influencing the shear strength capacity and to better understand the shear crack propagation.

From the analyses it was found that the lateral confinement effect on concrete compressive response plays a quite important role in the simulation of shear compression failure, especially for 3D FE models. The bond action between the concrete and the reinforcement strongly influence the shear crack propagation. The bond stiffness influences to some extent the mechanical behavior of the beam before the initiation of concrete cracks. After the beam cracks, relatively higher bond stiffness can result in higher concrete stresses close to existing cracks, leading to that additional shear cracks initiates earlier and propagates further towards the supports.

Key words: Reinforced Concrete beams, shear strength capacity, shear crack propagation, 3D FE model, bond-slip model, shear compression failure

# Contents

# Preface

This project was done at SP/CBI, Borås, and at the department of Structural Engineering, Chalmers University of Technology. To fulfil the requirements of the thesis of International Master Program, this project was supervised by Dr. Mathias Flansbjer, Dr. Kamyab Zandi Hanjari, and Dr. Jan Erik Lindqvist and examined by Associate Professor Mario Plos. The working period was from January to June 2012. This project was part of an on-going research project in cooperation between SP and CBI, which aims at investigating factors affecting the mechanical behaviour of reinforced concrete beams subjected to shear load. The project was done using the DIANA 9.4.3 FE program package. All the tests mentioned in the project have been carried out in the laboratory of SP and CBI by Mathias Flansbjer and Jan Erik Lindqvist.

We are thankful to our supervisors, Dr. Mathias Flansbjer, Dr. Kamyab Zandi Hanjari, and Dr. Jan Erik Lindqvist and examiner, Associate Professor Mario Plos for their continuous and helpful supervision and guidance during the working period. We thank Professor Karin Lundgren greatly for her valuable suggestions.

We also want to thank our opponents, Johannes Lundgren and Christoffer Palmqvist for their comments and good advices.

Göteborg May 2012

Hao Du

Ning Chen

# Notations

### Roman upper case letters

| | |
|---|---|
| $E$ | Young's modulus |
| $F$ | Force on support in horizontal direction |
| $P$ | Concentrated load |
| $V$ | Reaction force at support |
| $V_a$ | Shear resistance from aggregate interlock |
| $V_c$ | Shear resistance in compression zone |
| $V_d$ | Shear resistance from dowel action |
| $G_F$ | Fracture energy of concrete |
| $G_{F1}$ | Fracture energy in mode I of concrete |

### Roman lower case letters

| | |
|---|---|
| $a$ | Shear span |
| $c$ | Constant value in model Dörr (1980) |
| $d$ | Depth of beam |
| $\Delta u_t^{\,0}$ | Shear slip at which the Dörr curve reaches plateau |
| $k_{guess}$ | Stiffness of spring on the support |
| $s$ | Displacement of support in horizontal direction |
| $w/c$ | Water cement ratio |
| $f_{ct}$ | Concrete tensile strength |
| $f_{c,cube}$ | Cube compressive strength of concrete |
| $f_y$ | Yielding strength of steel |
| $f_u$ | Ultimate strength of steel |

### Greek lower case letters

| | |
|---|---|
| $\sigma_1$ | Principal tensile stress |
| $\beta$ | Shear retention factor |

# 1 Introduction

## 1.1 Background

Shear strength of reinforced concrete members adversely affects structural performance in various ways such as serviceability and durability. Reinforced concrete beams may fail in shear before attaining their full flexural strength if they are not adequately designed for shear. Unlike flexural failures, shear failures are very sudden and brittle. Significant efforts have been put all over the world to study this subject since the beginning of 20$^{th}$ century. Although the existing guidelines provide some design models for capacity prediction, more research on shear cracking process is needed in order to contribute to the improvement of the current models.

An on-going research project in cooperation between SP and CBI aims at investigating factors affecting the mechanical behaviour of reinforced concrete beams (RC beams) subjected to shear load. In the earlier stage of the project, shear tests have been performed on reinforced concrete beams, with two types of aggregate and two $w/c$ ratios. In addition to mechanical testing, the optical full-field deformation measurement system ARAMIS$^{TM}$ 4M by GOM based on Digital Image Correlation (DIC) and Acoustic Emission (AE) were used to monitor the initiation and propagation of cracks. More details about ARAMIS and AE are given by Flansbjer *et al.* (2011).

In this report, the master thesis project will be referred to as the project, and the experiments reported by Flansbjer *et al.* (2011) as the experiments.

## 1.2 Aim

In this project, the primary aim was to use non-linear finite element analysis to further examine the results of the beam tests. The shear cracking propagation of a reinforced concrete beam in experiments and finite element (FE) analyses was studied in detail in order to contribute to the understamding of the shear response. Results from the FE analysis were compared carefully with experimental results to study the shear cracking process at different load levels and the corresponding mechanical behaviour. Another aim was to better understand the shear cracking propagation and influencing factors during different stages of a shear failure.

## 1.3 Methods

The project started with literature study of shear failure pattern of RC beams and the study of FE analyses of reinforced concrete structures. Then, the FE-software DIANA was used to model the direct tensile test to verify the constitutive tensile models for concrete used in the analyses. Furthermore, the shear tests were modelled using three-dimensional nonlinear FE analysis. Three modelling choices for the bond between concrete and reinforcement were studied. First, the reinforcement was assumed to be fully embedded in concrete elements; this corresponds to full interaction between reinforcement and concrete. Afterwards, the model was modified so that the steel/concrete interaction was simulated with bond-slip relation. Finally, the bond model developed by Lundgren (2005), which describes the interaction between

concrete and reinforcement based on the relation between stresses and deformations, was applied.

The results from the finite element analysis were carefully compared with the test results with respect to shear capacity, and with respect to cracking process and pattern.

## 1.4 Limitations

The limitations applied on this project were as follows:

Not all the available experimental results were used in this study. For instance, only high strength concrete with one $w/c$ of 0.38 and fine aggregate of crushed rock material was studied.

The study was limited to one type of shear failure, i.e. shear compression failure, which governed the failure of the beams in the experiments.

The FE analysis was only carried out with one cracking model, i.e. smeared crack approach.

# 2 Review of background theory

## 2.1 Reinforced concrete beam in bending

Several types of failure modes may take place when RC beams are subjected to either a uniformly distributed load or a concentrated load. These are mainly anchorage failure, crushing failure, flexural failure and shear failure.

A beam can be divided into different regions based on stress states namely, compression, tension, anchorage and shear zone, see Figure 2.1. The failure modes associated with these zones are denoted as bending due to crushing, bending due to yielding of reinforcement, anchorage and shear failures. In compression zone, when the stresses caused by the increasing load exceed the compressive strength of concrete, crushing of concrete may lead to brittle failure of the beam. In the tensile zone, if the stresses in the reinforcement exceed the yielding strength of the reinforcement before crushing failure happens, the beam could fail for bending.

For RC beams in bending, the bending moment is resisted mainly by the steel reinforcement. After crack formation, the tensile force in the reinforcement at the end of the beam must be transferred to the surrounding concrete by bond action between the two materials; this is anchorage which requires a certain transmission length. Thus, the anchorage capacity depends on the transmission length, to a large extent. When cracks develop closer to the support, the transmission length gets shorter, and then the beam fails due to in-sufficient anchorage capacity. See Magnusson (2000).

RC beams may fail in shear if they are not adequately designed for shear. Shear load causes shear stresses, and high shear stresses can cause cracks in a concrete member. A crack is formed when the principal tensile stress, $\sigma_1$ in the concrete reaches the concrete tensile strength, $f_{ct}$. This results in initiation of diagonal cracks and the propagation of cracks determines the final failure of the beam. More details concerning shear-induced cracking and the corresponding failure are described in the following section.

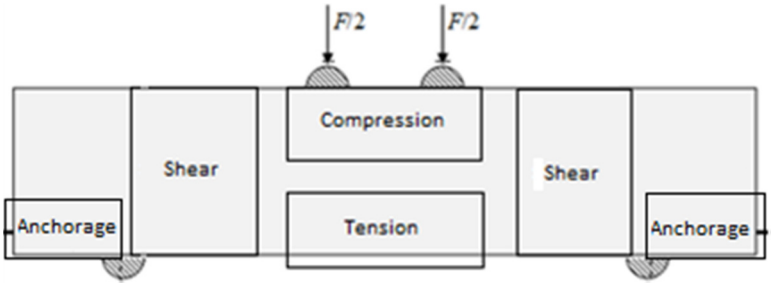


*Figure 2.1 Different zones of RC beam based on stress states.*

## 2.2 Shear induced cracking and failure

Several studies have shown that shear force is resisted by the combined action of three factors namely, the un-cracked concrete in the compression region, the aggregate interlocking and the shear acting across the longitudinal steel bars. See Zararis (2003). The shear force across the steel bars is also known as dowel force. Therefore, the corresponding shear transfer mechanism involves shear resistance in compression

zone ($V_c$), shear resistance from dowel action ($V_d$), and shear resistance from aggregate interlock ($V_a$), see Figure 2.2. The shear cracking process is mainly governed by the varying contribution of the three forces.

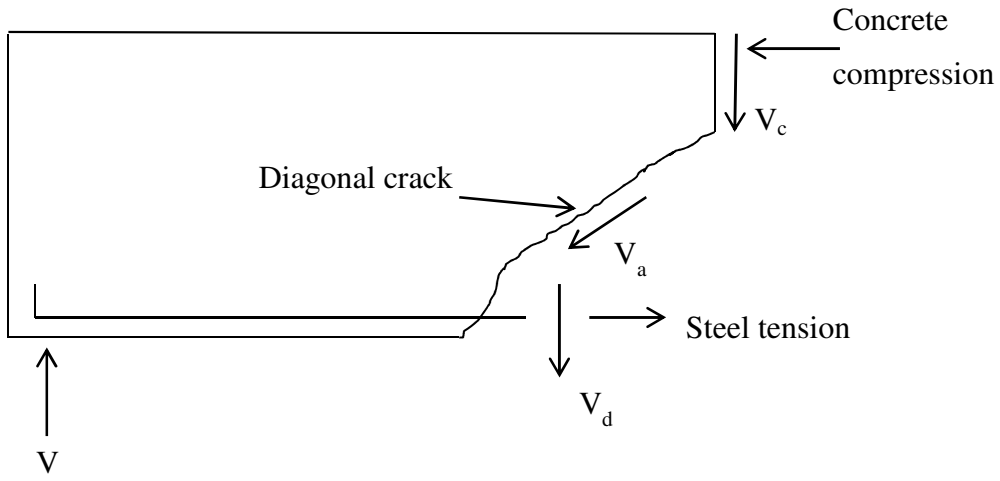


*Figure 2.2 Mechanism of shear transfer.*

Before cracking, a reinforced concrete beam acts like a homogeneous beam. After bending cracks appear, shear displacement occurs along an inclined crack and dowel action in reinforcements gets mobilized. When the two faces of a bending crack of moderate width are given a shear displacement relative to each other, a number of coarse aggregate particles projecting across the crack interlock with each other generate significant shear resistance.

As the applied shear force is increased, the dowel action is the first to reach the capacity after which a proportionally large shear force is transferred through aggregate interlock. The aggregate interlock mechanism is probably the next to fail, necessitating a rapid transfer of a large shear force to the concrete compression zone, which as a result of this sudden shear transfer, the beam often fails abruptly and explosively.

There are mainly four failure modes in shear (without web reinforcement) corresponding to different shear span to depth ratio ($a/d$).

**Diagonal tension failure**

This kind of shear failure is likely to happen when the ratio between the shear span and the effective height ratio, $a/d$, is above 2.0. In this mode, the diagonal crack starts from the flexural crack and turns gradually into a more inclined crack, see Figure 2.3. Typically, the diagonal crack encounters resistance as it propagates towards the compression zone and stops at some point. With increasing load, the tension crack extends slowly at a very flat slop until final failure occurs.

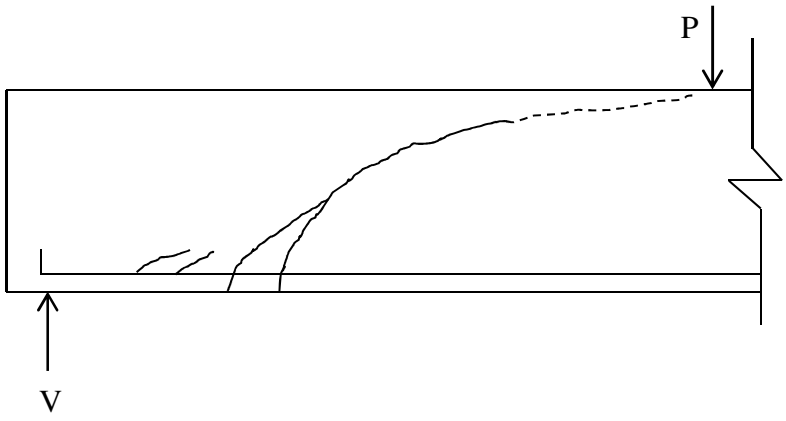


*Figure 2.3 Diagonal tension failure, adapted from Dileep Kumar (lecture notes).*

**Shear compression failure**

This failure occurs at a range of $a/d$ between 1.0 and 2.5. In this case, a 45 degree crack may be initiated across the neutral axis before a flexural crack appears. Such a crack tends to be self-propagating until stopped by the load or support reaction. A compression failure finally occurs adjacent to the shear load, see the shaded area in Figure 2.4 (left).

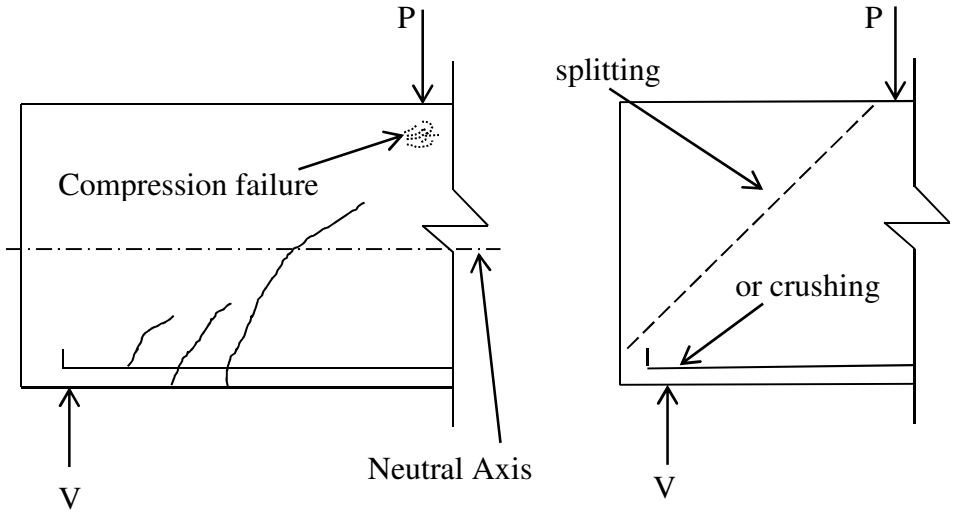


*Figure 2.4 Diagonal tension failure (left) and splitting shear failure (right), adapted from Dileep Kumar (lecture notes).*

**Splitting shear failure**

When the shear span, $a$, is less than the effective depth, d, i.e. $a/d < 1$, the inclined shear crack appears between load and the reaction. In such cases, shear strength is much higher and a splitting failure may take place, see Figure 2.4 (right), or the beam may fail in compression at the reaction.

**Shear tension failure**

Due to inadequate anchorage of the longitudinal bars, the diagonal cracks propagate horizontally along the reinforcement bars, which will lead to the final failure, see Figure 2.5.

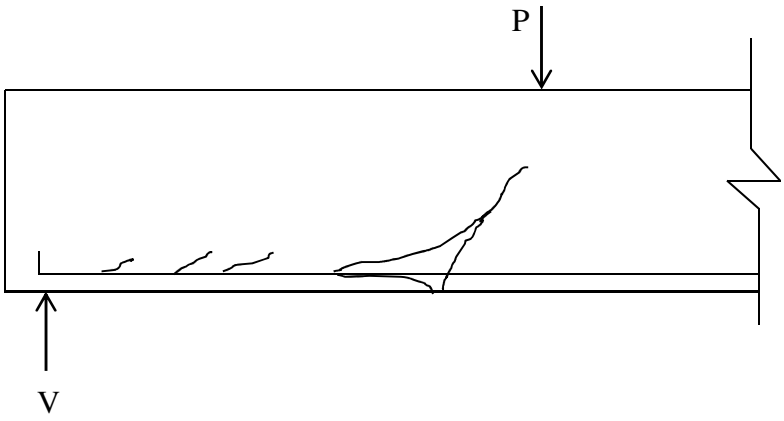


*Figure 2.5 Shear tension failure, adapted from Dileep Kumar (lecture notes).*

## 2.3 Material models for reinforced concrete

### 2.3.1 Concrete

Concrete is known to have a non-linear behaviour both in compression and in tension. To capture the behaviour of concrete structures, it is vital to include the non-linear behaviour of concrete in the finite element analysis. In the FE analysis carried out in this work, the smeared crack model, which allows introducing shear retention as shear retention factor, $\beta$, was mostly used. Three crack models used were: (a) rotating crack model based on total strain, (b) fixed crack model based on total strain, and (c) multi-directional fixed crack approach, see DIANA (2010).

(a) Rotating crack model based on total strain. Total strain crack models describe the tensile and compressive behavior of a material with one stress-strain relationship. The stress is evaluated in the crack directions. In a rotating crack model, the strain vector, transformed by the strain increment with the strain transformation matrix, influences the stress. The strain transformation matrix depends on the current strain vector, which means the stress-strain relationships keep updating with the strain vector in the rotating crack model. The axes of the principal stresses continuously rotate after cracking.

(b) Fixed crack model based on total strain. The decomposed crack model divides the total strain into an elastic strain and a crack strain. Local strains are transformed to global strains by a transformation matrix. In this model, the strain transformation matrix given by the incipient cracking and is fixed then. In this case, the compressive behavior is evaluated in the fixed coordinate system determined by the initial cracking direction.

(c) Multi directional fixed crack approach. In this model, the sub-decomposition of the crack strain allows modelling a number of cracks that occur simultaneously. The

components of this crack strain are the global strain increment owing to a primary crack, a secondary crack and so on. Each of these fixed cracks is assigned its own local strain vector, its own traction vector and its own transformation matrix. The overall stress-strain relation for the multiply cracked solid can be set up analogously to the relation for a cracked solid by assembling these individual vectors and matrices. However the use of fixed single cracks leads to an increasing discrepancy between the axes of the principal stress and the fixed crack axes. For such case, an angle can be set as a certain threshold angle; whenever the angle between the existing cracks and the direction of the principal stress exceeds this threshold value a new crack can be initiated. See Rots (1991).

For the concrete in compression, the constitutive model by Thorenfelt *et al*. (1991) was adopted as shown in Figure 2.6 (left). Moreover, the tension softening curve given by Hordijk (1987) was used; see Figure 2.6 (right).

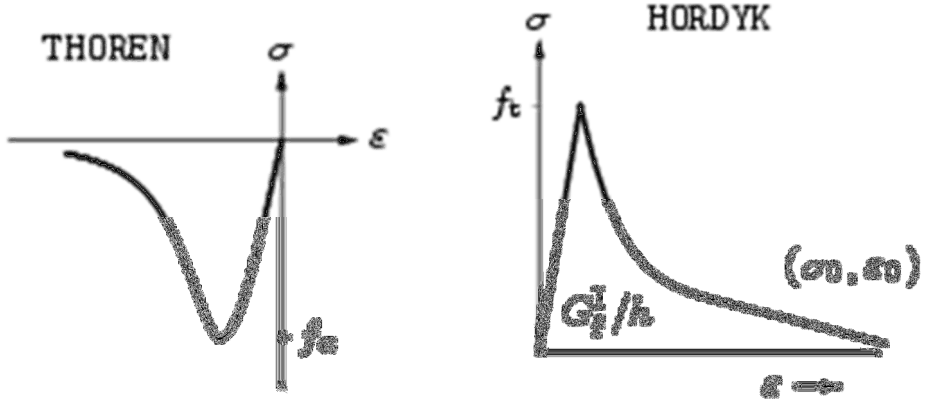


*Figure 2.6 Stress-strain relations for concrete in compression (left) and in tension (right), adapted from DIANA (2010).*

Ultimate strength and ductility of concrete are known to be significantly improved in the presence of lateral compressive stresses, Selby (1993). To consider the influence of lateral confinement for concrete in compression, the model proposed by Selby and Vecchio (1997) can be used for the model by Thorenfelt *et al.* (1991), see Figure 2.7 (left).

According to Broo *et al.* (2008), when capturing a correct localization is of importance, an elastic-ideal plastic relationship for concrete in compression can be used, see Figure 2.7 (right). This is another possible way to obtain correct cracking localization, however correct compression failure capacity may not be captured in this case.

Thus, for the compressive constitutive model of concrete in the project, two types of model were mainly used: (1) model by Thorenfelt *et al.* (1991) with consideration of lateral confinement effect; (2) elastic-ideal plastic model.

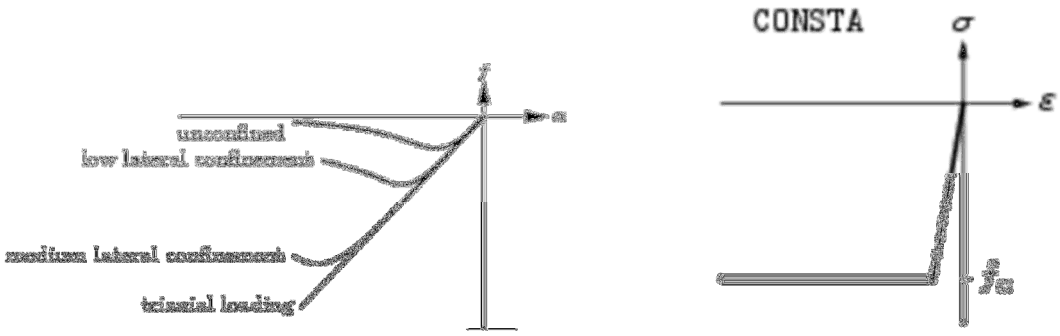


*Figure 2.7 Influence of lateral confinement on compressive stress-train curve (left) and elastic-ideal plastic relationship for concrete in compression (right), adapted from DIANA (2010).*

### 2.3.2 Reinforcement

The response of the reinforcing steel is linear elastic until yielding stress reached and then deforms plastically. The plasticity of the reinforcing steel is often modelled according to an isotropic plastic model with the Tresca or the Von Mises yield criterion as shown in Figure 2.8. The hardening behaviour can be obtained from uniaxial tests of reinforcement bars.

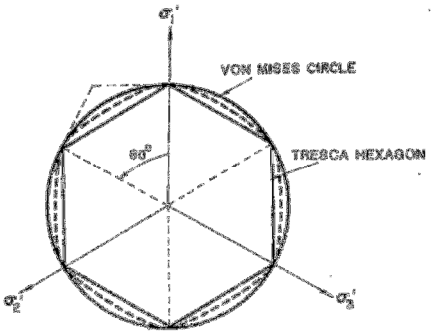


*Figure 2.8 Comparison of the Tresca and the Von Mises yield surfaces, adapted from Chen and Han (1988).*

According to Plos (2000), since the reinforcement units are generally one-dimensional and carry stresses mainly in the longitudinal direction, the reinforcement bars can be modelled in a simplified manner instead of continuum elements. In this case, the technique of embedding the reinforcement in the concrete elements should be adopted, which means no slip can occur between the reinforcement and the surrounding concrete.

To study the influence of the interaction between the reinforcement and the concrete on the cracking behaviour, the reinforcement has to be represented by separate elements. If so, the reinforcement should be modelled as truss/beam elements or three-dimensional solids elements together with interface elements.

### 2.3.3 Interaction between reinforcement and concrete

The localization of the deformation in concrete around the reinforcement bar is, to a large extent, determined by the stress transfer between the reinforcement and the surrounding concrete. For ribbed bars, the slip of steel bar results, not only, in the

shear stresses, but also, in stresses normal to the mean surface of the bar; the stress field around a deformed reinforcement bar has described by Tepfers (1973). One way to simulate the interaction is to use an interface model, and two types of interface bond model are stated below.

A less detailed way is to model the reinforcement with truss or beam elements, see Figure 2.9. Then a two-dimensional interface element or spring elements, which describe the bond stress-slip relationship, can model the interaction between the reinforcement and the concrete. The bond stress-slip is predefined and is not influenced by yielding of the reinforcement or the support pressure, see curve (a) in Figure 2.9 (right). This kind of interface model is suitable for modelling on component level, smaller concrete members or parts of concrete members.

In Figure 2.9 (right), bond-slip relationship curve (a) represents pull-out failure, which means the concrete surrounding the reinforcement is confined well and the reinforcement does not yield. Curve (b) describes the splitting failure or loss of bond due to yielding of the reinforcement. See Lundgren (2005).

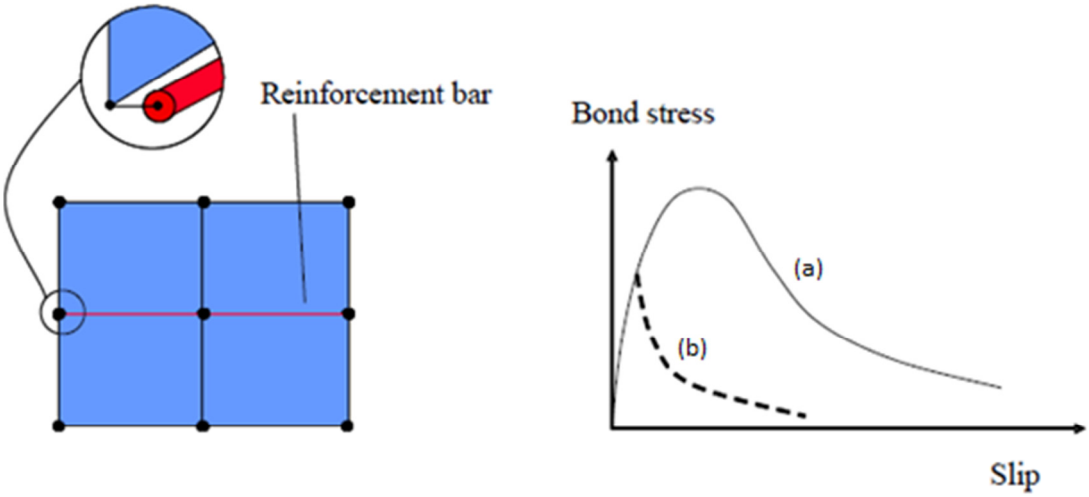


*Figure 2.9* *The truss elements for reinforcing steel with interface elements (left) using a predefined bond stress-slip relationship (right), adapted from Broo et al. (2008).*

For the model with both concrete and reinforcement modelled with three-dimensional elements, surface interface elements are used to describe the interaction between the reinforcement and the concrete. For this type of interface elements, a special bond model is needed, for example that of Lundgren (2005), see Figure 2.10, which includes not only the bond stresses but also the splitting stresses activated when the reinforcement slips in the concrete.

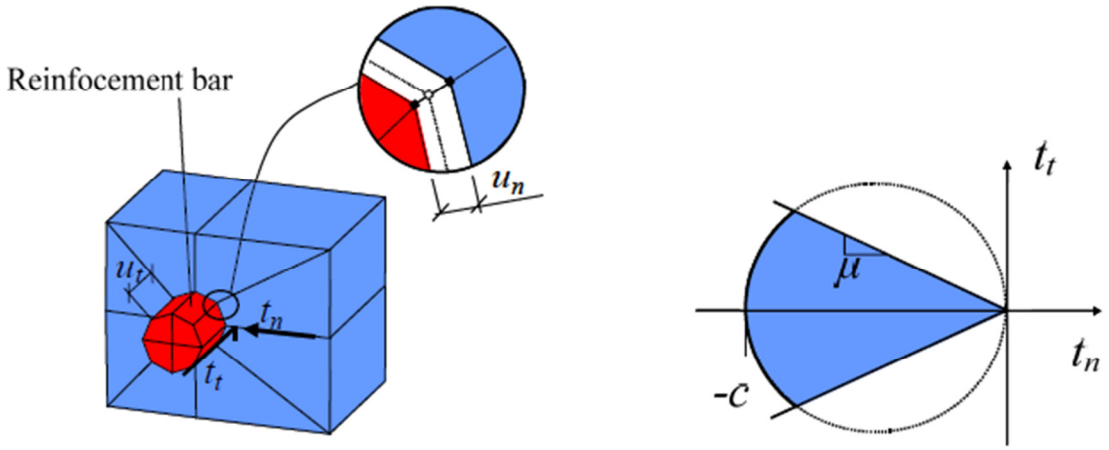


*Figure 2.10* *Both the concrete and the reinforcing bar are modelled with continuum elements and with three-dimensional interface elements between them (left). A plasticity model is employed to describe the special bond mechanism (right). Adapted from Lundgren (2005).*

In the FE program package DIANA, several simplified bond-slip model could be adopted, for example, the bond-slip model 'BONDSL 1' uses the cubic function proposed by Dörr (1980) to describe the nonlinear relation between the shear traction and the shear slip, see Figure 2.11. In this model, the relation between normal traction and the normal relative displacement is kept linear, DIANA (2010).

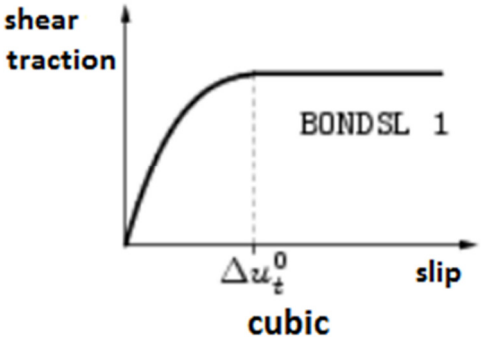


*Figure 2.11* *Bond shear traction-slip curve based on cubic function. Dörr (1980), adapted from DIANA 2010.*

# 3 Experiment description

## 3.1 Material properties

In this part, the direct tensile tests and RC beam tests have been performed in SP and CBI, which had four different concrete recipes including a $w/c$ of about 0.38 or 0.9 and fine aggregate (<8mm) of natural or crushed rock material. The detail of the material used in the tests is shown in Table 3.1. The cube compressive strengths, $f_{c,cube}$, were determined at 28 days and at the time of testing (208 days). The cubes (150x150x150 mm3) were stored along with the specimens. The tensile strength, $f_{ct}$, and fracture energy, $G_F$, were determined from direct tensile tests as described in Section 3.2.

*Table 3.1 Material description.*

| | C0.90* | N0.90* | C0.38* | N0.38* |
|---|---|---|---|---|
| $w/c$ | 0.94 | 0.90 | 0.38 | 0.38 |
| Fine aggregate 0-8 mm [kg/m$^3$] | 1126 | 1082 | 1064 | 900 |
| Coarse aggregate 8-16 mm [kg/m$^3$] | 720 | 815 | 708 | 900 |
| Water [kg/m$^3$] | 220 | 198 | 164 | 162 |
| Cement [kg/m$^3$] | 234 | 220 | 429 | 426 |
| Water reducer [kg/m$^3$] | 0 | 0 | 1.1 | 0.7 |
| $f_{c,cube}$ at 28 days [MPa] | 19.2 | 21.2 | 80.9 | 91.5 |
| $f_{c,cube}$ at 208 days [MPa] | 20.9 | 21.6 | 84.5 | 96.9 |

* N and C denote natural and crushed fine aggregate rock material, respectively.

The reinforcement steel used in RC beam tests was ribbed bars with Ø12mm. The yielding strength, $f_y$, and ultimate strength, $f_u$, were 550 MPa and 630 MPa, respectively. The young modulus, $E$, was 197 GPa.

## 3.2 Direct tensile test set-up

The direct tensile test aimed to obtain the softening behavior of the concrete material. Cubes (100x100x100 mm$^3$) were cut from the concrete blocks. Along two of the sides, a 10 mm deep and 5 mm wide notch was cut with a stationary diamond cutting-blade. The geometry of the specimens is shown in Figure 3.1.

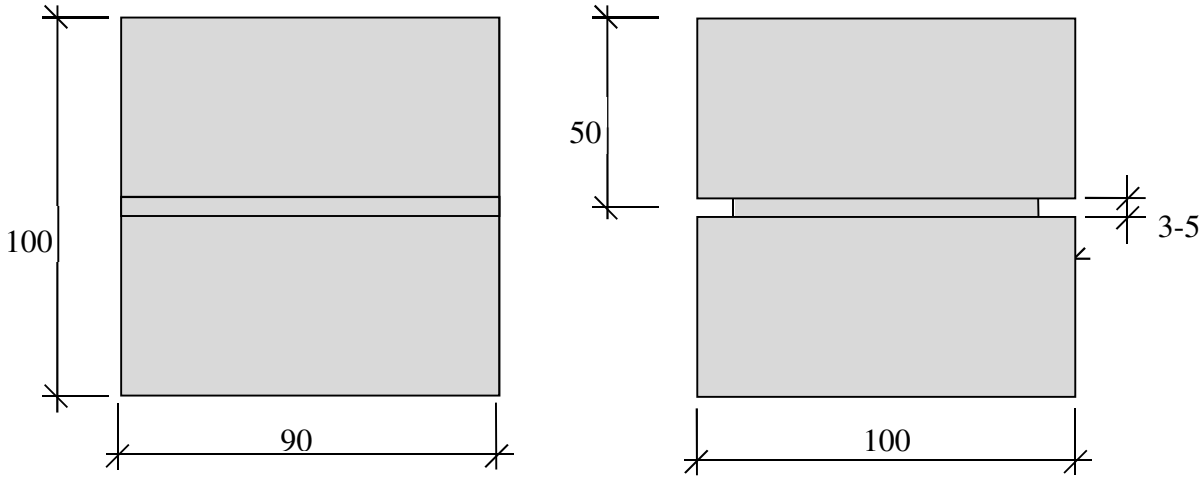


*Figure 3.1 Tensile test specimen geometry [mm].*

The specimen was precisely glued to the lower loading platen using a "glue device". The key of this operation was to make sure that center lines of the platen and the cylinder to coincide and the center axis of the specimen perpendicular to the face of the loading platen as close as possible. The lower loading platen, together with the glued specimen, is then bolted to the machine. Finally, the upper loading plate was glued to the top of the specimen. The load was applied as displacement control with a rate of 0.005 mm/min up to a displacement of 0.1 mm and then with a rate of 0.1 mm/min to failure. During the test, the stress and the deformation was registered during the testing by the use of the optical full-field deformation measurement system ARAMIS$^{TM}$ 4M by GOM and also the crack width was calculated.

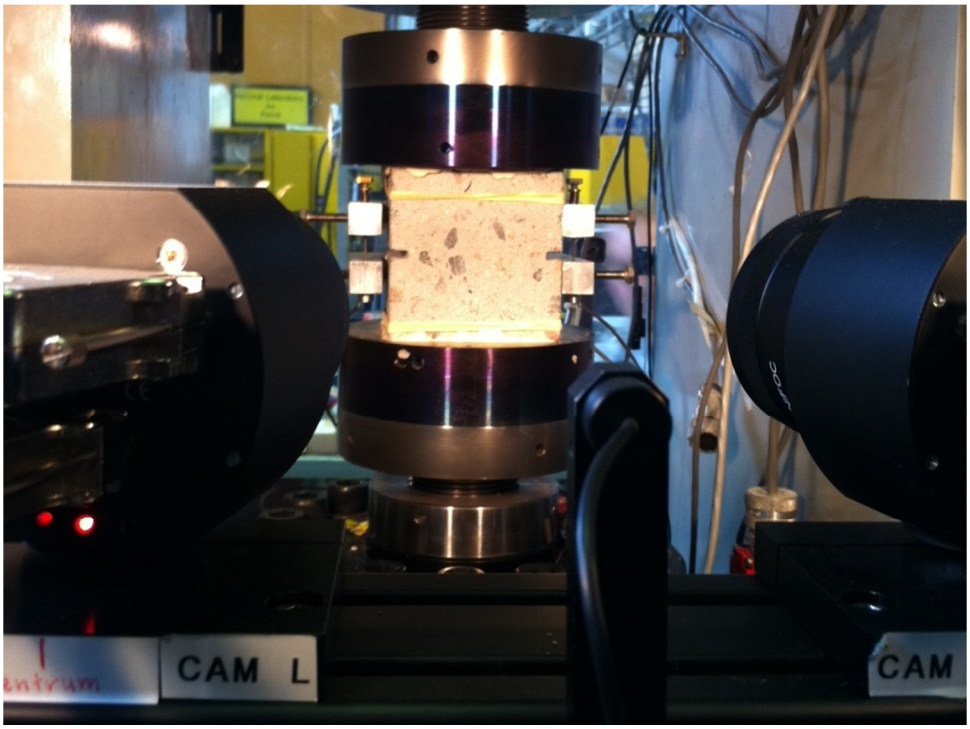

*Figure 3.2* *Experimental test setup for the direct tensile tests, where optical strain measurement system is seen in the foreground.*

## 3.3 RC-beam test set-up

The dimension of the RC beams is illustrated in Figure 3.4 and the bottom reinforcement is provided by 3 ribbed bars (Ø12mm). The details of the preparation of the specimens could be found in Flansbjer *et al.* (2011). In this project, only the beams with crushed aggregates and $w/c$ of 0.38 were studied (three RC beam specimens were tested for this type of concrete recipe), which are referred to as C0.38_1, C0.38_2 and C0.38_3 in the following.

*Figure 3.3* *The shear test set-up of the RC beams with the optical measuring system showing in the background and the placing of the AE-sensors at each end of the beam.*

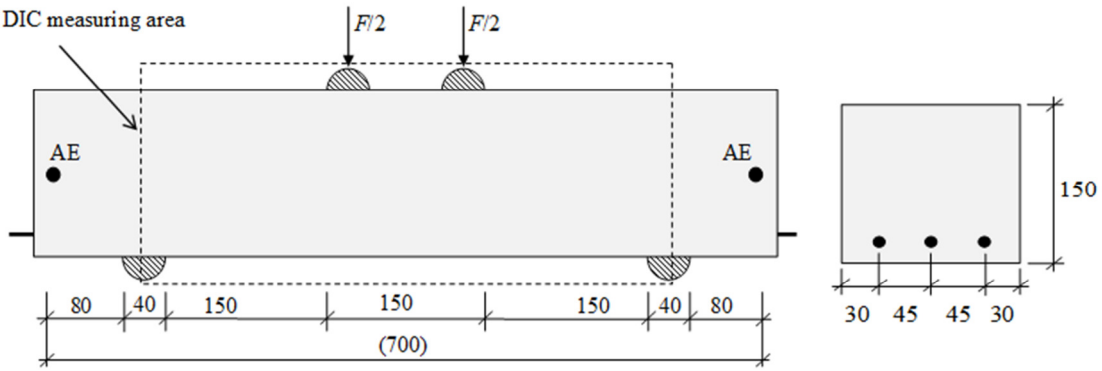


*Figure 3.4* *The RC beams geometry [mm].*

Two-point loading were applied on the RC beam specimens as shown in Figure 3.3 and 3.4. The beams were loaded through and supported by half-moon shaped steel rulers with a radius of 20 mm. The tests were carried out under displacement control with a rate of 0.5 mm/min.

During the process of loading, the crack propagation was registered in a detailed way at one side of the specimens by the use of the optical full-field deformation measurement system ARAMIS$^{TM}$ 4M by GOM. Moreover, the AE method, as mentioned above, was used to collect the acoustic activities. After the test, the micro- and meso-scale analysis was performed on the tested samples using fluorescence microscopy on thin sections of samples impregnated with fluorescent dye.

In this project, the FE analyses were compared with the test results extracted from the deformation measurement system ARAMIS$^{TM}$. The detail comparison and discussion were represented in the following chapters.

# 4 FE analysis for direct tensile test

The FE analysis started with the modelling of direct tensile test to verify the tensile model for concrete used in DIANA, and then the cracking behaviour of the same model was simulated with tensile loading in combination with shear. In all FE analyses, non-linear three-dimensional FE models with isoparametric continuum elements were used, and different constitutive models based on non-linear fracture mechanics using a smeared crack approach were adopted for concrete: (a) rotating crack model based on total strain denoted as TS-rotating, (b) fixed crack model based on total strain denoted as TS-fixed, and (c) multi-directional fixed crack approach denoted as Multi-dir, see DIANA (2010).

The model with a mesh of brick elements with 5mm size was used to model the direct tensile test described in Section 3.2, see Figure 4.1. In the model, the up and bottom face were fixed in vertical direction and the external load was applied as a prescribed displacement at the loading points in up face, see Figure 4.1. The material input data for concrete in the analysis are as shown in Table 4.1.

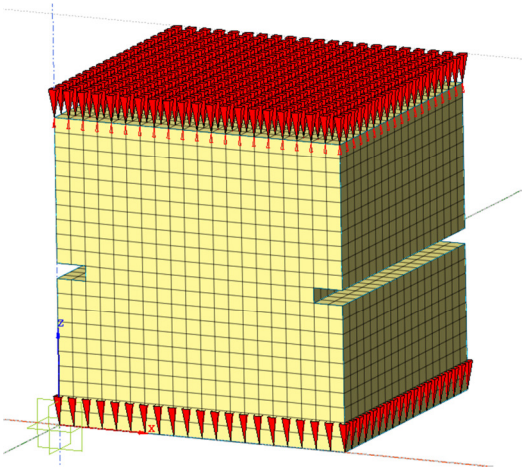

*Figure 4.1 FE model for direct tensile test.*

*Table 4.1 Material input data for concrete C0.38 in FE analysis.*

| C-0.38 | | Comments |
|---|---|---|
| Young modules [GPa] | 39.5 | From EC2 |
| Poison ratio | 0.2 | From EC2 |
| Density [kg/m$^3$] | 2400 | From |
| Tensile model | Tension softening curve | 'HORDYK' in DIANA |
| Tensile strength [MPa] | 4.9 | From experiment |
| GF1 (fracture energy in mode I) [N/m] | 208.7 | From experiment |
| Crack band width [mm] | 5 | Element size |

The results from numerical analyses with three constitutive models for concrete (TS-rotating, TS-fixed and Multi-dir) are compared with the experimental results (C0.38) in terms of stress-crack opening response in Figures 4.2 to 4.4.

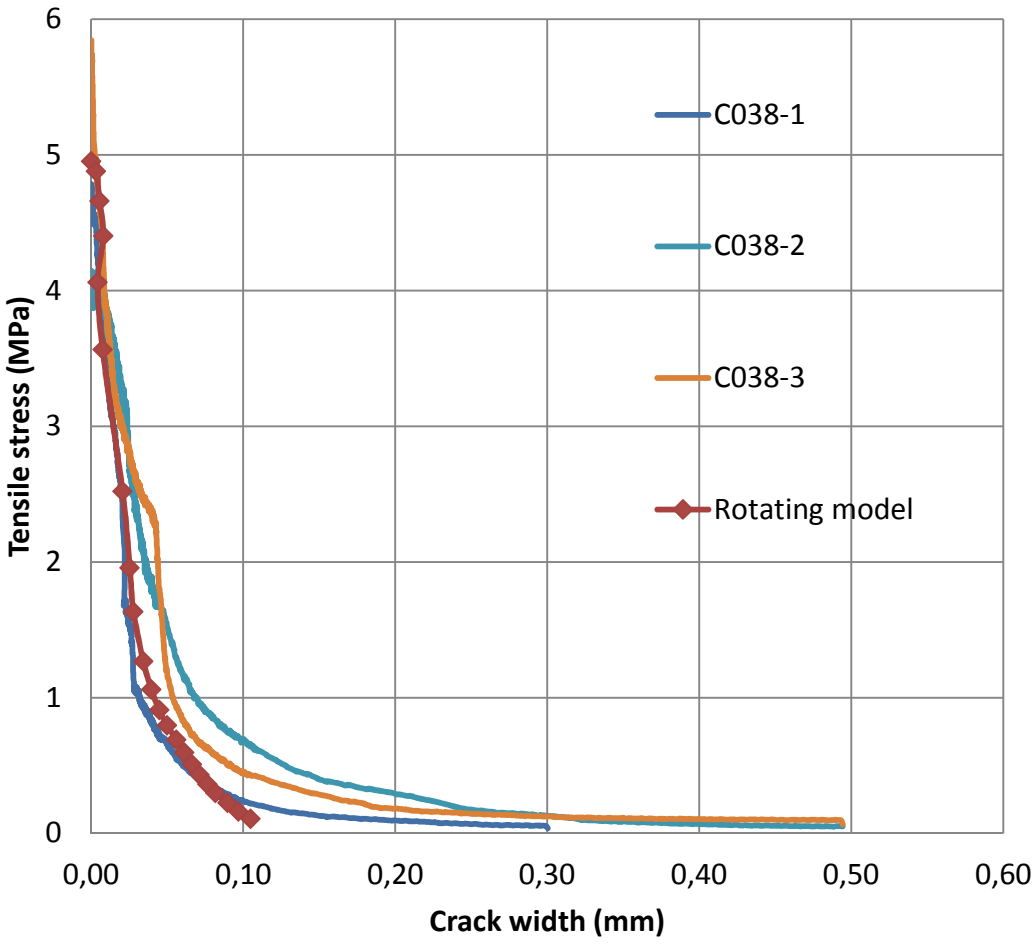


*Figure 4.2* *Stress-crack width response comparison between TS-rotating and test results.*

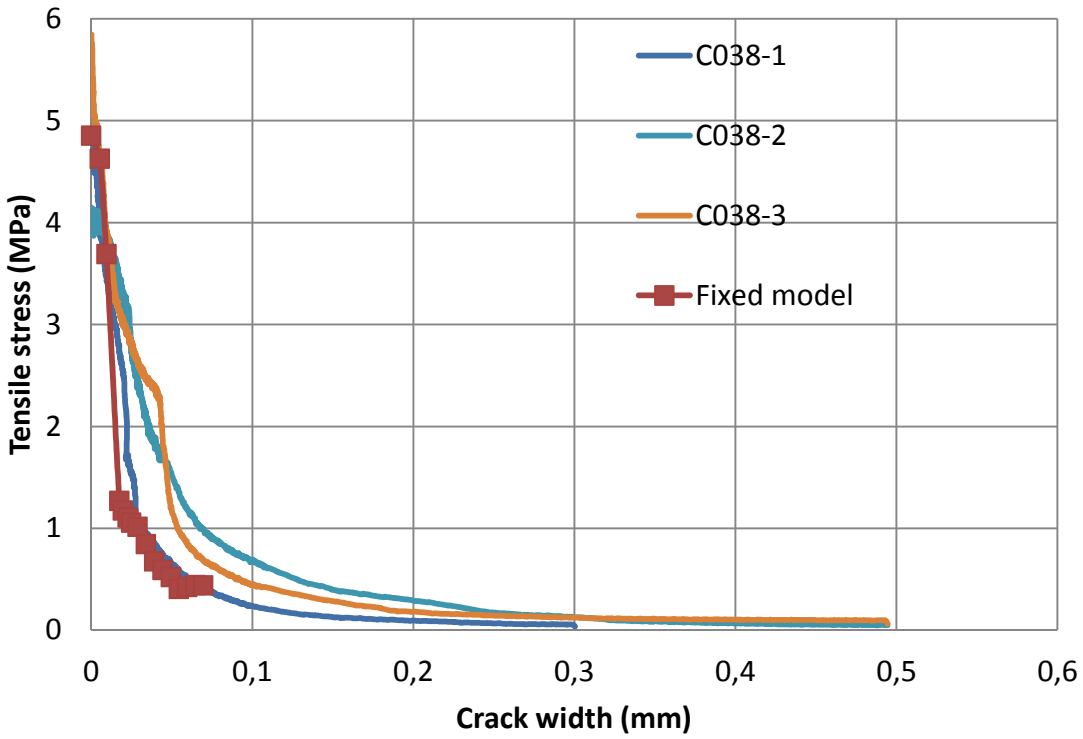


*Figure 4.3* *Stress-crack width response comparison between TS-fixed and test results.*

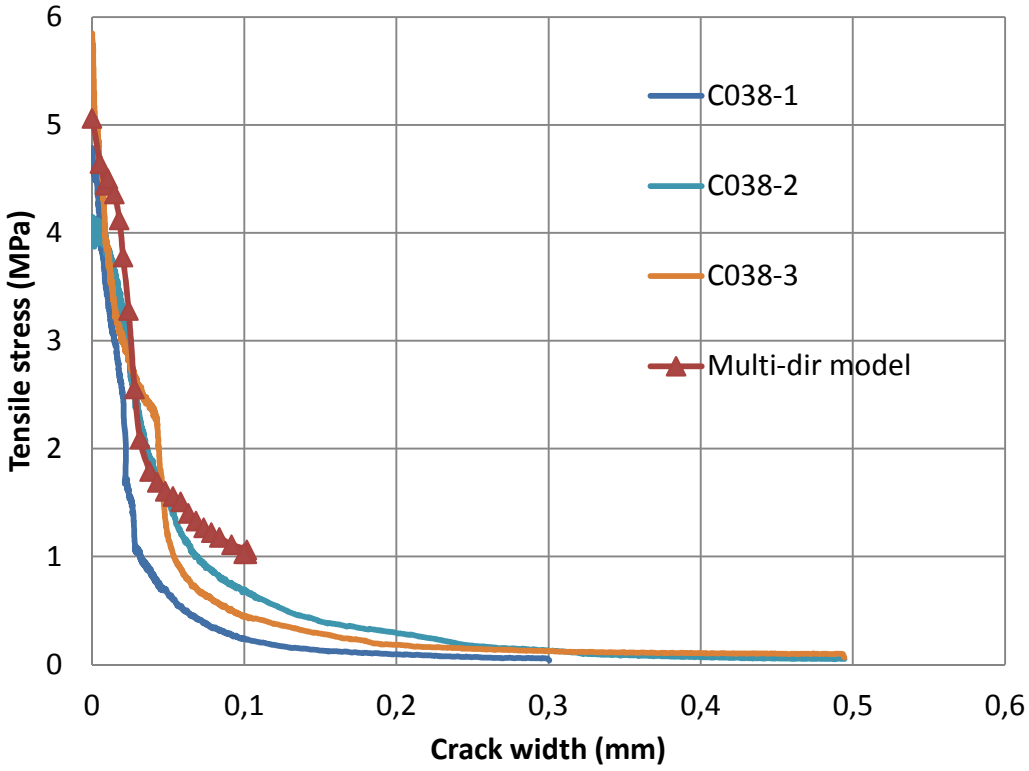


*Figure 4.4* *Stress-crack width response comparison between Multi-dir and test results.*

From the comparison above, we can draw the conclusion that the stress-crack opening of FE analyses based on rotating crack model (TS-rotating) constitutive model agrees well with the response measured in the tests over the entire loading period, at least for this test (C0.38). However, for TS-fixed and Multi-dir constitutive models, only parts of the crack-opening curve match that from the tests well. This means that the TS-fixed model can describe the cracking opening more correctly when the cracks initiated, and when the cracking width reached the range of 0.02-0.04 mm the Multi-dir model could work better.

To date, there is no consensus on the question of which type of model should be preferred. The distinction lies in the orientation of the crack, which either is kept constant (TS-fixed), updated in a stepwise manner (Multi-dir) or updated continuously (TS-rotating). In our coming simulation, the fracture starts in tension and subsequently proceeds in tension-shear. This behaviour generally implies that the axes of principal stress rotate after crack formation. For such cases, the use of TS-fixed leads to an increasing discrepancy between the axes of principal stress and the fixed cracks axes. However Multi-dir model provides an alternative. Whenever the angle of inclination between the existing cracks and the current direction of principal stress exceeds the value of a certain threshold angle, a new crack can be initiated. In this way, a system of non-orthogonal cracks is obtained. A prominent feature of TS-fixed and Multi-dir models is the inclusion of an explicit shear term for the fixed planes. Unfortunately, the identity ‘shear’ does not provide much insight into the behaviour of structures. A model which can monitor stress-strain relations in the rotating principal coordinate system is preferred, such as TS-rotating model. In TS-rotating model, new crack of slightly rotated orientation arises in each load step, and the previous cracks are erased from memory as soon as the new crack arises. And also, TS-rotating model allows the concrete material law to be satisfied exactly. See Rots (1991).

Based on what we discussed above, only TS-rotating constitutive model for concrete was used in the following analysis.

# 5 Finite element analysis for RC-beam test

## 5.1 FE model and numerical procedure

**(1) Mesh density**

In order to best capture the behaviour of the studied beams, the FE mesh must be sufficiently dense. Meanwhile, quite dense mesh could lead to relatively time consuming analyses. A balance should be obtained so that the results which are mostly concerned are achieved. As described in Chapter 1, one of the primary aims of this thesis is to study the shear cracking process in detail. Therefore, in order to correctly describe the shear cracking behaviour, element size should be appropriately chosen for the FE analysis.

To verify the effect of element size, two different mesh sizes were used in both 2D and 3D analyses for comparison. The discussion for comparison was shown in Table 5.1:

*Table5.1 Comparison of two element sizes.*

| Element size | | 2D model | 3D model |
|---|---|---|---|
| 5mm | Shear crack pattern | Being described clearly; | Being described clearly; |
| | Running time | 10 minutes on common computer | 20 – 50 hours in Cluster |
| 15mm | Shear crack pattern | Shear cracking was vague. | Being described clearly; |
| | Running time | 4 minutes on common computer | 1 – 10 hours in Cluster |

Based on the comparison above, it's reasonable to use 5mm element size for 2D model, and 15mm element for 3D model.

**(2) Element type**

For the 2D model, plane stress elements were used to model the shear response of the beams; see Broo *et al.* (2008). the loading acts in the plane of the plane stress elements. In DIANA, element CQ16M was selected which is an eight-node quadrilateral isoperimetric plane stress element. See Figure 5.1. It is based on quadratic interpolation and Gauss integration, TNO (2010).

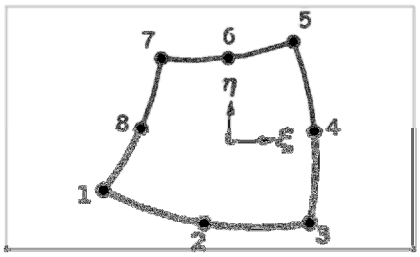


*Figure 5.1 CQ16M, TNO (2010)*

For the 3D model, three alternatives namely pyramid, wedge or brick elements can be chosen. If the 3D geometry is complex, pyramid or wedge elements are mostly used. If bond-slip model developed by Lundgren (2005) is used, the steel bars should be modelled with 3D elements too, therefore, pyramid element was the best choice.. pyramid elements of type TE12L were used in DIANA, which is a four-node, three-side isoparametric solid pyramid element based on linear interpolation and numerical integration, TNO (2010); see Figure 5.2.

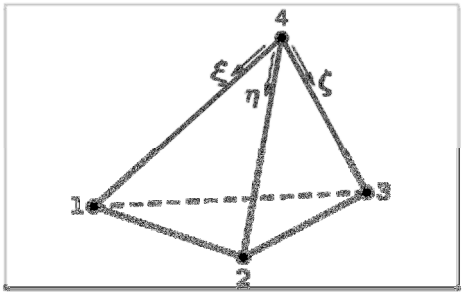


*Figure 5.2 TE12L,* TNO (2010)

For the 3D model with explicitly described bond action, interface elements, namely T18IF were used. It was built between two planes in a three-dimensional configuration; see Figure 5.3. The element is based on linear interpolation. Default integration scheme of 3-point was used.

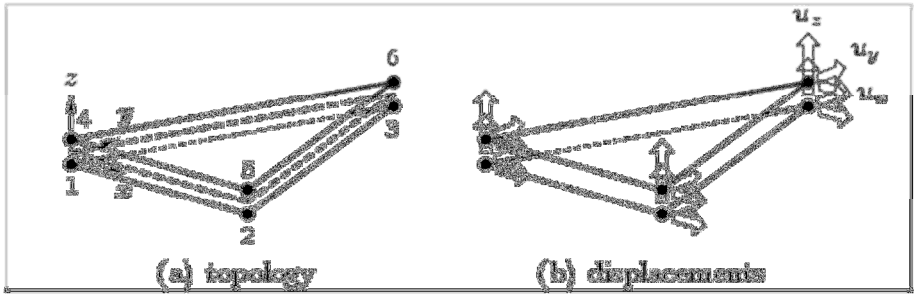


*Figure 5.3 T18IF,* TNO (2010)

**(3) Modelling of load**

**Self-weight:** Self weight of the RC beam was not included in the analysis; this was because the dimension of the beam is relatively small. Self-weight would have little influence on the analysis result and cracking behaviour.

**External load:** In order to correctly capture post-peak behaviour and precisely simulate the experiment conditions, the external load was imposed in a displacement-controlled regime.

**(4) Material input**

1) Concrete

The concrete was modelled with rotating crack approach, denoted by TS-rotating, based on total strain according to non-linear fracture mechanics. The reason for the choice of rotating crack approach was earlier discussed in Chapter 4.

The tension softening curve given by Hordijk (1987) was used to describe tensile behaviour of concrete. For the behaviour of concrete in compression, either the model given by Thorenfeldt *et al.* (1987) or an elastic-ideally plastic model was adapted. The relevant material parameters are shown in Table 5.2. When the lateral confinement for compressive behaviour was taken into account, VECCHI model proposed by Selby and Vecchio (1993) was used; see DIANA (2010).

*Table 5.2 Material parameters input*

| C0.38 | | Comments |
|---|---|---|
| E-modul at 208 days [GPa] | 39.49 | From EC2 |
| Poison ratio | 0.20 | From EC2 |
| $f_t$ at 208 days [MPa] | 4.90 | From experiment |
| Mode-I fracture energy [MPa] | 208.7 | From experiment |
| Crack band width [mm] | | Equal to element size except for the specially noted cases |
| $F_{c,cyl}$ at 208 days [MPa]=$f_{c,cube} \cdot 0.85$ | 71.83 | From experiment |

2) Reinforcing steel and half-moon shaped steel rulers

The reinforcing steel bars and steel rulers were modelled according to isotropic plastic model with Von Mises yield criterion. Hypothesis of strain hardening was considered in Von Mises. All the material parameters for steel are from the experiments; see Appendix B and Table 5.3.

*Table 5.3 Material input for reinforcing steel bars and half-moon shaped steel rulers*

| | E-modulus [GPa] | $f_y$ [MPa] | Poison ratio | Density [kg/m$^3$] | $f_u$ [MPa] |
|---|---|---|---|---|---|
| Reinforcing steel bars | 197 | 550 | 0.300 | 7800 | 630 |

| | | | | | |
|---|---|---|---|---|---|
| Steel ruler | 210 | 490 | 0.30 | 7800 | 630 |

**(5) Control for nonlinear analysis**

To actually perform FE analysis, some key parameters controlling nonlinear calculation procedure have to be defined:

- Loading increments: It is important that the increments are small enough to capture e.g. strain localization.
- Iterative method and convergence criteria: it is well known that divergence problem often occurs in analyses of reinforced concrete structures. In order to overcome these difficulties and get valuable information, some parameters should be appropriately set. For example, convergence norm and tolerance cannot be very strict to some extent, and the allowable number of iterations should be chosen wisely.

Based on the criteria mentioned above, some key parameters controlling nonlinear analysis were shown in Table 5.4.

*Table 5.4 Parameters input for control of nonlinear analysis.*

| Loading increment | Maxi-num of Iterations | Iterative method | Convergence norm | Convergence tolerance | If no convergence |
|---|---|---|---|---|---|
| 0.05mm | 500 | Regular Newton | Energy | 0.01 | Terminate |

## 5.2 FE model with embedded reinforcement

In FE analysis of reinforced concrete, the steel/concrete interface can be modelled with the assumption of full-interaction or with the introduction of an explicitly defined bond-slip law; see Plos (2000). The most advanced method is to implement a bond action in which the bond stresses does not only depend on the slip along the reinforcement but also on the normal stresses, similar to that developed by Lundgren (2005).Full-interaction between reinforcement bar and the surrounding concrete is realized by embedded reinforcement which adds stiffness to the finite element in the rebar direction. No separate elements or degree of freedom are held by an embedded rebar. Therefore, the strain of embedded rebar is calculated from the surrounding concrete elements. Consequently, nodal forces are computed from both concrete and rebar responses.

In general, the assumption of full-interaction is an easier method, than the application of a bond-slip law or an explicitly defined bond action, to simulate the steel/concrete interaction, although it cannot express the real mechanical behaviour. Therefore, in the earlier part of the project, in order to make the simulation easier, FE analyses were carried out with embedded reinforcement and later on an explicitly defined bond action developed by Lundgren (2005) was adopted.

### 5.2.1 2-D FE model

In the earlier part of the thesis work, an analysis based on 2D FE model with embedded reinforcement was performed. Half of the beam was modelled due to the symmetric geometry and loading. The FE mesh and the boundary conditions are shown in Figure 5.4. An elastic-ideally plastic model was used to describe the compressive behaviour.

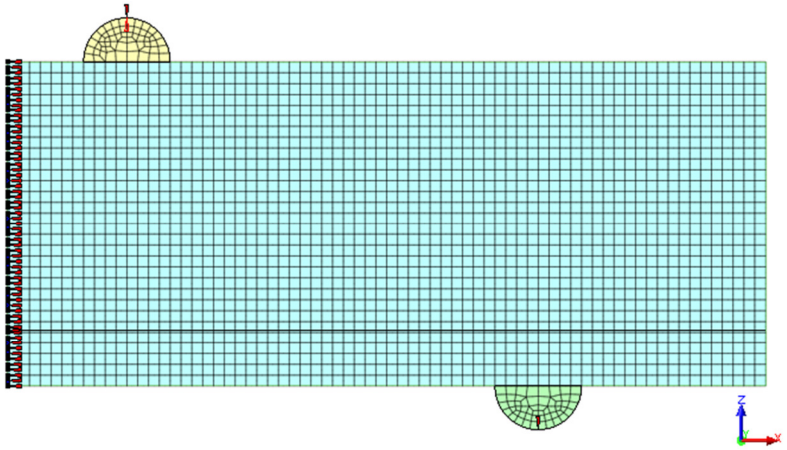

*Figure 5.4 FE mesh and boundary conditions.*

Analysis results and experimental results were shown in Figures 5.5-5.6. It can be seen in Figure 5.5 that the stiffness and failure load from FEA are close to those from experiment. However, the failure mode in FEA was triggered by the yielding of steel bars and crushing of concrete at the same time, which differed from that in the experiment. Until the load level of 178kN, no inclined shear cracking and clear bending cracking presented. After the load level of 178kN, two inclined cracks suddenly appeared on each half beam, which should be seen as shear cracking. Figure 5.6 shows the shear cracking pattern from FEA and the experiment at the same load level. The inclined cracking in FEA differed from that in the experiment both in position and in orientation, and did not cross the reinforcing bars.

Base on the discussion above, it can be concluded that a simplified 2D model is not suitable for the detailed study of the shear process in this project. More detailed 3D model will be discussed in the flowing chapters.

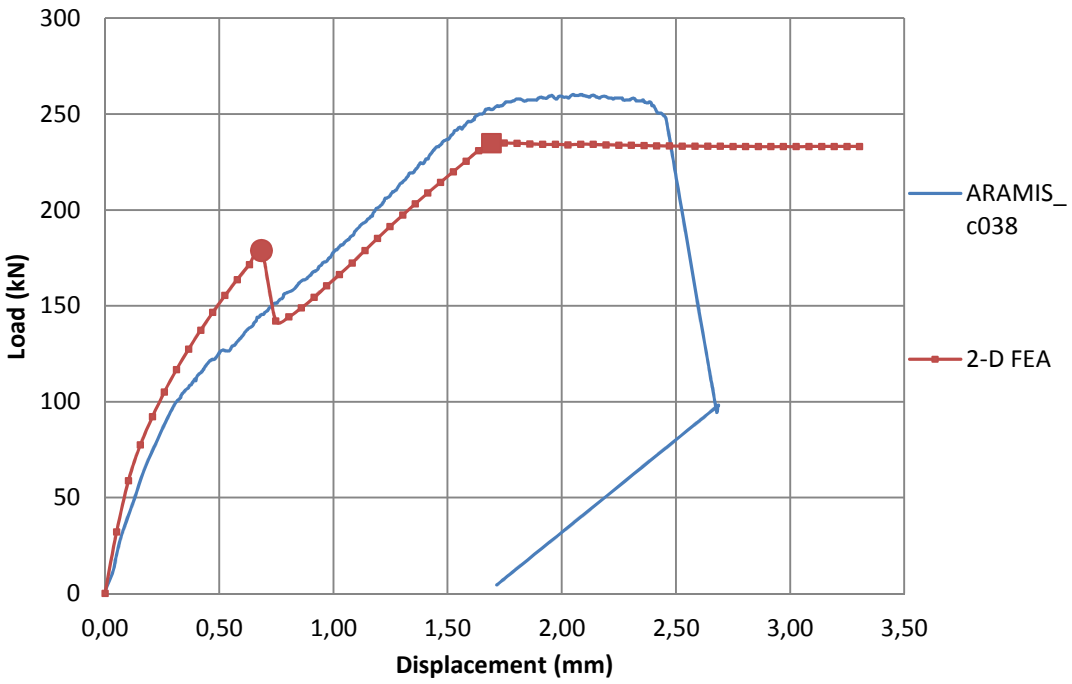


*Figure 5.5* *Load-displacement relations. Larger marked square point shows the yielding of the bars; larger marked circle point shows the primary shear cracking.*

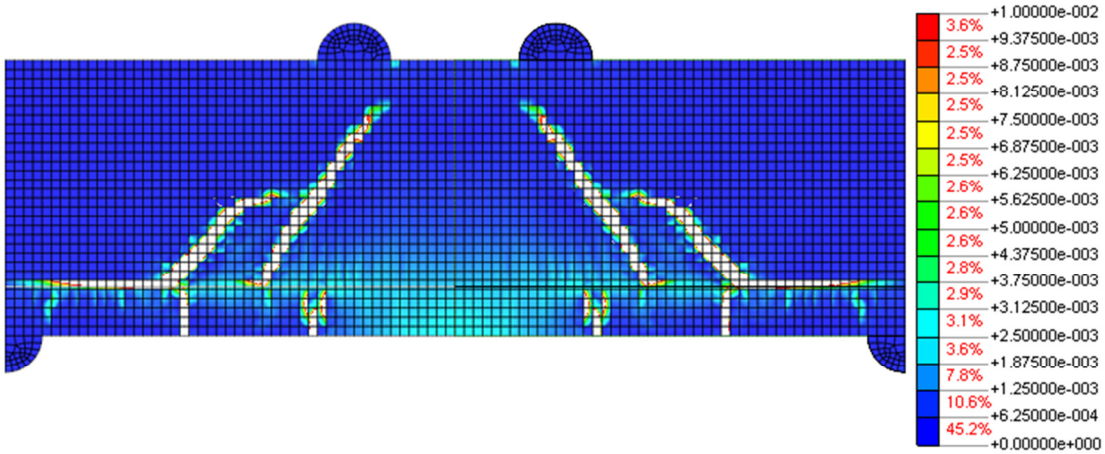


(a)

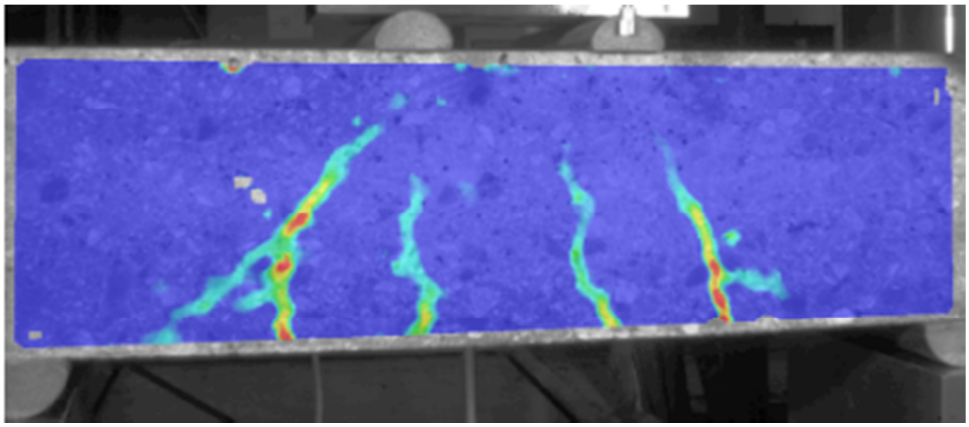

(b)

*Figure 5.6* *(a) First principal strain distribution at load=148kN shortly after the sharp drop in the load level; (b) Crack pattern from experiment at load=148kN.*

### 5.2.2 3D Symmetric model with embedded reinforcement

Due to the symmetric geometry and symmetric external load, the first attempt was to model one fourth of the RC beam (half of a beam length and half of a beam cross section); see Figure 5.7.

For boundary conditions, the displacement was constrained in the global Z-direction at both support plate and load plate. The displacement was also constrained in the global X-direction at the beam symmetry plane, and in the global Y-direction at the section symmetry plane respectively; see Figure 5.8.

The material input was the same as the ones given in Section 5.1. Model given by Thorenfeldt *et al.* (1987) was used to describe compressive behaviour of concrete.

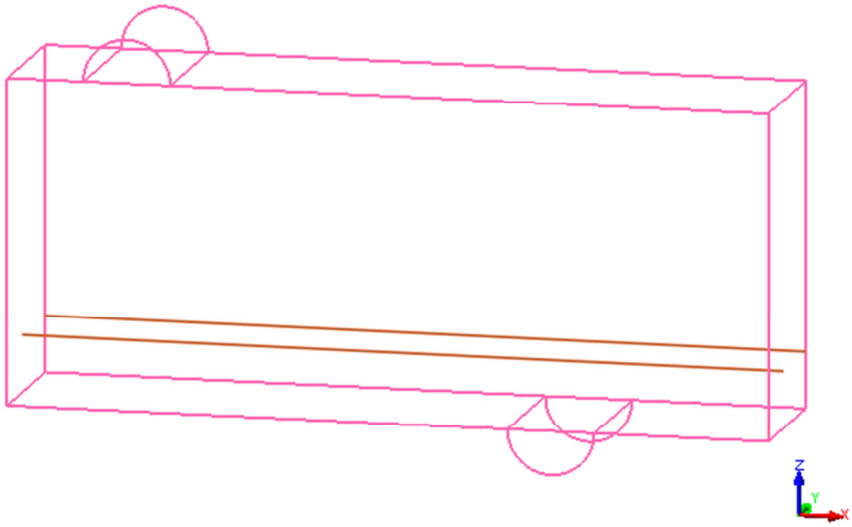


*Figure 5.7* *Symmetric geometric model (one fourth RC beam) with embedded reinforcing bar*

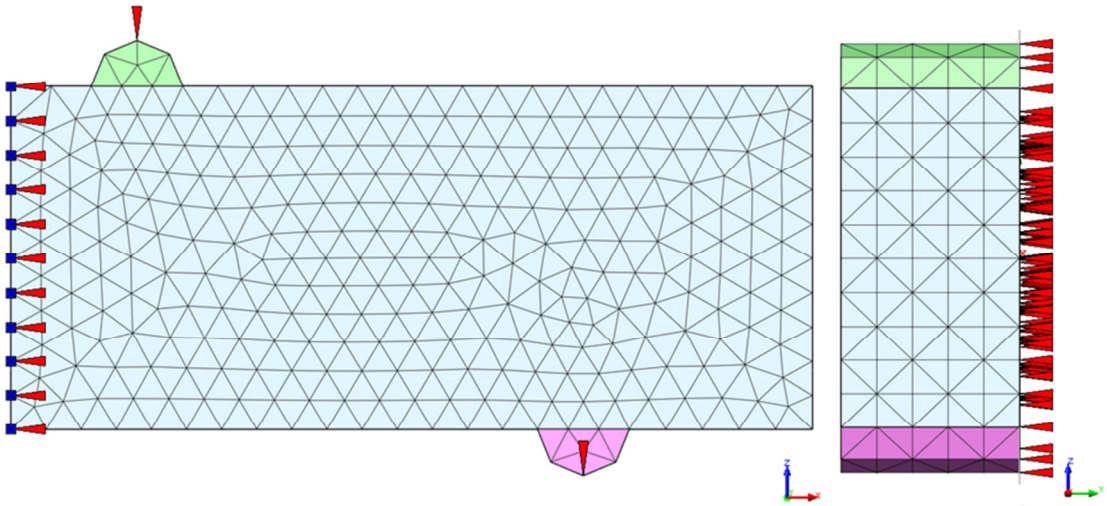

*Figure 5.8* *Symmetric geometric models with the FE mesh and boundary conditions; x-direction is longitudinal, y-direction is transversal, and z-direction is vertical.*

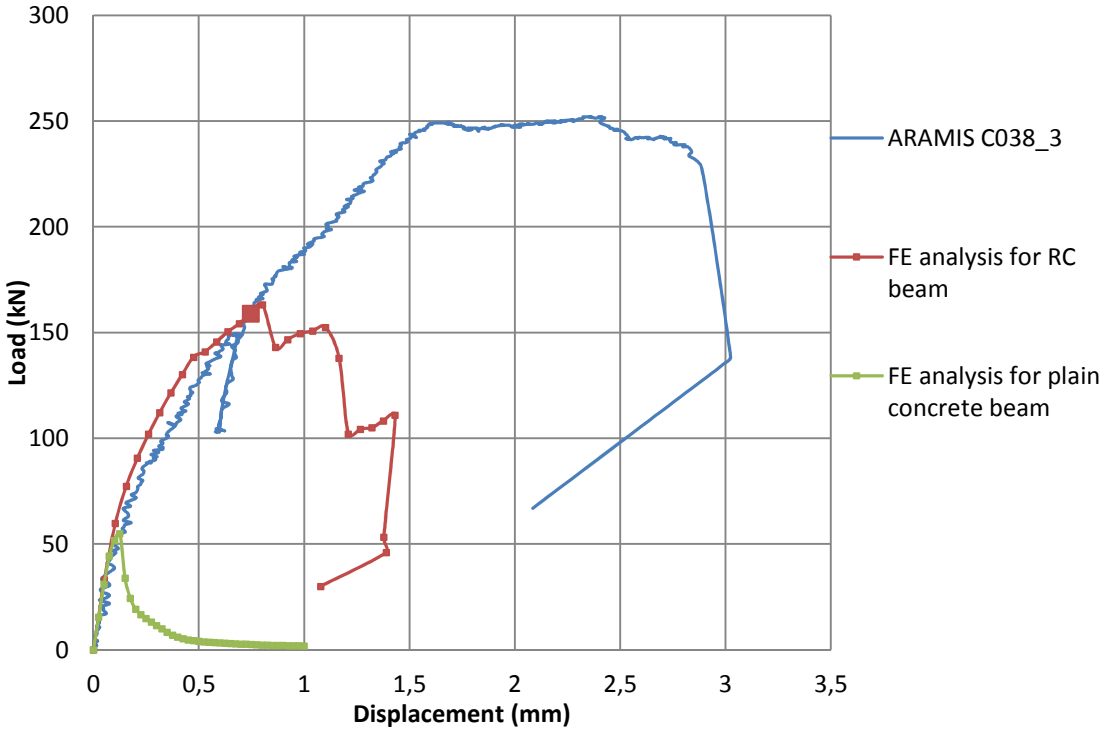


*Figure 5.9* *Load-displacement relations. Bigger marked point shows the yielding of the bar.*

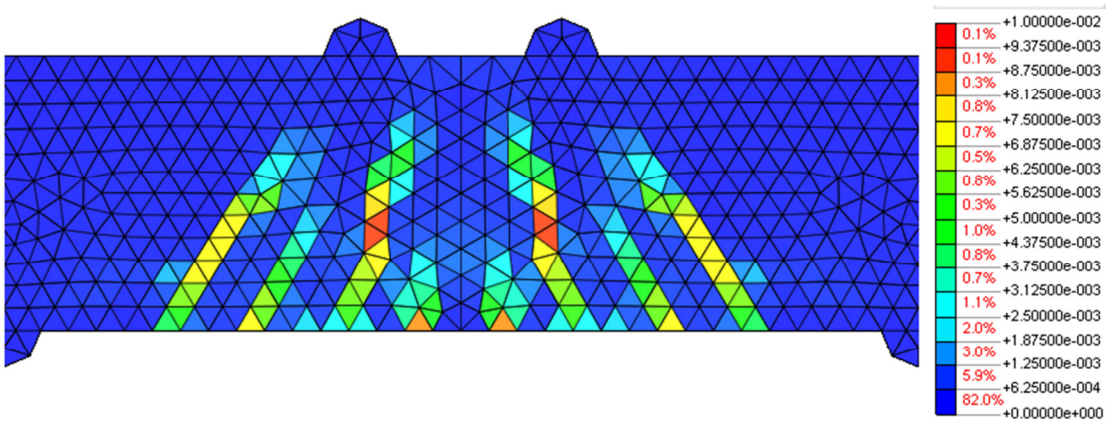


*(a)*

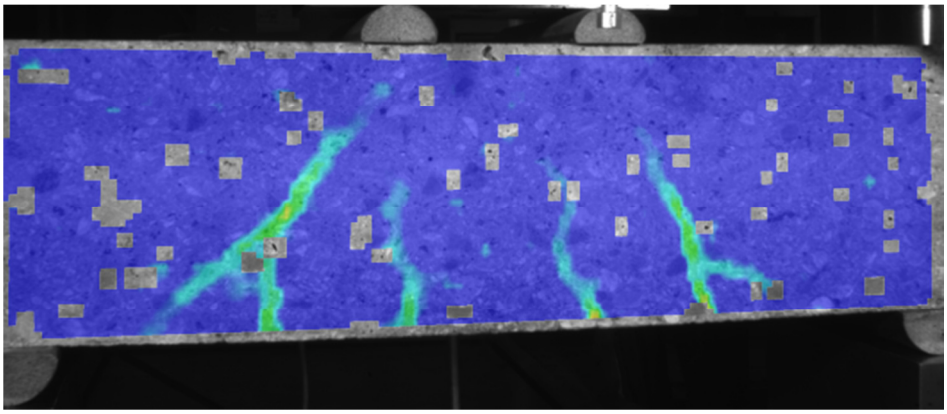

*(b)*

*Figure 5.10 (a) First principal strain distribution at load=163kN; (b) Crack pattern from experiment at load=163kN.*

The results for load-displacement relationship and cracking pattern were shown in Figure 5.9 and 5.10. The load level at first cracking was also estimated using hand calculations. The results showed that the initial stiffness from both FE analyses and hand calculations agreed very well, but slightly differed from that in the experiment. The load at first bending crack from FE analyses, hand calculation and experiment agreed well.

After the initial bending cracking of concrete, beam stiffness from FE analysis is slightly higher than that from experiment. One reason for this, among others, could be related to the choice of relatively fine mesh (15 mm element size). Over estimation of stiffness in FE analysis with fine mesh has been reported by other researchers too. The FE analysis also showed very early yielding of rebar and much lower load at the failure. However, the final failure was triggered by crushing of concrete in compressive zone, which agreed well with the failure mode observed in the experiment. One possible reason leading to lower failure load might be as follows: in finite element analysis, there are no separate elements or degree of freedom for embedded rebar. Therefore, the end of rebar at beam symmetry plane and longitudinal cross-section of rebar at section symmetry plane were not possible to be constrained, so that the symmetric boundary condition could not be fulfilled.

Based on discussion above, it can be concluded that in order to model the RC beam with embedded rebar in this project, an entire geometry model had to be used.

### 5.2.3 3D FE model with embedded reinforcement for entire beam

#### 5.2.3.1 FE model with modifying horizontal constraint

The entire geometry with embedded reinforcement was modelled as shown in Figure 5.11.

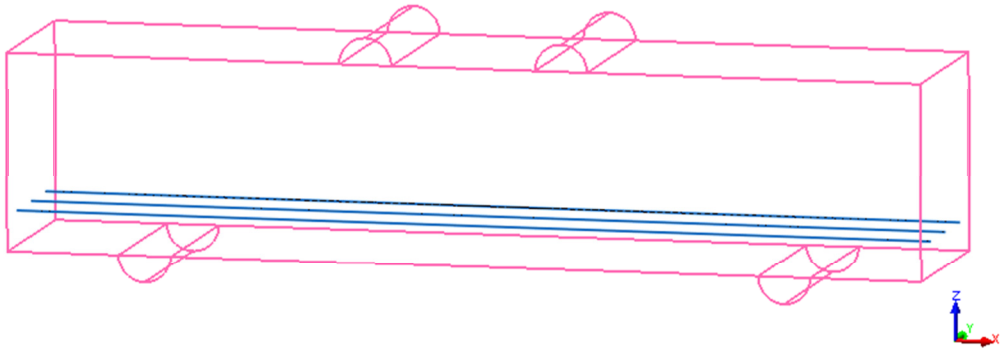

*Figure 5.11 Geometry model for the entire RC beam*

In the experiment, the half-moon shaped rulers were supported by steel blocks. The interface between them cannot be friction free. The friction resists the free deformation to some extent in the global X-direction, which delays crushing of concrete and lead to a higher load bearing capacity. In order to find an appropriate way to simulate the boundary condition as precisely as possible, four types of constraining methods in the FE model were tried.

- **BC1**: the displacements were constrained in global X-direction at one support plate, and in global Z-direction at both support plates; see Figure 5.12.

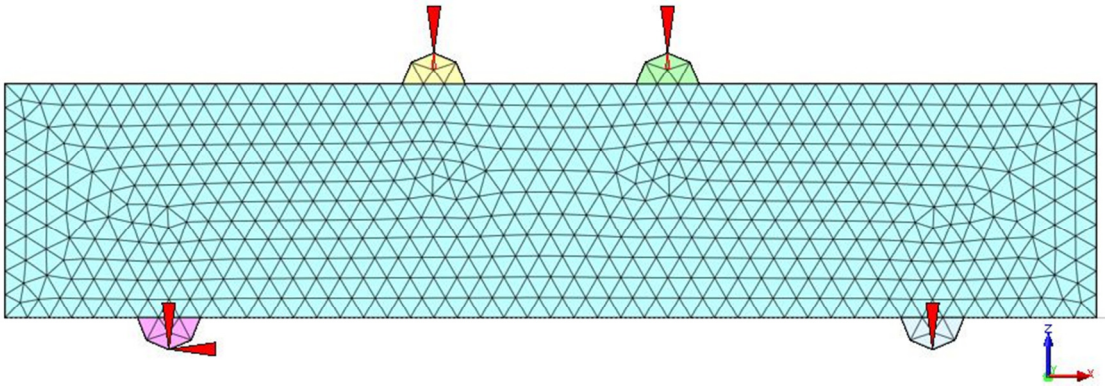

*Figure 5.12 Entire geometry model in case of BC1.*

- BC2: the displacements were constrained in global X-direction and Z-direction at both support plates; see Figure 5.13.

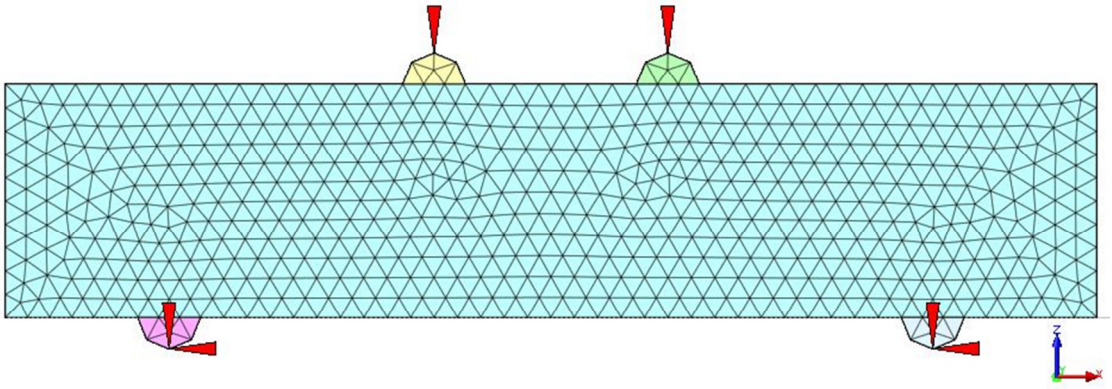

*Figure 5.13 Entire geometry model in case of BC2.*

- BC3: the displacements were constrained only in global Z-direction at both support plates; see Figure 5.14.

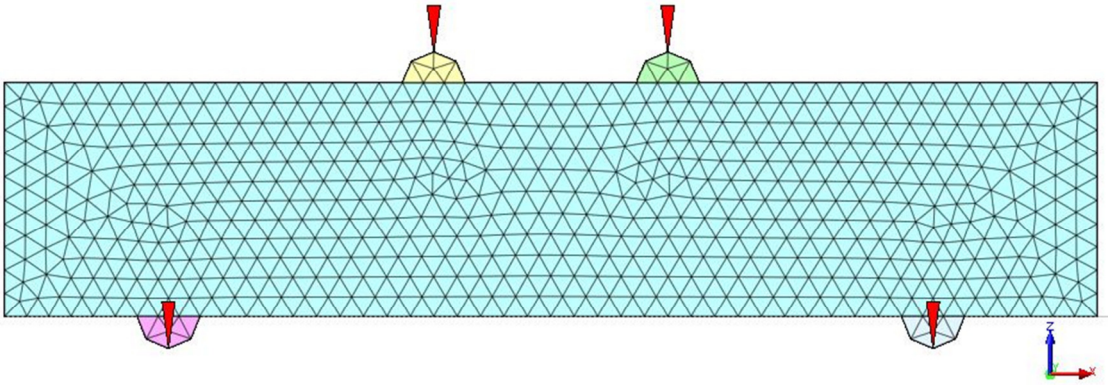

*Figure 5.14 Entire geometry model in case of BC3.*

- BC4: the displacements were constrained in global Z-direction at both support plates. The tension springs were added in global X-direction at both support plates; see Figure 5.15.

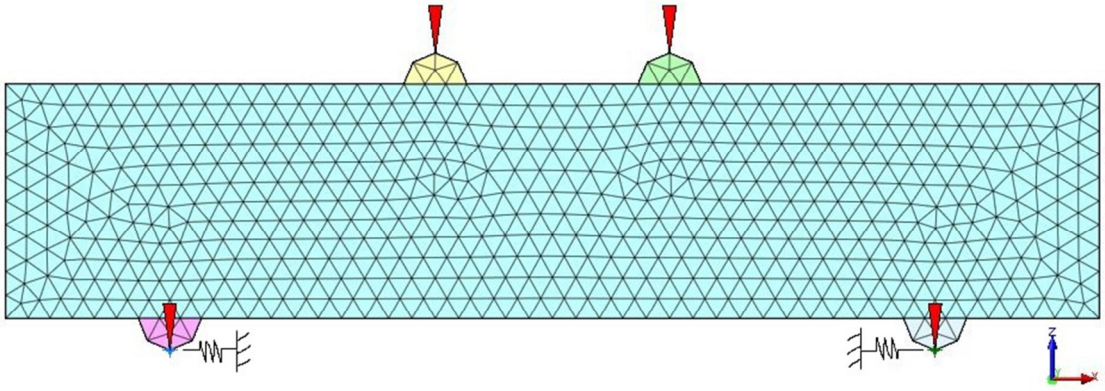

*Figure 5.15 Entire geometry model in case of BC4*

The material inputs were kept the same as before. Model given by Thorenfeldt *et al.* (1987) was used to describe compressive behaviour of concrete.

As a result, case BC1 shared the same load-displacement relationship with the case BC3, which was as expected. Case BC1 still presented lower load capacity compared with the experiment. Case BC2 presented almost the same failure load as the experiment but much higher stiffness; see Figure 5.16. That is because the fully constraint for the support on horizontal direction leads to a very large beam stiffness in the initial loading procedure. The failure mode was not a shear compression failure, but was triggered by the crushing of the concrete surrounding the ruler support; see Figure 5.17. Obviously, case BC2 cannot simulate reality reasonably. However it prompted us to find a case in between BC1 and BC2. That is the reason why case BC4 was considered.

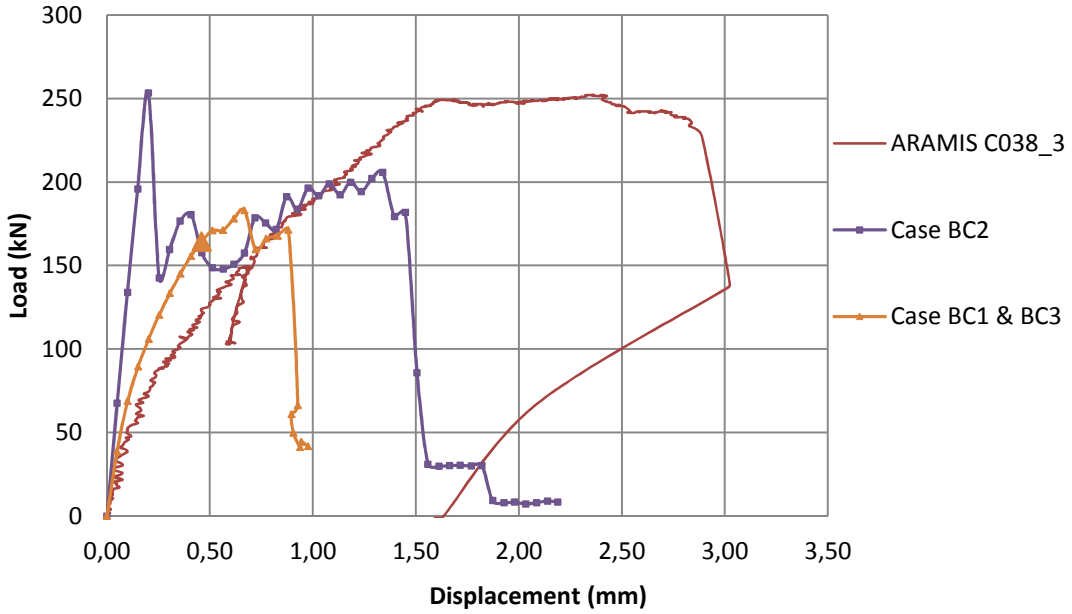


*Figure 5.16 Load-displacement relations. Larger marked point shows the yielding of the bar; no yielding presents in case of BC2.*

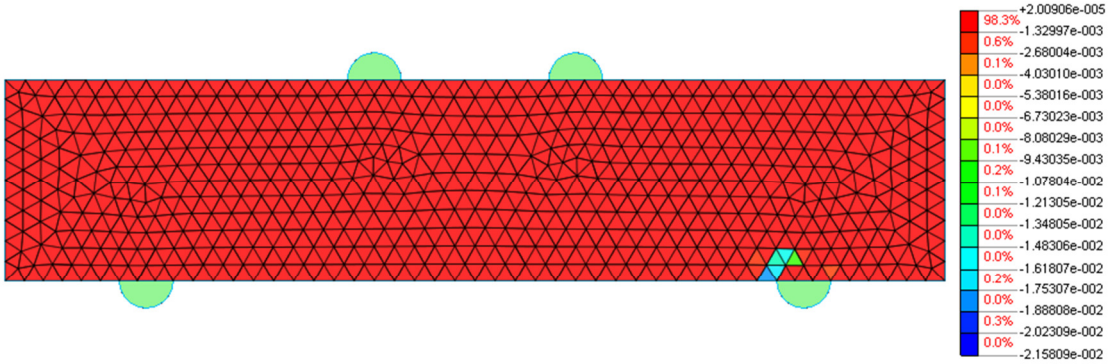


*Figure 5.17 First principal strain for the case BC2, Load=253kN.*

For the case BC4, the spring's stiffness highly influenced mechanical behaviour of the beam, e.g. beam's stiffness. However, choosing an appropriate stiffness value was very complicated. In the beginning of the analysis, a stiffness value could be roughly estimated. The reaction force on one support in X-direction in the case of BC2 was F = 30kN. The displacement on one support in X-direction in the case of BC3 was s = 1.1mm. Then, F = 15kN and s = 0.55mm could be got by linear interpolation, which yielded $k_{estimated}$=(15kN)/(0.55mm)=2.73e7N/m. Based on $k_{estimated}$, other spring's stiffness within the same order of magnitude as $k_{estimated}$ were tried in the analysis.

Firstly constant stiffness was used from beginning of the loading process. As a result, very high beam stiffness was observed during the entire loading process, which did not make sense. In very early loading procedure, e.g. before concrete cracking, the friction between the supports' surfaces were very small. The sliding friction increased with the increase of vertical load. Therefore it is not realistic to simulate the friction with constant spring stiffness. However, searching for a sound relationship between stiffness and load was not within the scope of this work; therefore, a simplified multi-linear relationship was adopted; see Figure 5.18. The springs' stiffness in both case (a) and case (b) were activated after the initial cracking of concrete and before yielding of the rebar, although this was taken place much earlier in case (a) compared to case (b).

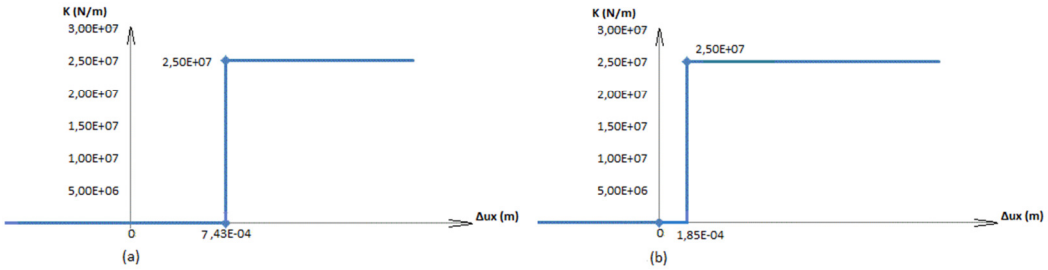


*Figure 5.18 Spring's stiffness diagram. 'K' denotes spring's stiffness, '$\Delta u_x$' denotes deformation of spring.*

The results by using the two stiffness diagrams were shown in Figures 5.19-5.21. The failure load increased more in case (b) than in case (a), and almost reached the same level as the experiment. However, in case (b), the beam stiffness was much higher than that in the experiment, and there was no clear shear cracking pattern shown at the failure load level. Therefore, it should be concluded that spr(a) could describe the real mechanical behaviour more reasonably compared with spr(b), although spr(a) still could not present a higher failure load. In order to better understand how stiffness influences the failure mode, other analysis with varying stiffness values or spring activation points were also tried. The results showed that it was nearly impossible to find an appropriate expression for spring's stiffness where both beam stiffness and failure load could be correctly predicted. The high spring stiffness and an early activation of the spring led to a higher failure load but incorrect beam stiffness at the same time.

From discussion above, a conclusion can be drawn that the friction between the half-moon shaped rulers and steel blocks did show effects, but could not completely work as a horizontal constrain. Therefore, that effect would not be considered in the following analysis work. However, if the effect of friction was simulated by spring element, the beam stiffness, failure load and cracking pattern varied sensitively with variation of the spring's stiffness in a certain range. Additional research is required for establishing an appropriate spring's stiffness model.

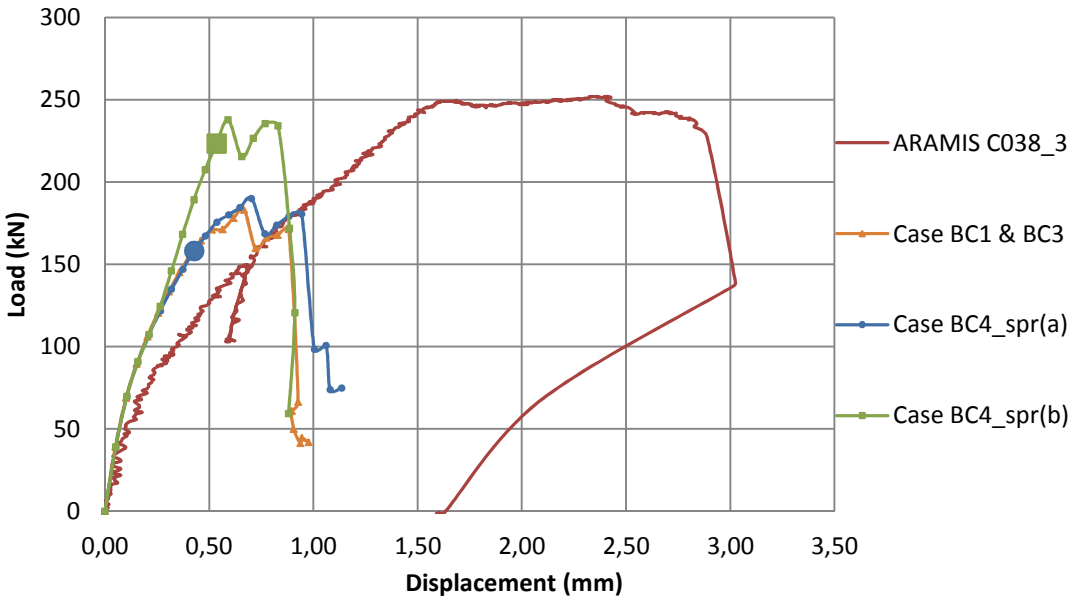


*Figure 5.19* *Load-displacement relations. Larger marked point shows the yielding of rebar.*

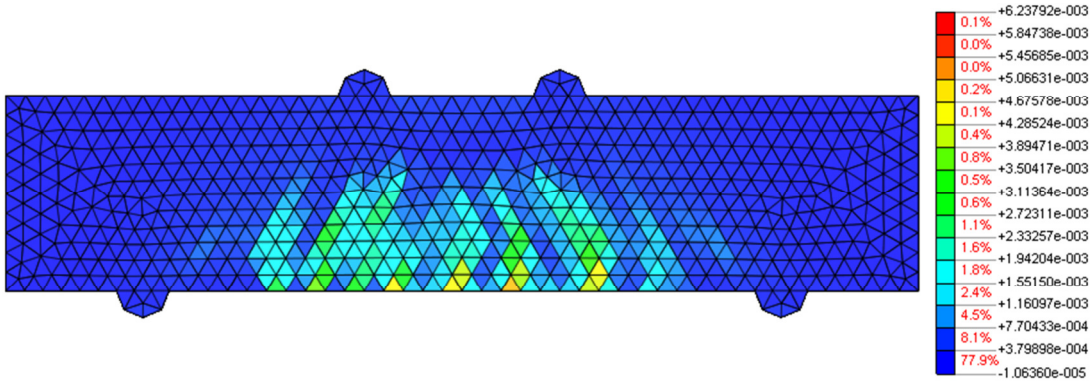


*Figure 5.20* *First principal strain for the case of BC4_spr(b), Load=237kN.*

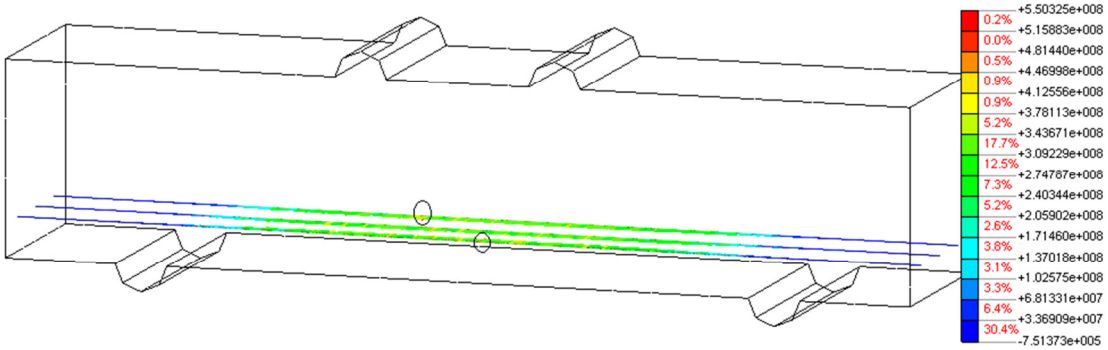


*Figure 5.21* *Yielding distribution of 3 bars for Case BC4_spr(a). Marked points present the yielding positions.*

### 5.2.3.2 FE model with controlling elements' positions

As the beam is symmetric on both load and geometry, the three embedded bars should reach yielding symmetrically in the same cross section. However, it can be seen from Figure 5.21 that the yielding points scattered and did not appear in the same cross section, which prompted us to check the embedded situation inside the FE model.

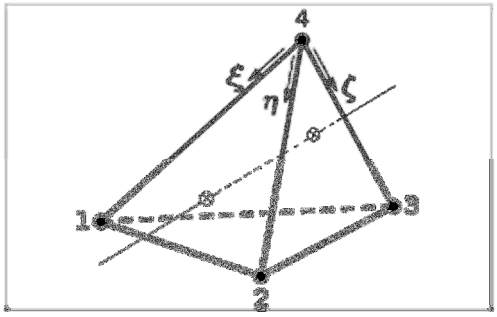


*Figure 5.22 BAR particle in TE12L.*

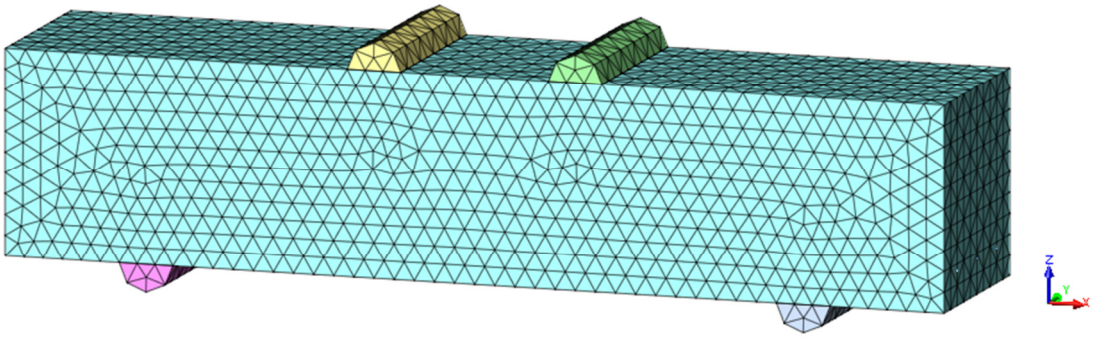

*Figure 5.23 Auto-meshed model for the entire beam.*

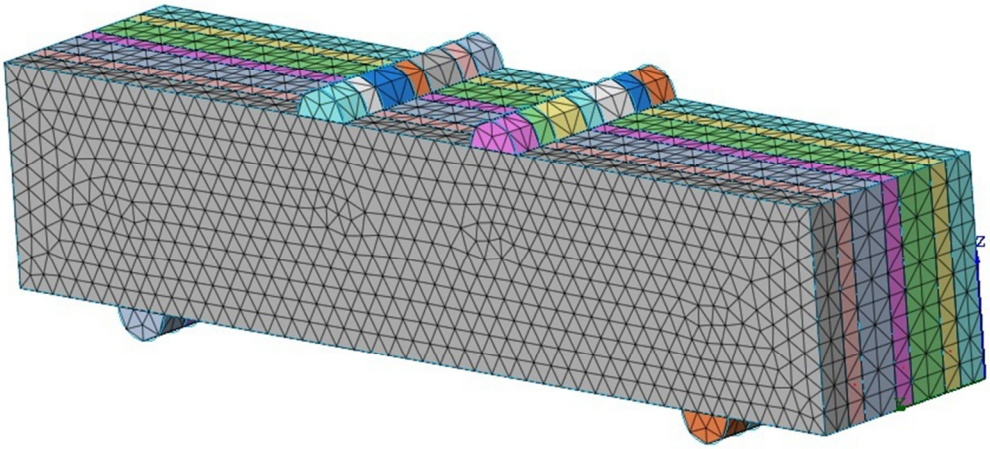

*Figure 5.24 Meshed model for the entire beam with controlling the relative positions of embedded bar and its surrounding solid elements.*

In DIANA reinforcing bar can be embedded in all solid elements. To embed a bar in solid elements, DIANA needs the location points of the particle that is embedded in each element, TNO (2010). See Figure 5.22. In the previous section, auto-mesh method was used for the entire geometry without controlling the relative positions of embedded bars and its surrounding solid elements; see Figure 5.23. That might cause errors in calculating the right embedded situation in DIANA, which led to incorrect yielding distribution as shown in Figure 5.21. To solve this problem, the geometry model was divided into 7 blocks along Y-direction, as shown in Figure 5.24. In this way, three bars shared the same relative positions to their corresponding surrounding solid elements.

The yielding distribution calculated from new model was shown in Figure 5.25. It can be seen that yielding points appear in the symmetric cross-section of the three bars. Therefore, this new mesh configuration should be used for the following analysis. Since the yielding of bars and final crushing failure of concrete still were triggered very early in this new model, see Figure 5.26-5.27, further improvement was performed in the following sub-chapter.

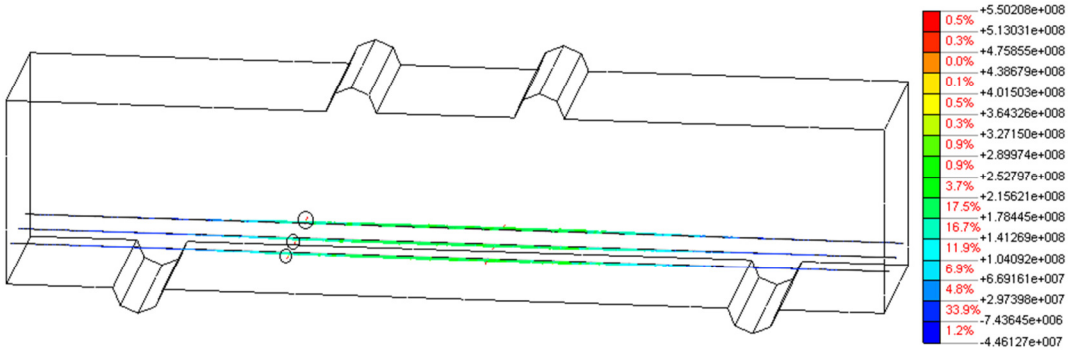


*Figure 5.25 Yielding distribution of the three bars. Marked points present the yielding positions.*

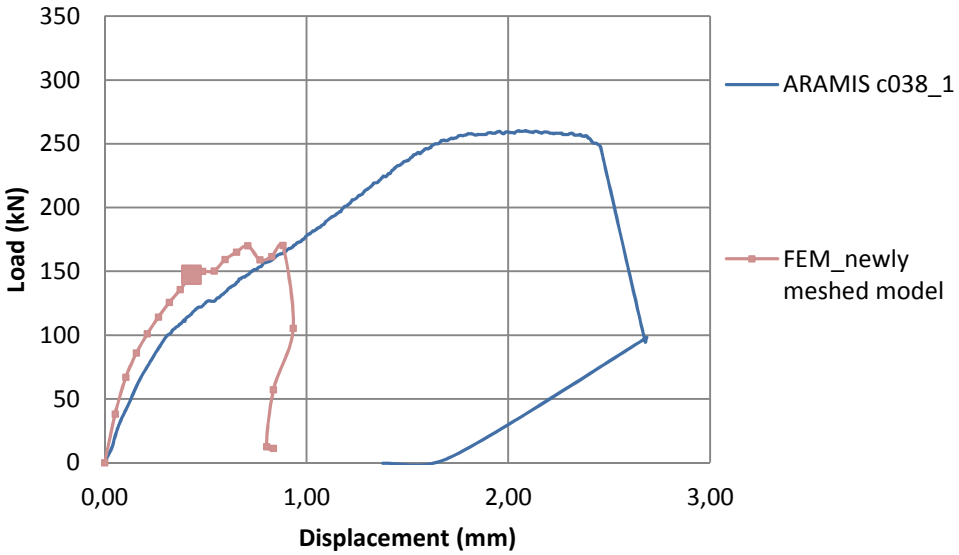


*Figure 5.26 Load-displacement relations. larger marked point shows the yielding of rebar.*

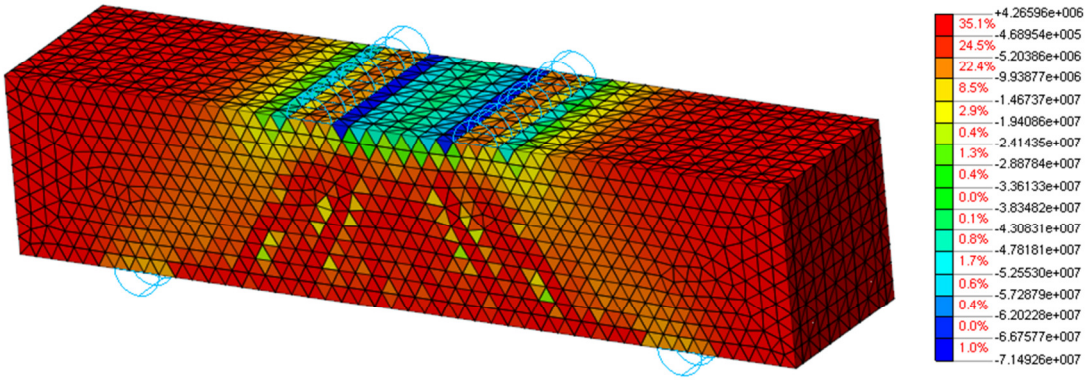


*Figure 5.27 3rd principal stress distribution. Load=170kN.*

#### 5.2.3.3 FE model with controlling elements' positions and considering lateral influence

After all the analyses mentioned above, a reasonable load-displacement relation close to the experiment result still could not be achieved. Yielding of bars and final crushing failure of concrete were triggered too early. Model given by Thorenfeldt *et al.* (1987) used in all the 3D analyses above, played a leading role in capturing the failure mode caused by the concrete's crushing. That prompted us to perform more detailed research on compressive behaviour of concrete in the following work.

Figure 5.27 shows the 3rd principal stress distribution when crushing failure was triggered. Compressive failure was localised in one element row on horizontal cross-section close to upper half-moon ruler. The size of that failure region was too small to correspond to the size of the specimens used to calibrate the Thorenfeldt compression law; this potentially leads to a premature compressive failure, see Zandi Hanjari *et al.* (2011). That is one reason for underestimation of the failure load in the analysis above. Therefore, in order to correctly capture the compressive strain localization, the compressive stress-strain law given by Thorenfeldt *et al*. (1987) which is shown in Figure 2.6 should be modified for the element size.

However, in commercial programs available today, it may not always be possible to combine a compressive-softening curve with the adjusting for the size of the compression zone, Broo *et al*. (2008). In order to capture a correct localization, compressive model with an elastic-ideal plastic relationship, namely CONSTA in DIANA (shown in Figure 2.7), could be tried. The load-displacement results are shown in Figure 5.28.

Although compressive model with an elastic-ideal plastic relationship is capable of presenting the correct localization, it overestimates the compressive capacity. After the compressive strength is firstly reached within a very small area in the compression zone, no softening took place in that area. Compressive capacity kept constant and compressive failure did not happen until compressive strength was continuously reached within all other areas in the compressive zone. Therefore, the failure load calculated from analysis based on elastic-ideal plastic compressive model is overestimated.

Other important factor that should be considered, especially in 3D FE analysis, is lateral influence including lateral confinement and lateral tensile strain. For lateral tensile strain, it does not influence the analysis in this project much because the

localised areas in compressive zone subject compressive stress in three principal directions. Although 1st principal strain still shows positive in these areas, it is not large enough to influence the compressive response. For lateral confinement, it is an essential factor which could influence the compressive capacity. Lateral confining stresses increase the strength, stiffness and strain at peak stress of concrete elements, Selby (1993). In DIANA, the strength enhancement is modelled by modifying the peak stress of the base curve, i.e. Thorenfeldt compression curve, based on the theory developed by Selby *et al.* (1993).

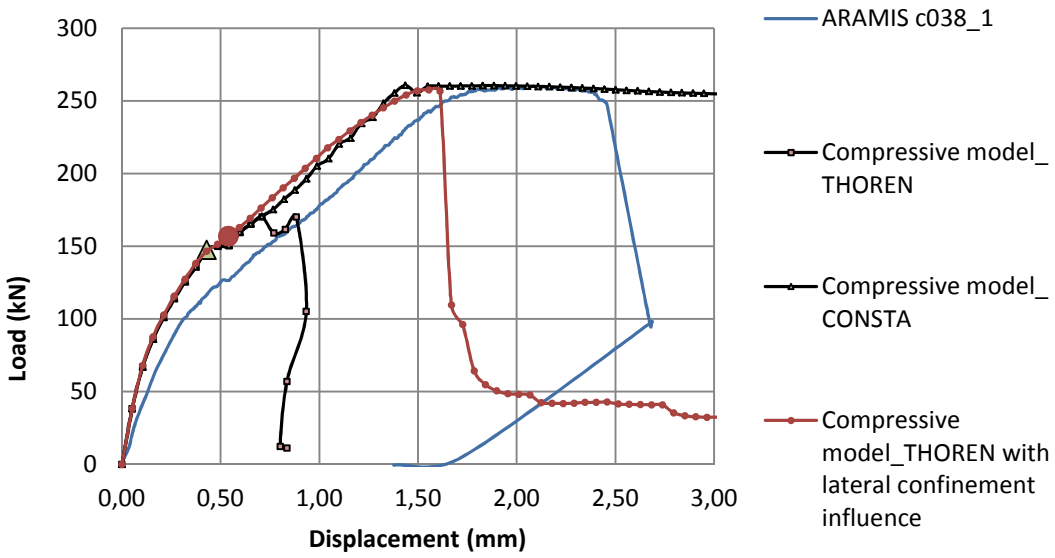


*Figure 5.28 Load-displacement relations. Bigger marked point shows the yielding of rebar.*

The load-displacement results are shown in Figure 5.28. It can be seen that THOREN model with lateral confinement influence is capable of predicting the failure load very well. CONSTA model can also obtain almost the same failure load as that in the experiment; however, it does not capture the drop in the load after the failure. The stiffness was slightly overestimated in all the analysis, especially after the shear cracking occurred, which is believed to be caused by the effect of perfect bond between reinforcing bars and concrete. However, none of these models can predict a correct load at which the reinforcement reached yielding.

In conclusion, THOREN model with lateral confinement influence will be used for the following analysis. Furthermore, as cracking process is one of the primary focuses in this thesis, a more detailed discussion about shear cracking pattern will be performed in Chapter 6.

## 5.3 FE model with explicitly described bond action

It is well known that embedded reinforcement can only simulate the ideal mechanical behaviour for the interaction between rebar and surrounding concrete. The perfect bond would lead to higher stiffness than reality, which was verified in the analysis

above. Therefore, FE analyses considering a more realistic bond action between bar and concrete will be built in the following.

The model was still built based on entire beam for the convenience of comparison with model considering embedded bars; see Figure 5.29. The bars were modelled by four-node, three-side isoparametric solid pyramid element - TE12L, the same as concrete element type. The cross-section of the rebar was estimated with a quadrangle shape, and a total area 339mm$^2$, the same as in the experiment. The interface elements, namely T18IF in DIANA, were generated between two planes in the 3D configuration. General material input was same as given in Section 5.1. THOREN model with lateral confinement influence was used to describe compressive behaviour of concrete.

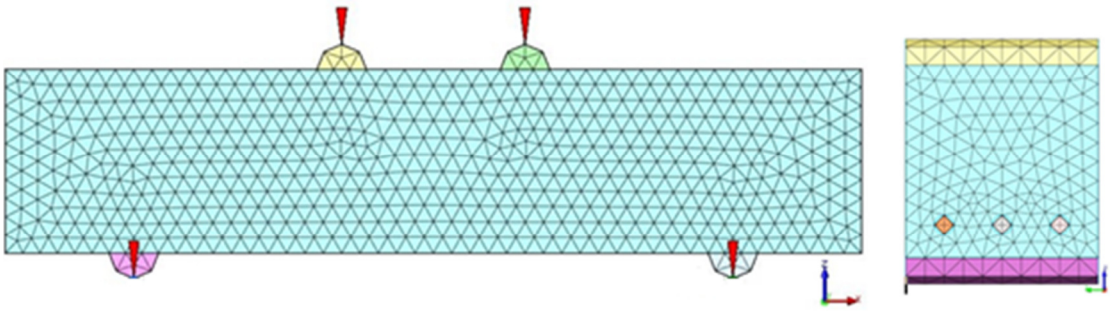

*Figure 5.29 Geometric model with meshes and boundary conditions; x-direction is longitudinal, y-direction is transversal, and z-direction is vertical.*

The interaction between the reinforcing bar and its surrounding concrete was described by two models, Lundgren (2005) and Dörr (1980). The modelling approach developed by Lundgren (2005) is especially suited for detailed three-dimensional finite element analyses, where both the concrete and the reinforcement are modelled with solid elements. Surface interface elements are used at the steel/concrete interaction to describe a relation between the stress, σ, and the relative displacement, u, in the interface. The bond model is a frictional model that uses elasto-plastic theory to describe the relations between stresses and deformations, and it consists of two yield functions: one explains the friction assuming that the adhesion is negligible, and the other describes the upper limit for a pull-out failure determined from the stress in the inclined compressive struts that result from the bond action. The model by Dörr (1980) however describes the interaction between the bar and its surrounding concrete with an explicitly defined bond-slip law. The advantage of such an approach is the simplicity and the possibility to be used in both 2D and 3D analyses. However, in such a model, the bond stress is solely a function of slip and does not depend on the stresses generated due to surrounding confinement.

In the model by Lundgren (2005), tensile strength and compressive strength of concrete as well as radius of bar were needed as the input data. For Dörr (1980), value c and $\Delta u_t^0$ were chosen as tensile strength of concrete and 0.06mm respectively, which is recommended by DIANA user's manual. See Figure 5.30 and Function (5.1) for model description.

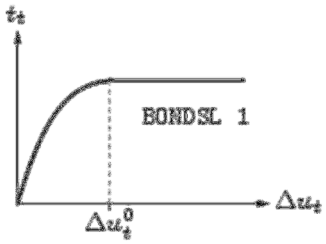


*Figure 5.30 Shear traction-slip relation, Dörr (1980)*

$$\tau_t = \begin{cases} c\left(5\left(\frac{\Delta u_t}{\Delta u_t^0}\right) - 4.5\left(\frac{\Delta u_t}{\Delta u_t^0}\right)^2 \cdots \right. \\ \quad \left. +1.4\left(\frac{\Delta u_t}{\Delta u_t^0}\right)^3\right) & \text{if } 0 \le \Delta u_t < \Delta u_t^0 \\ 1.9\,c & \text{if } \Delta u_t \ge \Delta u_t^0 \end{cases} \quad (5.1)$$

The load-displacement relations achieved from analyses above and the experiment are shown in Figure 5.31, and results from the model with prefect bond are also shown for comparison. The stiffness in the analyses including bond action is still slightly higher than that in the experiment, but still better estimate the stiffness in the experiment than the model with perfect bond. The yielding load from both Lundgren (2005) and Dörr (1980) are higher and further closer to experiment. The failure mode was trigger by crushing of concrete, which was the same as in the experiment. However, the failure loads in the analyses with Lundgren (2005) and Dörr (1980) are underestimated by about 22kN and 31kN respectively. That is most likely because horizontal constraint due to the friction between half-moon support ruler and the brick under it was not modelled in analyses.

From the discussion above, it can be concluded that better agreement with experiment, in terms of stiffness and capacity, was observed in the analyses with explicitly described bond action. More detailed discussion focusing on shear cracking process will be performed in Chapter 6.

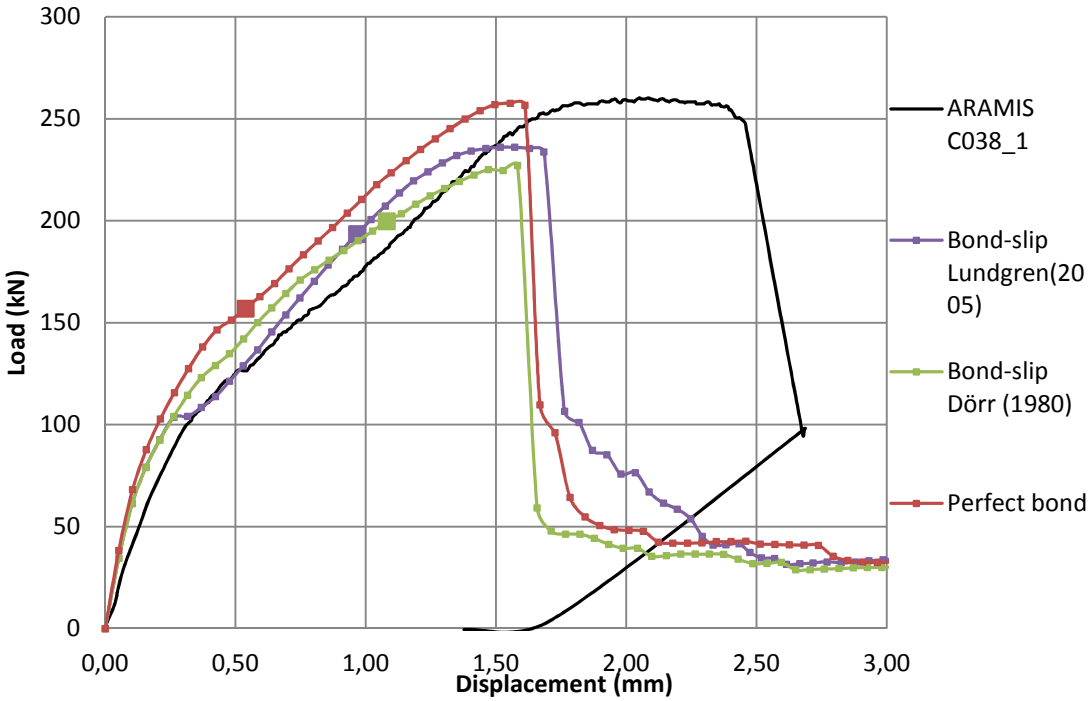


Figure 5.31 Load-displacement relations. Bigger marked point shows the yielding of rebar.

# 6 Discussion of results in terms of cracking patterns

From the description and comparison of the results in Chapter 5, it was seen that the influence of lateral confinement played quite an important role in the shear response of the analysed beam. The results of the analyses including the lateral influence on the concrete compressive response are more trustworthy and reasonable, especially when the bond action was included; therefore, in this chapter, cracking patterns from these FE analyses will be discussed in detail.

## 6.1 FE analyses including bond action and lateral influence on the concrete response

As mentioned in Section 5.3, the bond slip models from Lundgren (2005) and Dörr (1980) were used in the FE analysis to incorporate the bond action. In this chapter, the cracking patterns from the analyses are compared with that in the experiment, with respect to cracks' initiation, propagation and localization etc. Meantime, the possible factors, which might influence the shear cracking behaviour, are analysed in detail for different stages of crack development. The bond model given by Lundgren (2005) and the bond-slip law given by Dörr (1980) will be denoted as Model L and Model D, respectively.

### 6.1.1 Comparison of shear crack behaviour

Theoretically, without the consideration of concrete's plastic property, the first flexural crack should form when the tensile stress at the bottom edge reaches the tensile strength of the concrete ($f_t$ = 4.9MPa) see Table 4.1. From hand calculation, the corresponding load is around 35kN in the experiment, see Appendix A. Since the first flexural crack had a width of a few micrometres, it could not be observed visually directly, neither in the experiment nor in the FE analyses.

In the experiment, the first visible flexural crack was found when the load reached approximately 100kN. In Figure 6.1, comparison of the crack patterns from the analyses and the experiment is illustrated at the load level of 104kN. There were four clearly visible cracks totally in this stage of the experiment, while the cracks from the FE analyses, both with Model L and Model D, were not yet fully localized.

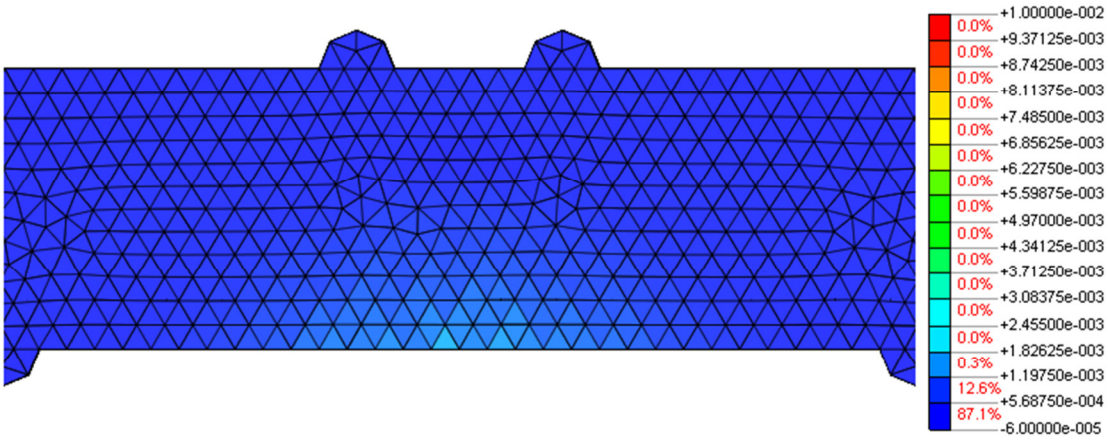

*(a)*

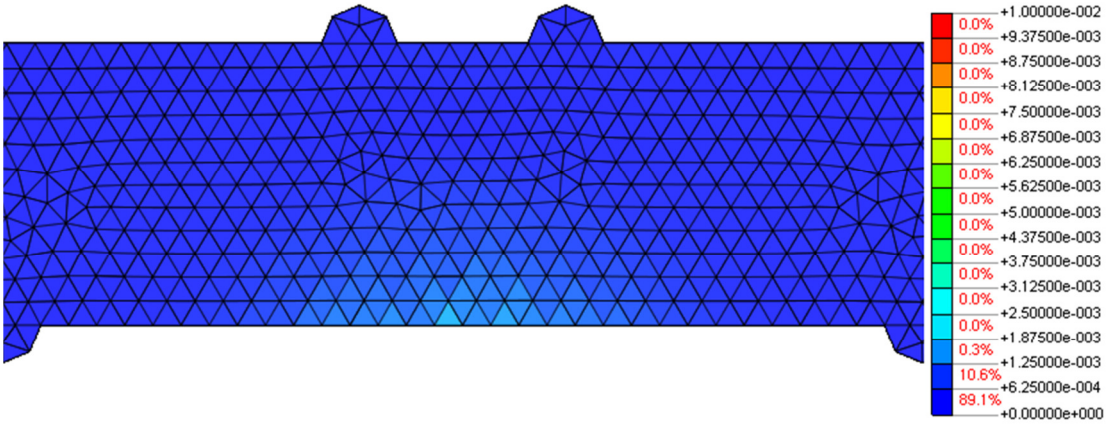


*(b)*

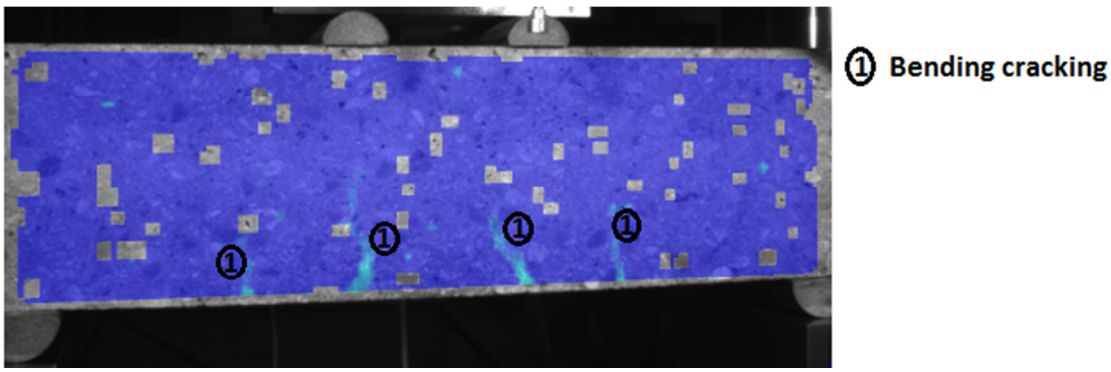


*(c)*

*Figure 6.1* *Cracking patterns: (a) 1st principal strain distribution based on Model L at load 104kN; (b) 1st principal strain distribution based on model D at load 104kN; (c) DIC from the experiment at load 104kN.*

As can be seen from Figure 6.2 (c), after the load reached about 120kN, an inclined shear crack began to develop from the tip of the flexural crack closest to the support, this was called 1st shear cracking. From now on, the critical crack propagation would be governed by shear rather than by bending. The initiation of inclined shear crack was not exactly symmetric. A possible reason might be an uneven distribution of the properties of the concrete.

In the two FE analyses, flexural cracking was initiated in the central zone of the beam. No fully localized shear crack was presented in this stage. However, a number of microscopic inclined shear cracks had initiated from the tip of flexural cracks. Still flexural cracking was dominating the crack behaviour. See Figure 6.2.

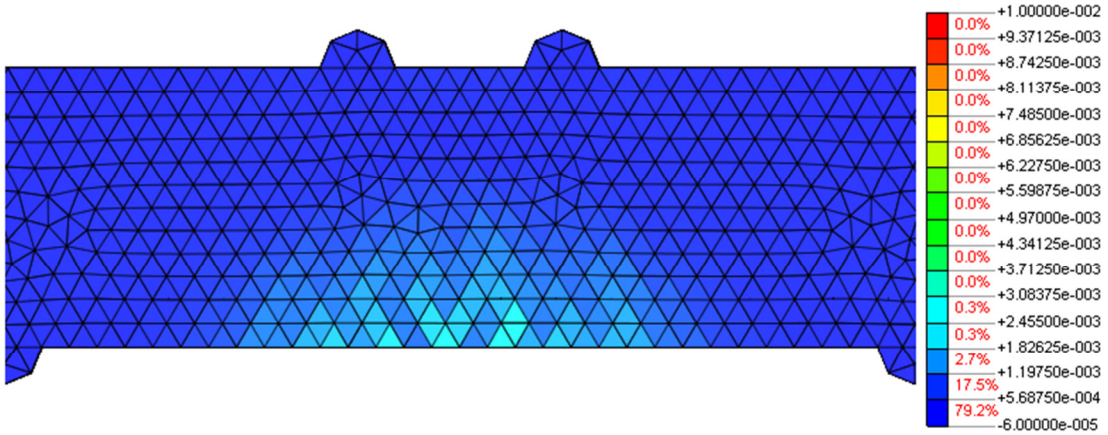


*(a)*

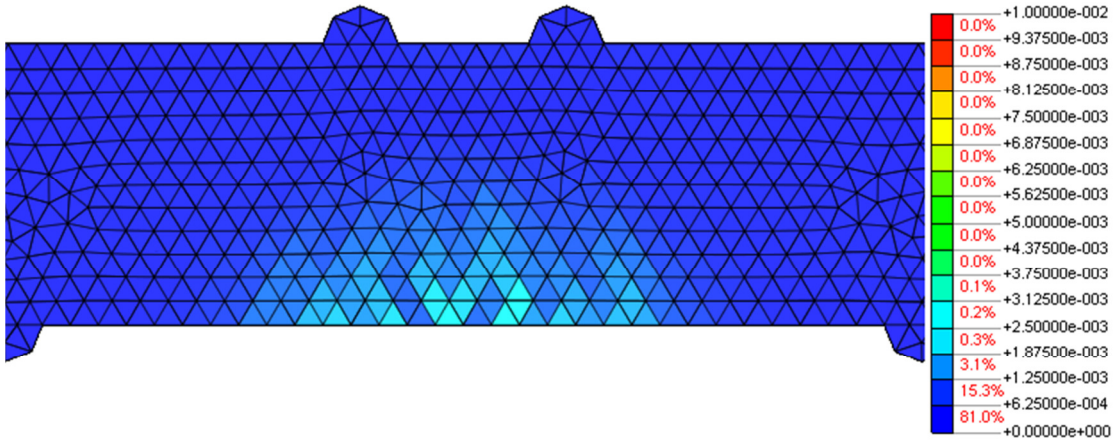


*(b)*

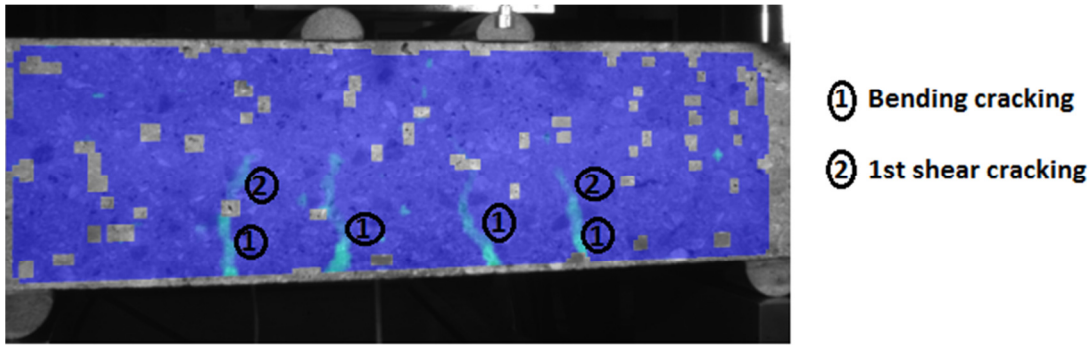


*(c)*

*Figure 6.2* *Cracking patterns: (a) 1st principal strain distribution based on Model L at load 121kN; (b) 1st principal strain distribution based on Model D at load 123kN; (c) DIC from the experiment at load 121kN.*

As shown in Figure 6.3 (c) and (d), the 1st shear cracks kept propagating towards the load plates at load level 141kN-149kN. The initiation of the 2nd shear crack on left hand side started at around 141kN along the bar and then rotated to connect with tip of the flexural crack close to the support at around 149kN.

In the two FE analyses, the 1st shear cracks had initiated and propagated towards load plates, which could match the experiment well at this stage. The crack pattern along the reinforcement in the case of Model D was more diffuse than that of Model L, which could be regarded as a sign of initiation of the 2nd shear cracks.

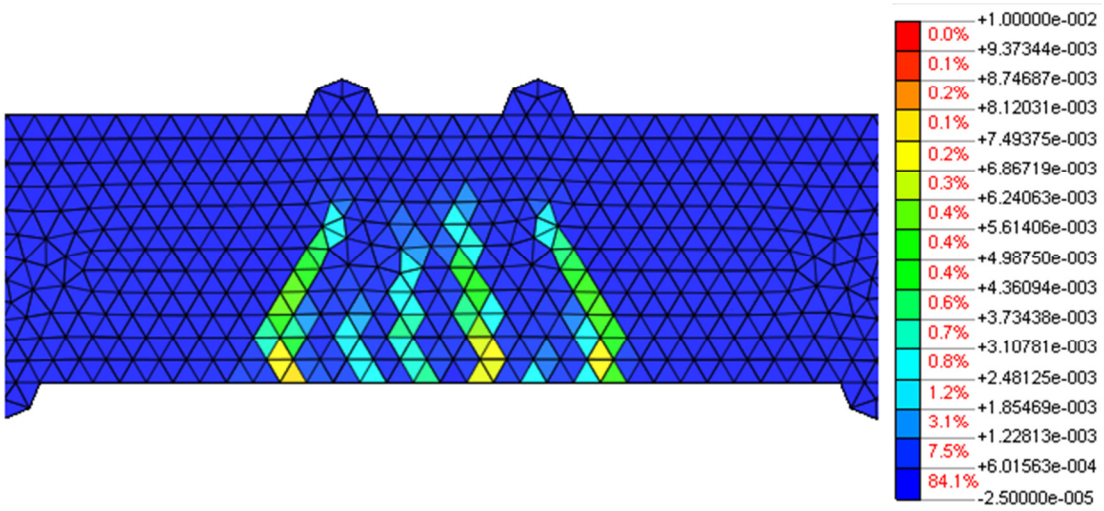


*(a)*

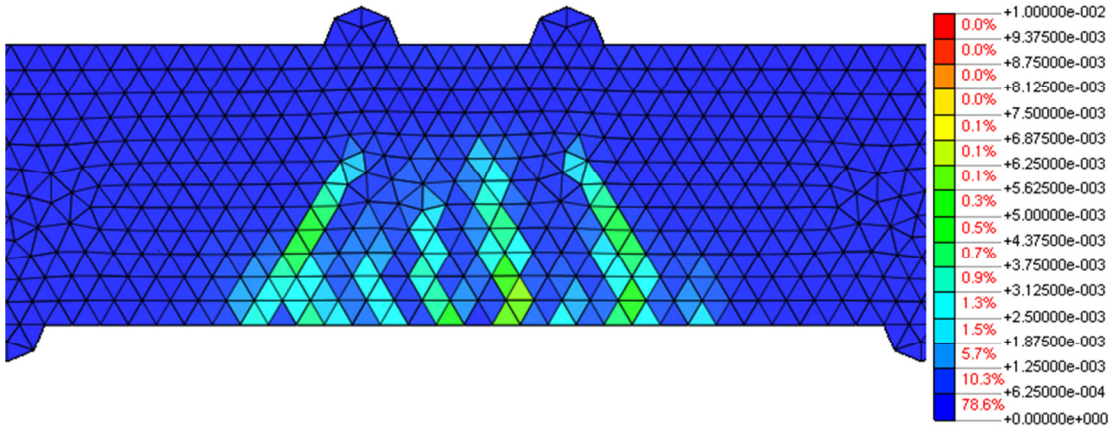


*(b)*

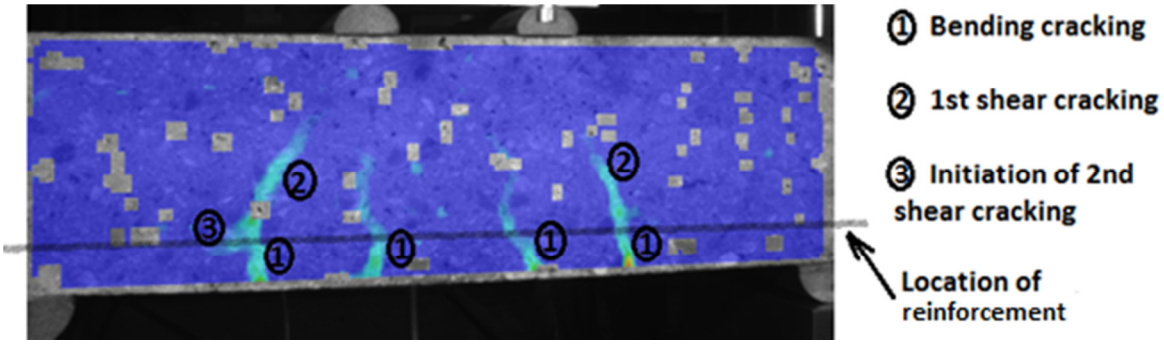


*(c)*

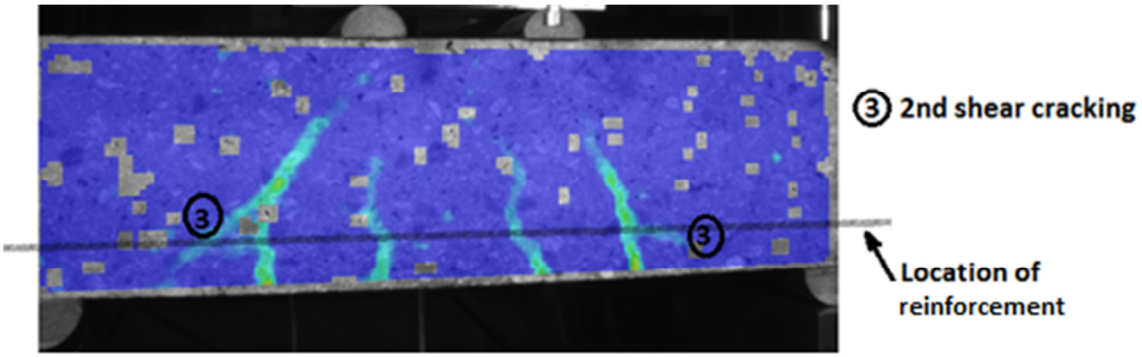


*(d)*

*Figure 6.3 Cracking patterns: (a) 1st principal strain distribution based on Model L at load 145kN; (b) 1st principal strain distribution based on Model D at load 142kN; (c) DIC from the experiment at load 141kN; (d) DIC from the experiment at load 149kN.*

As can be seen from Figure 6.4 (c), at the load level of 180kN, the 2nd shear crack on the left hand had developed towards the bottom edge. The triangular area encircled by the tip of the flexural crack, the 2nd inclined shear crack and the crack along the reinforcement exhibited many micro-crack. On the right hand, the 2nd shear crack stopped developing along the reinforcement, but propagated towards the 1st shear crack.

For the analysis including Model L, the 1st shear crack propagated further upwards to the load point, which could match the experiment well. Only the initiation of the 2nd shear crack along the bar was presented in this stage, which was later than in the experiment; see Figure 6.4 (a). The analysis using Model D could predict the shear crack pattern more correctly than that using Model L at this load level; see Figure 6.4 (b). The 2nd shear crack could be captured on the reinforcement level. It was initiated from the tip of flexural crack, developed along the reinforcement and propagated slightly upwards to the 1st shear crack. However, the crack pattern was more diffuse than in the experiment. The weak triangular area observed in the experimental crack pattern could almost be simulated in the analysis from Model D, although it was not exactly triangular in Figure 6.4 (b) due to the influence of coarse element mesh.

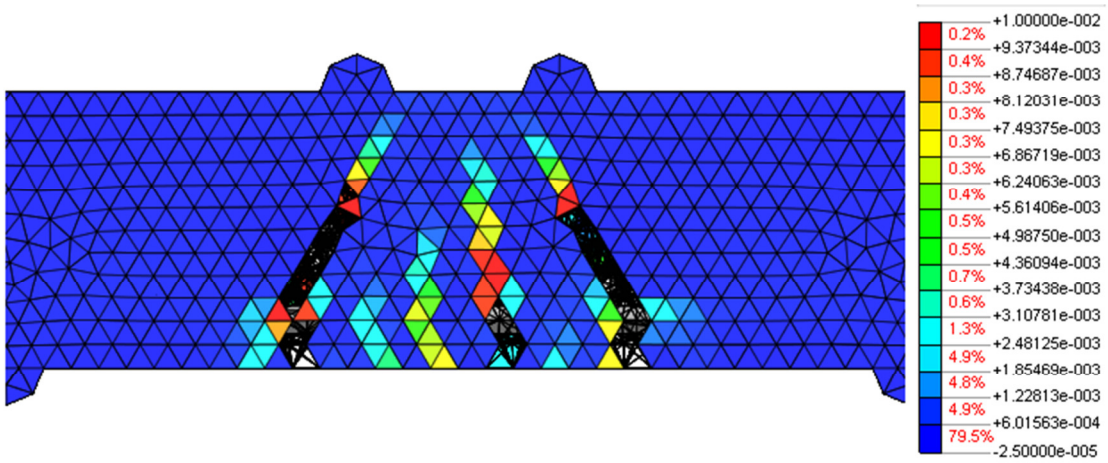


*(a)*

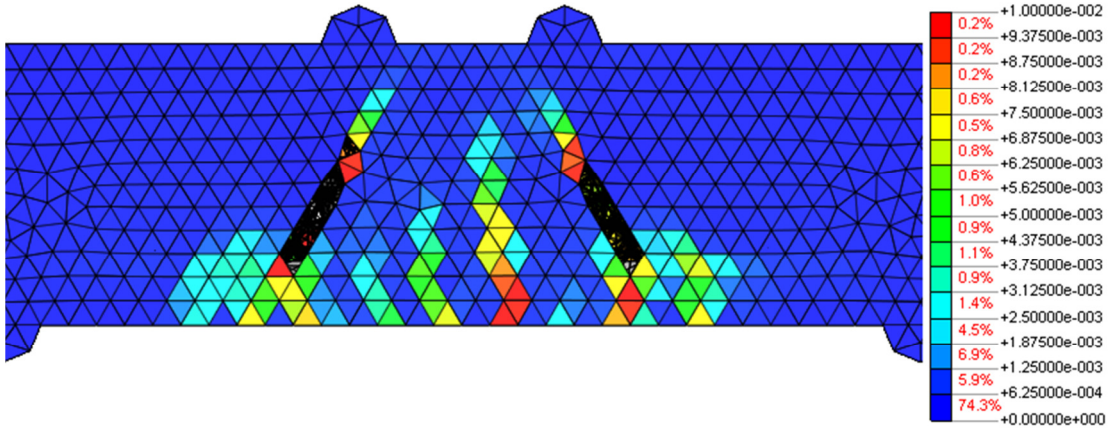


*(b)*

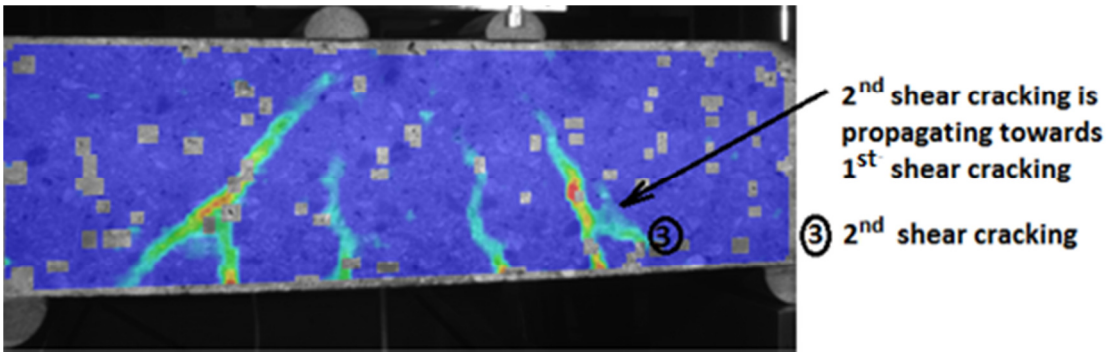


*(c)*

*Figure 6.4* *Cracking patterns: (a) 1st principal strain distribution based on Model L at load 178kN; (b) 1st principal strain distribution based on Model D at load 181kN; (c) DIC from the experiment at load 180kN.*

In Figure 6.5, the crack patterns were compared when the beam almost reached the failure. For the analyses and the experiment, one common characteristic is that, with increasing load, the 1st shear cracks developed further into the compression zone between the loading points, and the width of the 1st shear cracks became larger. In the experiment, the 1st shear cracks from both sides propagated with a smaller angle and coalesced at the compression zone. Therefore, the beam worked in arch action and

finally failed due to crushing of concrete in the compression zone. The crack pattern in the compression zone was simulated in the analysis to some extent; see Figure 6.5 (b).

At the same time, the propagation of the 2nd shear cracks in the experiment continued towards the bottom edge of the beam. Then the 1st and 2nd shear cracks were combined into one diagonal shear crack, which directly linked the loading plate and the bottom edge. Meanwhile, the 3rd shear crack formed separately from the 1st and 2nd shear cracks; see Figure 6.5 (f). Because of no constrain due to the absence of stirrups, the 3rd crack could not be propagated to be another primary shear crack.

The shear crack behavior in both FE analyses can match the experiment correctly. For the case of Model L, in addition to the propagation of the 1st shear crack towards the load plate, a splitting crack initiated from the 2nd shear crack and propagated along the reinforcement (the anchorage length) and ended to the bottom. A similar shear crack behavior presented in Model D. The main difference is that the 2nd shear crack propagated further and ended closer to the support, and was fairly diffused at bottom of the beam.

Same failure mode, shear compression or crushing failure, was observed both in the experiment and in the analyses. In Figure 6.5 (f) and (g), the formation of the crushing failure started and the compression zone was progressively crushed after failure; see Figure 6.5 (h). Accordingly, large compressive strain was viewed in the compression zone in the analyses, which means that correct failure mode was captured in the simulation. Comparing with the analysis using Model D, the failure mode from the analysis using Model L seems more reasonable, since more matching compressive strain distribution was found in the analysis from Model L, see Figure 6.5 (c) and (d).

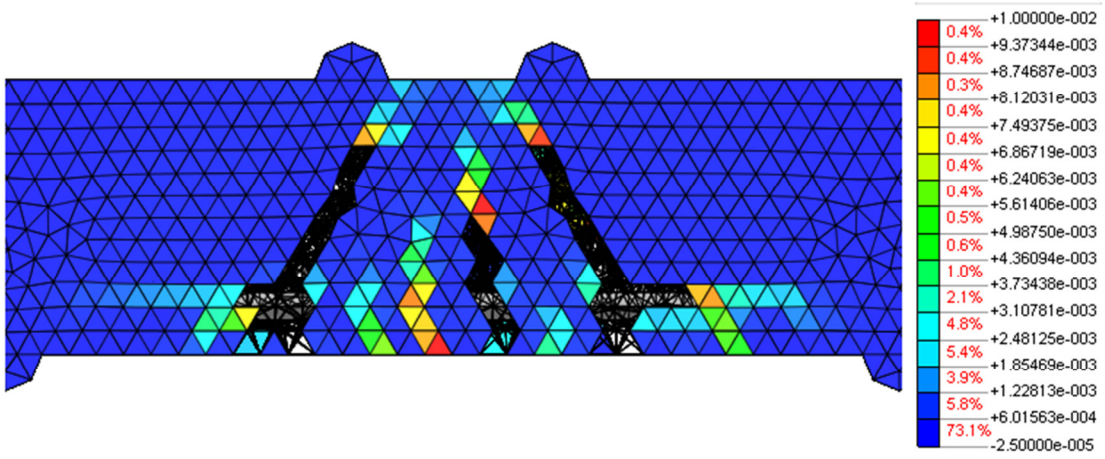


*(a)*

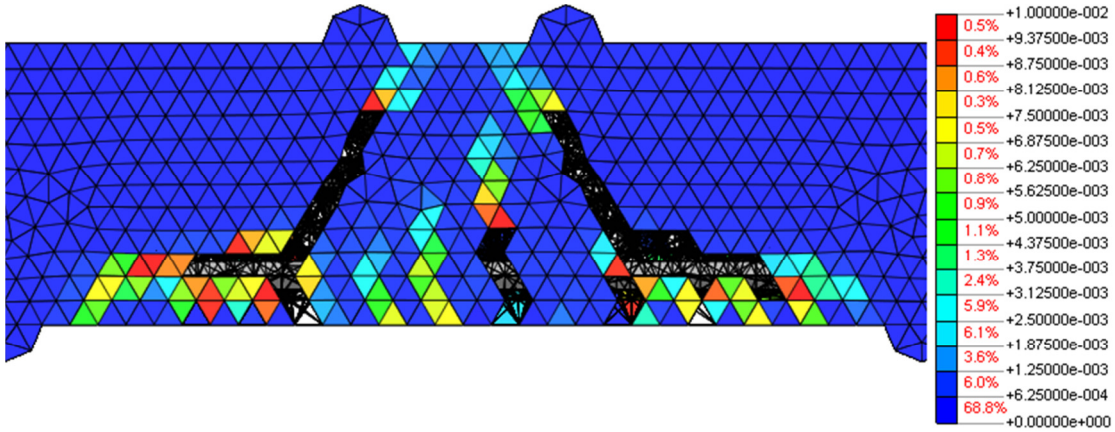
0.5% +1.00000e-002
0.4% +9.37500e-003
0.6% +8.75000e-003
0.3% +8.12500e-003
0.5% +7.50000e-003
0.7% +6.87500e-003
0.8% +6.25000e-003
0.9% +5.62500e-003
1.1% +5.00000e-003
1.3% +4.37500e-003
2.4% +3.75000e-003
5.9% +3.12500e-003
6.1% +2.50000e-003
3.6% +1.87500e-003
6.0% +1.25000e-003
68.8% +6.25000e-004
+0.00000e+000

*(b)*

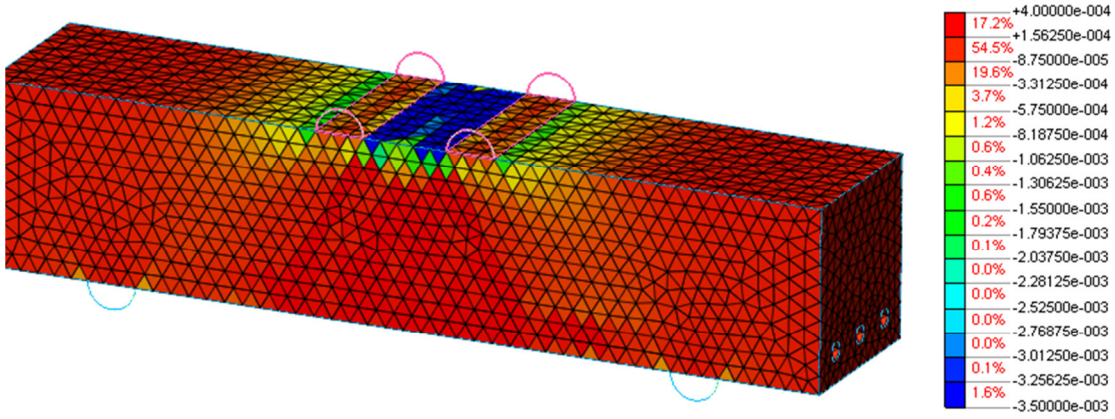
17.2% +4.00000e-004
54.5% +1.56250e-004
19.6% -8.75000e-005
3.7% -3.31250e-004
1.2% -5.75000e-004
0.6% -8.18750e-004
0.4% -1.06250e-003
0.6% -1.30625e-003
0.2% -1.55000e-003
0.1% -1.79375e-003
0.0% -2.03750e-003
0.0% -2.28125e-003
0.0% -2.52500e-003
0.0% -2.76875e-003
0.1% -3.01250e-003
1.6% -3.25625e-003
-3.50000e-003

*(c)*

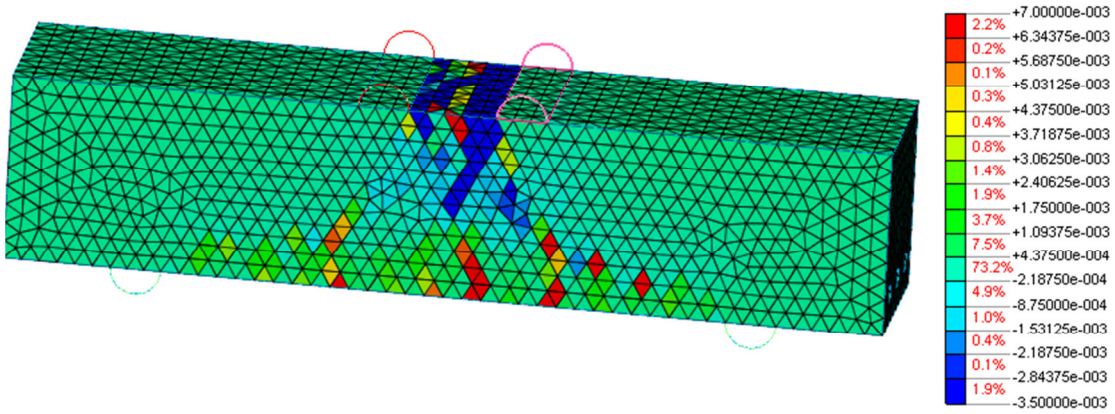
2.2% +7.00000e-003
0.2% +6.34375e-003
0.1% +5.68750e-003
0.3% +5.03125e-003
0.4% +4.37500e-003
0.8% +3.71875e-003
1.4% +3.06250e-003
1.9% +2.40625e-003
3.7% +1.75000e-003
7.5% +1.09375e-003
73.2% +4.37500e-004
4.9% -2.18750e-004
1.0% -8.75000e-004
0.4% -1.53125e-003
0.1% -2.18750e-003
1.9% -2.84375e-003
-3.50000e-003

*(d)*

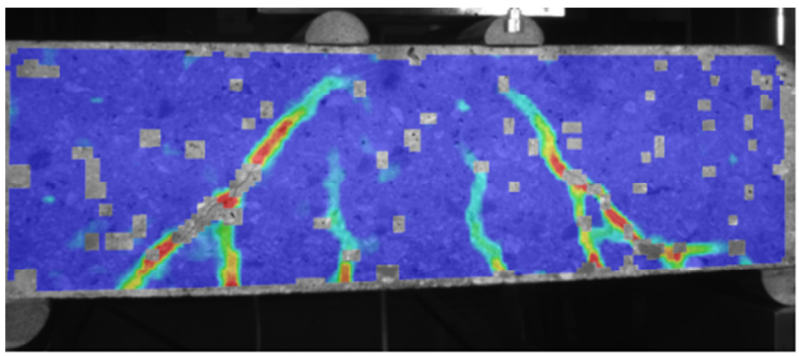

*(e)*

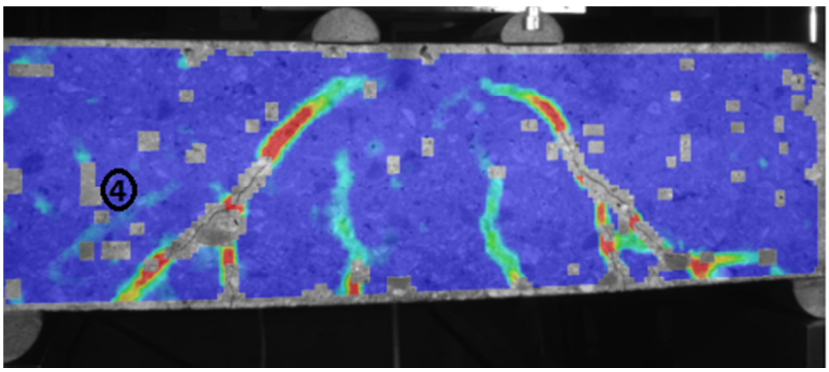


*(f)*

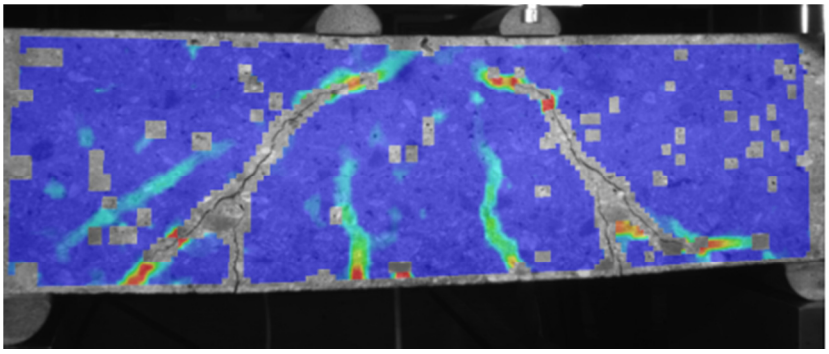

*(g)*

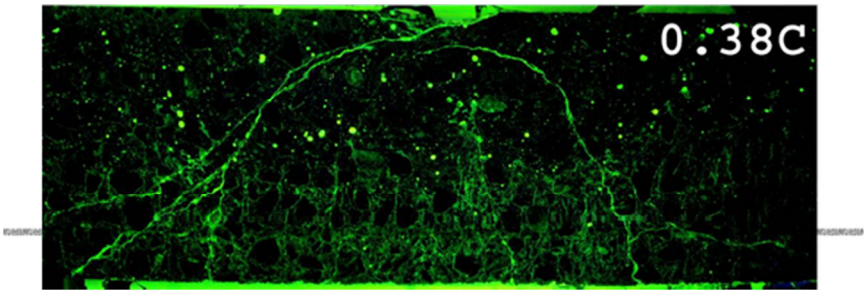


*(h)*

*Figure 6.5* *Cracking patterns: (a) 1st principal strain distribution based on Model L at load 232kN; (b) 1st principal strain distribution based on Model D at 227kN; (c) X-strain distribution based on Model L; (d) X-strain distribution based on Model D; (e) DIC from the experiment at load 233kN; (f) DIC from the experiment at load 246kN; (g) DIC from the experiment at failure (243kN); (h) DIC from the experiment at failure in meso-scale.*

### 6.1.2 Discussion of results

There is no doubt that a successful simulation for shear crack behaviour depends on different factors such as material models, element's density and control of nonlinear analysis. The bond slip model is one of the most important influencing factors. Neither the FE-models including Model L nor that including Model D could predict a correct shear crack pattern completely from the beginning to the end. Furthermore, neither case could predict the flexural cracking completely correctly. However, both

cases can predict the 1st shear crack pattern correctly with regard to localization and propagation, but the 1st shear crack initiated later than in the experiment. Both cases could predict the 2nd shear crack almost correctly. In the case of Model D, the 2nd shear crack was more correct with regard to the initiation. However, it propagated closer to the support and was fairly diffused, which did not exactly match the experiment. On the contrary, the 2nd shear crack from Model L did not propagate accurately to the support comparing to the experiment.

In order to discuss effectively how the bond slip model can influence the shear crack behavior, bond-slip curves were extracted from the two cases, see Figure 6.6. For the case including Model D, the bond-slip response is the same as the input given. For Model L, the bond-slip is not given as input, but is rather a result of the three-dimensional constitutive model for the interface between the reinforcement and surrounding concrete. For this case, the bond stress and the slips were extracted from 3 typical cross-sections, as shown in Figure 6.6(b). Cross-section 1 (CS1) is located at the free-end, cross-section 2 (CS2) is located close to the support, and cross-section 3 (CS3) is located in the middle between the support and the load plate. "Model L CS1" keeps a linear behaviour because no cracking occurred here during the entire process. "Model L CS2" and "Model L CS3" has a linear response up to load levels of 164kN and 128kN, receptively, where the initiation of concrete cracks at the corresponding cross-sections leads to increased slips. The maximum bond stresses for the two curves were reached when failure of the beam occurred. It can clearly be seen that bond stiffness of Model L is larger than Model D before initiation of concrete crack, but smaller after that.

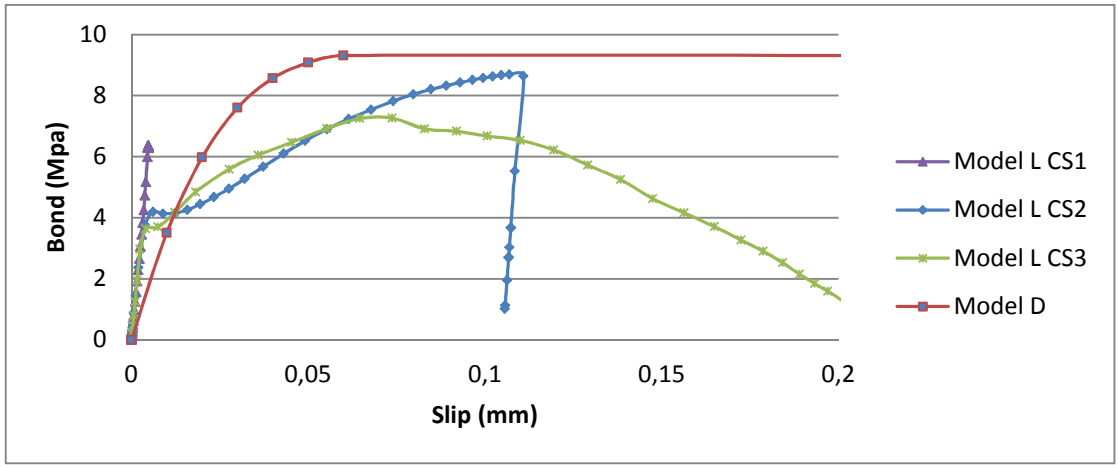


(a)

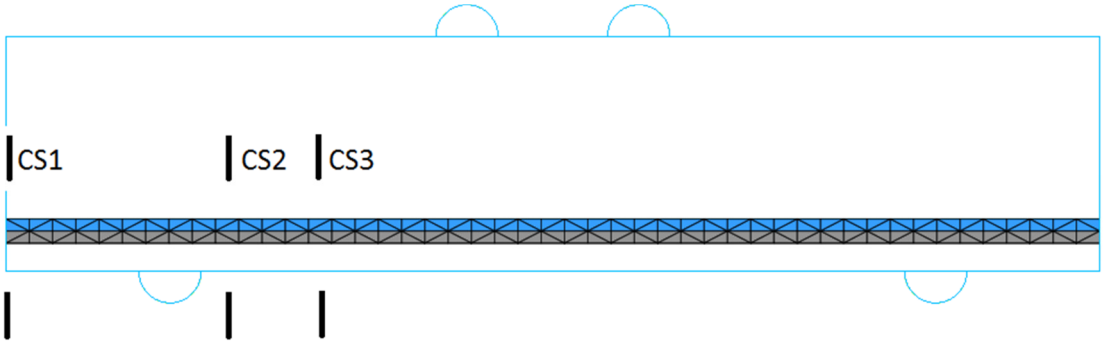


(b)

*Figure 6.6* *(a) Bond-slip curve for case including Model L and Model D; (b) Positions of the 3 cross sections.*

In the beginning of the load process, neither the FE analysis with Model L nor that with Model D could predict a correct flexural crack. The different bond stiffness between Model D and Model L, before initiation of concrete crack, did not influence the flexural crack behaviour because concrete stiffness governed the beam's stiffness at this stage. Bond action together with steel stiffness had a small influence on the beam's stiffness.

However, after the initiation of flexural cracks and the 1st shear crack, the FE analysis with Model D predicted an earlier initiation of the 2nd shear crack than that with Model L, but this crack ended closer to the support and was fairly diffused. The possible reason might be the higher bond stiffness for Model D at this stage. After the 1st shear crack appeared, a relatively larger bond action was needed to transfer load to the un-cracked concrete close to the support, so that the 2nd shear crack could be triggered. After shear cracking, the shear force was transferred through a compression strut, more or less parallel to the shear crack, from the loading point to the support area. The compression force in the inclined strut was balanced by a tensile force on the reinforcement level. In addition, aggregate interlock in the shear crack, shear transfer in the uncracked top compression zone and the dowel effect of the reinforcement bars contributes to the transfer of shear force. Concrete tension stiffening contributed to the stiffness of the beam. Larger bond stiffness will lead to higher concrete stresses closer to the crack, so that the 2nd shear crack developed along the bar and towards the support. Generally, it might be concluded that, for the FE analysis of this shear test, a more appropriate value of bond stiffness between Model L and Model D is preferred in order to capture more correct shear crack behaviour.

However, the cracking development along the reinforcement could not be infinitely towards support, because the largest first principal strain leading to the 1st shear crack in the web zone was rotating with the formation of the 1st shear crack and with increased load. This rotating of the 1st principal strain caused another inclined shear crack which was finally connected to horizontal crack along the bars. Subsequently, a weak triangular area exhibiting several micro-cracks formed as mentioned in Section 6.1.1. The two FE analyses could predict the weak area, thanks to the rotating crack model based on total strain. A fixed crack model based on total strain and multi directional fixed crack approach was not able to predict the rotating crack well, which was verified in our previous analyses but was not described in this report. In further load steps, more cracks showed up along the reinforcement and towards the support due to the same effects as described above.

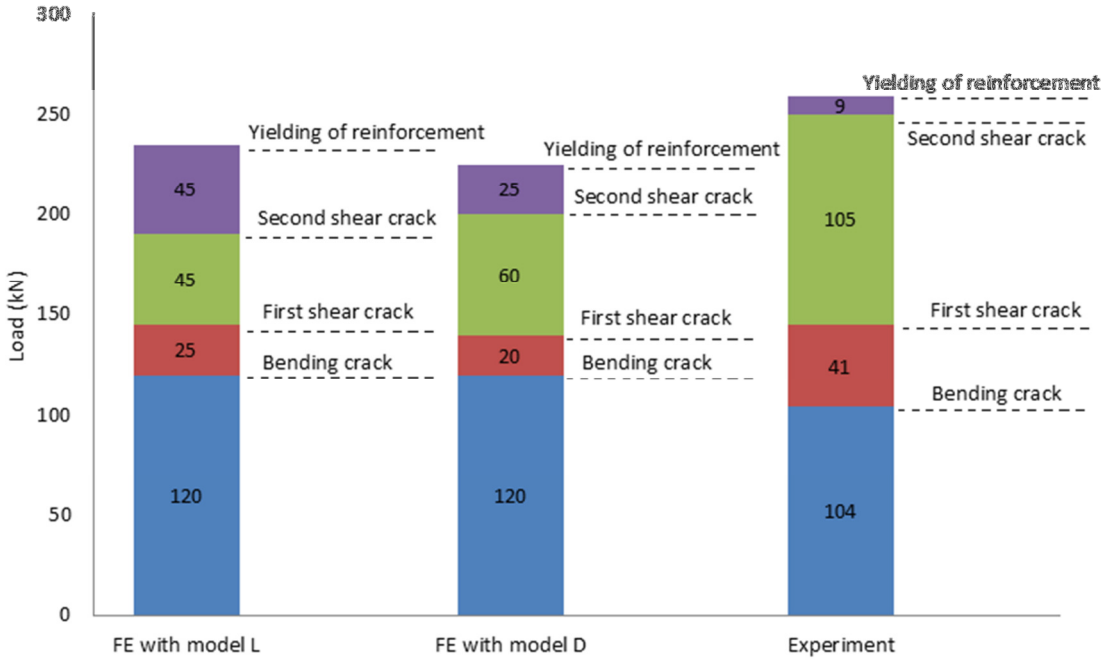


*Figure 6.7* *Load levels for different characteristic events in the FE analyses and the experiment.*

In conclusion, the bond-slip model and the concrete fracture model are two of the most important factors which influence the shear crack pattern. Although no completely correct shear pattern was captured in previous analyses, some valuable findings still could be obtained to shed light on the following research in the future.

## 6.2 FE analyses with embedded reinforcement and lateral influence on the concrete response

As mentioned in Section 5.2.3, the model with embedded reinforcement did not obtain the correct yielding load, possibly because some unclear rules in the 3D simulation work performed in DIANA influenced the yielding capacity. Considering the uncertainties of the analysis using embedded reinforcement, no detailed comparison and discussion of the results were made step by step in this case. Only the shear pattern from the moment of the final failure in the analysis was compared with the experiment.

It can be seen from Figures 6.8 that in overall, realistic cracking was simulated well in the FE analysis except for the development of the 2nd shear cracks. The 2nd shear crack in the FE analysis was formed separated from the first shear crack, while in the experiment the 2nd shear crack was connected to the 1st shear crack on the tip of the initial flexural crack and propagated from this point towards the support.

It can also be observed that the cracking pattern in the FE analysis was more diffused than that in the test, especially around the reinforcement. This was probably caused by the perfect bond assumption which gives rise to irregularities and distortions in the neighborhood of the reinforcement (Rots J.G. 1989).

Although the analysis result using embedded bar is not trustworthy due to its lower yielding load, the effect of bond between the reinforcing bar and the concrete can be obtained to some extent by analyzing the shear crack pattern. Comparing the shear crack pattern obtained from the FE-model using Model L, Model D and full bond, it could be concluded that, higher bond capacity leads to a more distinct shear crack pattern.

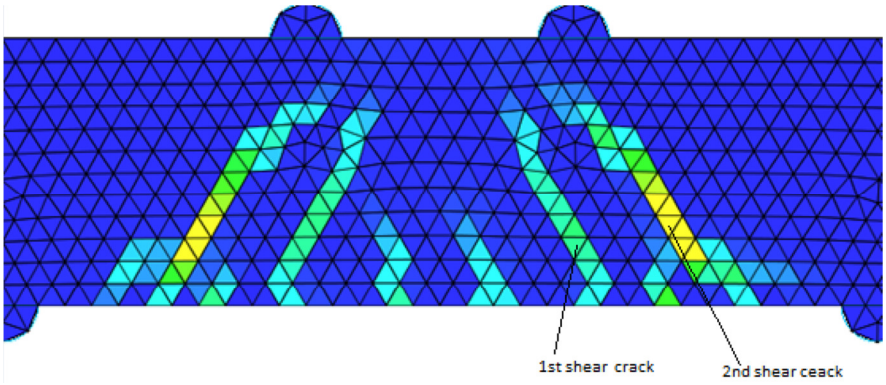


*(a)*

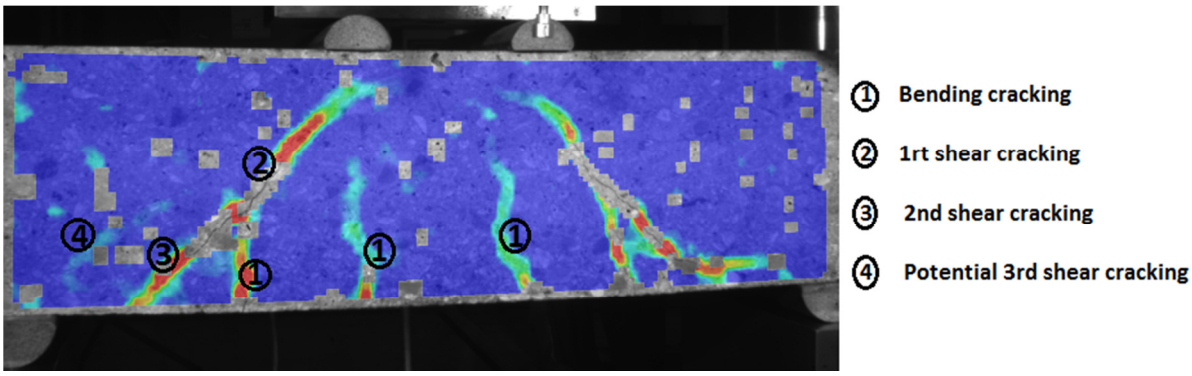


*(b)*

*Figure 6.8* *(a) 1st principal strain distribution at load 253kN; (b) Cracking patterns from DIC from the experiment at load 250kN.*

# 7 Conclusions

## 7.1 General conclusion

In this project, 3D nonlinear finite element analysis was used to study the shear response, especially the shear cracking behavior, of concrete elements. Two approaches were adopted to model the reinforcement: embedded reinforcement and solid elements for the reinforcement bars including steel/concrete interaction.

For the analysis with embedded reinforcement, after incorporating several improvements to the model, the cracking patterns, failure mode and load-displacement relationship agreed relatively well with what was observed in the experiment. These improvements included adjustments of horizontal constraint at the supports, controlling the elements' positions around the embedded reinforcement and including the lateral influence on the concrete compressive behavior. The results showed that the horizontal constraint had a minor influence on the overall behavior. Controlling the elements' positions had a significant effect for the case with embedded reinforcement. Moreover, including the lateral influence on concrete compressive behavior affected the load-displacement relationship, leading to a more correct failure load.

Based on the modifications in the model with embedded reinforcement, the FE analyses including the bond-slip model were improved with the inclusion of the lateral influence on the concrete compressive behavior. Moreover, in order to study the bond-slip relationship's influence on shear crack behavior, two types of bond models were adopted, the model developed by Lundgren (2005) (Model L) and the model by Dörr (1980) (Model D). For the studied case, at lower load levels, i.e. before initiation of concrete cracks, the bond stiffness weakly influences the mechanical behavior of the beam. After the beam has cracked, relatively higher bond stiffness can attract stiffness to the concrete adjacent to previous cracks, so that shear cracks initiate earlier and propagate further to the supports.

The study of the shear crack behavior in this project contributes to the development of a general analysis method for simulation of shear response of RC beams, so that the crack pattern, the failure load and the overall response can be predicted and determined with a high degree of accuracy.

## 7.2 Suggestions for future research

Further studies on the use of smaller element sizes would be of interest, in order to capture more correct shear crack pattern. In this project, only an element size of 15 mm was used.

The friction between the supports and the steel blocks needed to be simulated by more appropriate model. Alternative choice is to improve the set-up of experiment, for example using smooth rollers as supports to eliminate the friction.

To study the aggregate interlock effect between the shear crack surfaces by introducing a shear retention factor, TS-fixed model would be of interest as well. This would be perfectly possible as the experimental program includes test results with two types of aggregates (natural and crushed) and water/cement ratio.

# 8 References


Broo H. (2008): *Shear and Torsion in Concrete Structures*, Doctoral thesis, Chalmers University of Technology, Gothenburg, Sweden.

Broo H., Lundgren K. and Plos M. (2008): *A guild to non-linear finite element modelling of shear and torsion in concrete bridges,* Report 2008:18, Chalmers University of Technology, Gothenburg, Sweden.

Chen W. F. and Han D. J. (1988): *Plasticity for Structural Engineers.* Spring-Verlag, New York, 606 pp.

Dörr K. (1980): *Ein Beitrag zur Berechnung von Stahlbetonscheiben unter besonderer Berücksichtigung des Verbundverhaltens*. PhD thesis, University of Darmstadt.

Dileep Kumar P. G. : *Shear strength of R.C.C Beams without web reinforcement,* Lecture notes, Dept. of Civil Engg. Govt. Engg. College, Palakkad.

Flansbjer M., Lindqvist J. E. and Silfwerbrand J. (2011): *Quantitative fracture characteristics in shear load*, Fib Symposium, Prague, 12 pp.

Gebreyouhannes E. and Maekawa K. (2011): *Numerical Simulation on Shear Capacity and Post-Peak Ductility of Reinforced High-strength Concrete Coupled with Autogenous Shrinkage*, Journal of Advanced Concrete Technology Vol. 9, No, 1, pp. 73-88, Feb. 2011.

Hordijk D. A. (1991): *Local Approach to Fatigue of Concrete*, Doctoral thesis, Delft University of Technology, Delft, Netherlands.

Jan S. (2010): *Fracture propagation in cementitious materials*, Doctoral thesis, Technical University of Denmark, Denmark.

Jirásek M. (2004): *Modelling of localized inelastic deformation –Lecture notes*, Czech Technical University, Prague, 2004.

Lundgren K. (2005): *Bond between ribbed bars and concrete. Part 1: Modified model*, Magazine of Concrete Research, Vol. 57, No. 7, pp. 371–382.

Magnusson J. (2000): *Bond and Anchorage of Ribbed Bars in High-strength Concrete*, Doctoral thesis, Chalmers University of Technology, Gothenburg, Sweden.

Nooru-Mohamed MB (1992): *Mixed-mode fracture of concrete: an experimental approach*. Phd thesis, Delft University of Technology, Delft, The Netherlands.

Plos M. (2000): *Finite element analyses of reinforced concrete structures*, Compendium 96:14, Chalmers University of Technology, Gothenburg, Sweden.

Rots J.G. (1991): *Smeared and discrete representations of localised fracture,* International Journal of Fracture, Vol 51, pp. 45-59.

Rots J.G. (1989): *Bond of reinforcement*, Fracture Mechanics of Concrete Structures, Chapman and Hall, ISBN 0412306808, pp. 245-261.

Selby R.G. and Vecchio F. J. (1997): *A constitutive model for analysis of reinforced concrete solids*, Can. J. Civ. Eng. 24: 460-470 (1997).

Selby R.G. (1993): *Three-Dimensional Constitutive Relations for Reinforced Concrete,* Doctoral thesis, University of Toronto.

Tepfers R. (1973): A Theory of Bond Applied to Overlapped Tensile Reinforcement Splices for Deformed Bars, Division of Concrete Structures, Chalmers University of Technology, Publication 73:2, Gothenburg, Sweden, 328 pp.

Thorenfeldt E., Tomaszewicz A. & Jensen J. J. (1987): *Mechanical properties of high-strength concrete and applications in design*, Conference on Utilization of High-Strength Concrete, Stavanger, Norway.

TNO (2010): *DIANA Finite Element Analysis, User's Manual, release 9.3. TNO BV*, Delft, the Netherlands, 2010.

Zararis P. D. (2003): *Shear Compression Failure in Reinforced Concrete Deep Beams,* Journal of Structural Engineering, pp. 544-553, Apr. 2003.

Zandi Hanjari, K., Kettil, P. and Lundgren, K. (2011). *Modeling the structural behavior of frost-damaged reinforced concrete structures,* Structure and Infrastructure Engineering, First published on: 07 March 2011, URL: DOI:10.1080/15732479.2011.552916.

# Appendix A: Hand calculation for verification

**Cracking force**

The force at which the first crack is formed and starts to localize

$$f_{ct} = \frac{M \cdot y}{I} \Rightarrow M = \frac{f_{ct} \cdot I}{y}, \Rightarrow N_{cr} = 32.4kN$$

Where $N_{cr}$ is the cracking force in kN

$f_{ct}$ is the concrete tensile strength in MPa

$y$ is the height of the of concrete beam in m

$I$ is the moment of inertia of concrete beam cross-section in $m^4$

$$f_{ct} = 4.9MPa$$

$$y = 0.15m$$

$$I = 4.22 \times 10^{-5} m^4$$

**Yielding force**

The force at which reinforcement starts to yield

$$M_E = A_s \cdot f_y \cdot d \cdot 0.9 = 18.92kN \cdot m$$

$$N_y = \frac{M_E}{a} \times 2 = 219.03kN$$

Where $N_y$ is the yielding force in kN

$a$ is the distance from the support to the shear loading in m

$d$ is the distance from the reinforcement to the upper surface of the concrete beam in m

$f_y$ is the yielding strength of reinforcement steel in MPa

$A_s$ is the cross sectional area of reinforcement in $m^2$

$$a = 0.19m$$

$$d = 0.124m$$

$$f_y = 550MPa$$

$$A_s = 3.39 \times 10^{-4} m^2$$

# Appendix B: Tested material properties of steel bars

**Dragprovning**

| Provets märkning | Nominell diameter | Nominell tvärsnitts-area | Övre sträckgräns | Brott-gräns | Förhållande | Gränstöjning |
|---|---|---|---|---|---|---|
| | d mm | $S_0$ mm² | $R_{eH}$ N/mm² | $R_m$ N/mm² | $R_m/R_{eH}$ | $A_{gt}$ % |
| Prov 1 | 12 | 113 | 551 | 634 | 1,15 | 11,4 |
| Prov 2 | 12 | 113 | 548 | 632 | 1,15 | 12,1 |
| Prov 3 | 12 | 113 | 552 | 634 | 1,15 | 12,5 |

*Mätosäkerhet - övre sträckgräns:* < 2,1 %
*Mätosäkerhet - brottgräns:* < 2,1 %
*Mätosäkerhet - förhållande:* < 2 %
*Mätosäkerhet - gränstöjning:* < 7 % av angivet värde

| TestNo | Diameter (mm) | Area (mm2) | Reh (MPa) | Rp0.2 (MPa) | Fm (kN) | Rm (MPa) | E-auto (GPa) | Fp0.2 (kN) | Agt (%) | Ag (%) |
|---|---|---|---|---|---|---|---|---|---|---|
| 1 | 12.00 | 113.10 | 551.31 | 540.22 | 71.71 | 634.03 | 197.66 | 61.10 | 10.74 | 10.42 |
| 2 | 12.00 | 113.10 | 548.08 | 539.11 | 71.43 | 631.61 | 197.95 | 60.97 | 10.87 | 10.55 |
| 3 | 12.00 | 113.10 | 552.30 | 539.40 | 71.71 | 634.03 | 197.72 | 61.00 | 10.75 | 10.43 |
| Medelvärde | 12.000 | 113.100 | 550.563 | 539.577 | 71.617 | 633.223 | 197.777 | 61.023 | 10.786 | 10.467 |
| S.D. | 0.000 | 0.000 | 2.207 | 0.576 | 0.162 | 1.397 | 0.153 | 0.068 | 0.069 | 0.072 |

Kommentar Testno 1 : Prov 1:ReH, brott på fri del
Kommentar Testno 2 : Prov 2:ReH, brott på fri del
Kommentar Testno 3 : Prov 3:ReH, brott på fri del

Primärprotokoll: Kamstänger, ~~Nordcert~~

Utfärdad: 2011-11-16, utgåva 4

## Dragprovning - Kamstänger

Uppdragsgivare:

Uppdragsnummer: PX20105

Provningstemperatur: 21°C

Provningsmetod: SS-EN ISO 15630-1

| | | | |
|---|---|---|---|
| Provningsmaskin: | Sintech | Dragprovning, datum/sign : | 19/4-12 J.H |
| Extensometer: | | Mått och vikt, datum/sign: | — |
| Skjutmått: | 403279 | Talmeter: | — |
| Våg: | — | ~~Kamprofilsutrustning~~ inv nr 901008: | ☐ |

| Provets märkning | Diameter D mm | Längd L mm | Vikt m g | Tvärsnitts-area $S_0$ $mm_2$ | Övre flytkraft $F_{eH}$ kN | Maximal provkraft $F_m$ kN | För-hållande $F_m/F_{eH}$ | [illegible] | Brott-gräns $R_m$ N/mm² | För-hållande $R_m/R_{eH}$ | Gränstöjning Agt $X_0$ mm | Gränstöjning Agt X mm | Kam-märkning |
|---|---|---|---|---|---|---|---|---|---|---|---|---|---|
| Prov 1 | 12 | | | | | | | | | | 100 | 111,1 | 6+5 |
| prov 2 | 12 | | | | | | | | | | 100 | 111,8 | |
| prov 3 | 12 | | | | | | | | | | 100 | 112,0 | |
| | | | | | | | | | | | | | |
| | | | | | | | | | | | | | |
| | | | | | | | | | | | | | |
| | | | | | | | | | | | | | |
| | | | | | | | | | | | | | |
| | | | | | | | | | | | | | |
| | | | | | | | | | | | | | |
| | | | | | | | | | | | | | |
| | | | | | | | | | | | | | |
| | | | | | | | | | | | | | |
| | | | | | | | | | | | | | |
| | | | | | | | | | | | | | |
| | | | | | | | | | | | | | |
| | | | | | | | | | | | | | |

Kammärkning 6+5 = Celsa Mo i Rana, Norge

# Appendix C: Input data file (*. dat file)

## 1. Input data for one forth beam model with embedded reinforcement

```
Translated from FX+ for DIANA neutral file (version 1.2.0).

'UNITS'
FORCE N
LENGTH M
MASS  1.00000E+000

'DIRECTIONS'
   1  1.00000E+000  0.00000E+000  0.00000E+000
   2  0.00000E+000  1.00000E+000  0.00000E+000
   3  0.00000E+000  0.00000E+000  1.00000E+000

'COORDINATES'
   1  3.50000E-002 -7.50000E-002  7.50000E-002
   2  4.83333E-002 -7.50000E-002  7.50000E-002
   3  6.16667E-002 -7.50000E-002  7.50000E-002
                                .
                                .

'ELEMENTS'
CONNECT
 122 TE12L  114 105 100 104
 123 TE12L  97 100 112 96
 124 TE12L  8 117 99 103
                                .
                                .
```

### Material properties' input

```
'MATERI'
   1 NAME   CONCRETE
     YOUNG   3.94900E+010
     POISON  2.00000E-001
     TOTCRK ROTATE
     TENCRV HORDYK
     TENSTR  4.90000E+006
     GF1     2.08700E+002
     CRACKB  1.50000E-002
     COMCRV THOREN
     COMSTR  7.18300E+007

   2 NAME   REBAR
     YOUNG   2.22000E+011
     POISON  3.00000E-001
     YIELD  VMISES
     HARDEN STRAIN
     HARDIA  5.50000E+008  0.00000E+000  6.30000E+008
1.25000E-001
```

```
   3 NAME   PLATE
     YOUNG   2.10000E+011
     POISON  3.00000E-001
     YIELD  VMISES
     HARDEN STRAIN
     HARDIA  4.90000E+008  0.00000E+000  6.30000E+008
1.14000E-001
```

**Geometry and Data properties' input**

```
'GEOMET'
   1 NAME   CONCRETE
   2 NAME   PLATE
   3 NAME   BAR1
     CROSSE  1.13000E-004
   4 NAME   BAR2
     CROSSE  5.65000E-005

'DATA'
   1 NAME   CONCRETE
   2 NAME   REBAR
   3 NAME   PLATE
   6 NAME   BAR1
   7 NAME   BAR2
```

**Assignment of material, data and geometry**

```
MATERI
/ 285-7260 / 1
/ 122-284 / 3
DATA
/ 285-7260 / 1
/ 122-284 / 3
GEOMET
/ 122-284 / 1
/ 285-7260 / 2
```

**Definition of embedded reinforcement**

```
'REINFORCEMENTS'
LOCATI
   1 BAR
     LINE   1676 1675

   2 BAR
     LINE   1678 1677
```

**Assignment of embedded reinforcement**

```
MATERI
/ 1 2 / 2
GEOMET
/ 1 / 3
/ 2 / 4
DATA
```

```
/ 1 / 6
/ 2 / 7
```

### Definition of loads

```
'LOADS'
DEFORM
6    TR 3 -1.00000E-003
DEFORM
14   TR 3 -1.00000E-003
DEFORM
108  TR 3 -1.00000E-003
DEFORM
111  TR 3 -1.00000E-003
DEFORM
114  TR 3 -1.00000E-003
DEFORM
117  TR 3 -1.00000E-003
```

### Element groups

```
'GROUPS'
ELEMEN
  49 "Load-plate" / 122-202 /
  50 "Support-plate" / 203-284 /
  51 "Concrete" / 285-7260 /
```

### Boundary conditions and constrains

```
'SUPPOR'
/ 156-161 181-190 449-498 / TR 1
/ 156-161 181-190 449-498 / RO 2
/ 9-16 25 45-54 119-122 155 156 167-448 139-142 / TR 2
/ 9-16 25 45-54 119-122 155 156 167-448 139-142 / RO 1
/ 6 14 108-117(3) 17 139 144-153(3) / TR 3

'END'
```

## 2. Input data for entire beam model with embedded reinforcement

```
Translated from FX+ for DIANA neutral file (version 1.2.0).

'UNITS'
FORCE N
LENGTH M
MASS  1.00000E+000

'DIRECTIONS'
   1  1.00000E+000  0.00000E+000  0.00000E+000
   2  0.00000E+000  1.00000E+000  0.00000E+000
   3  0.00000E+000  0.00000E+000  1.00000E+000

'COORDINATES'
   1  7.00000E-001  8.32667E-017  0.00000E+000
```

```
   2  7.00000E-001  1.50000E-002  0.00000E+000
   3  7.00000E-001  3.00000E-002  0.00000E+000
                                .
                                .

'ELEMENTS'
CONNECT
   1 TE12L  3769 2981 3555 3755
   2 TE12L  375 1593 456 376
   3 TE12L  3769 3691 2536 2736

                                .
                                .
```

**Material properties' input**

```
'MATERI'
   1 NAME   CONCRETE
     YOUNG   3.94900E+010
     POISON  2.00000E-001
     TOTCRK ROTATE
     TENCRV HORDYK
     TENSTR  4.90000E+006
     GF1     1.04700E+003
     CRACKB  1.50000E-002
     COMCRV THOREN
     COMSTR  7.18300E+007

   2 NAME   REBAR
     YOUNG   2.22000E+011
     POISON  3.00000E-001
     YIELD  VMISES
     HARDEN STRAIN
     HARDIA  5.50000E+008  0.00000E+000  6.30000E+008
1.25000E-001

   3 NAME   PLATE
     YOUNG   2.10000E+011
     POISON  3.00000E-001
     YIELD  VMISES
     HARDEN STRAIN
     HARDIA  4.90000E+008  0.00000E+000  6.30000E+008
1.14000E-001
```

**Geometry and Data properties' input**

```
'GEOMET'
   1 NAME   CONCRETE
   2 NAME   PLATE
   3 NAME   BAR
     CROSSE  1.13000E-004

'DATA'
   1 NAME   CONCRETE
   2 NAME   PLATE
```

```
   3 NAME   REBAR
```

**Assignment of material, data and geometry**

```
MATERI
/ 1-22721 / 1
/ 22722-23341 / 3
DATA
/ 1-22721 / 1
/ 22722-23341 / 2
GEOMET
/ 1-22721 / 1
/ 22722-23341 / 2
```

**Definition of embedded reinforcement**

```
'REINFORCEMENTS'
LOCATI
   1 BAR
     LINE   5129 5130

   2 BAR
     LINE   5132 5131

   3 BAR
     LINE   5134 5133
```

**Assignment of embedded reinforcement**

```
MATERI
/ 1-3 / 2
GEOMET
/ 1-3 / 3
DATA
/ 1-3 / 3
```

**Definition of loads**

```
'LOADS'
DEFORM
4990 TR 3 -1.00000E-003
DEFORM
4993 TR 3 -1.00000E-003
DEFORM
4994 TR 3 -1.00000E-003
DEFORM
4995 TR 3 -1.00000E-003
DEFORM
4996 TR 3 -1.00000E-003
DEFORM
4997 TR 3 -1.00000E-003
DEFORM
4998 TR 3 -1.00000E-003
DEFORM
4999 TR 3 -1.00000E-003
```

```
DEFORM
5000 TR 3 -1.00000E-003
DEFORM
5001 TR 3 -1.00000E-003
DEFORM
5002 TR 3 -1.00000E-003
DEFORM
5024 TR 3 -1.00000E-003
DEFORM
5025 TR 3 -1.00000E-003
DEFORM
5026 TR 3 -1.00000E-003
DEFORM
5027 TR 3 -1.00000E-003
DEFORM
5028 TR 3 -1.00000E-003
DEFORM
5029 TR 3 -1.00000E-003
DEFORM
5030 TR 3 -1.00000E-003
DEFORM
5031 TR 3 -1.00000E-003
DEFORM
5032 TR 3 -1.00000E-003
DEFORM
5033 TR 3 -1.00000E-003
DEFORM
5034 TR 3 -1.00000E-003
```

**Element groups**

```
'GROUPS'
ELEMEN
   2 "Concrete" / 1-22721 /
   3 "Load Plate1" / 22722-22875 /
   4 "Load Plate2" / 22876-23031 /
   5 "Sup Plate1" / 23032-23185 /
   6 "Sup Plate2" / 23186-23341 /
```

**Boundary conditions and constrains**

```
'SUPPOR'
/ 4990 4993-5002 5024-5034 5060 5063 5065-5073 5094 5097-5106
/ TR 3
/ 5060 5063 5065-5073 / TR 1

'END'
```

## 3. Input data for entire beam model with bond-slip model

```
Translated from FX+ for DIANA neutral file (version 1.2.0).

'UNITS'
FORCE N
LENGTH M
```

```
MASS  1.00000E+000

'DIRECTIONS'
   1  1.00000E+000  0.00000E+000  0.00000E+000
   2  0.00000E+000  1.00000E+000  0.00000E+000
   3  0.00000E+000  0.00000E+000  1.00000E+000

'COORDINATES'
   1  3.50000E-001  4.50000E-002  3.35200E-002
   2  3.35106E-001  4.50000E-002  3.35200E-002
   3  3.20213E-001  4.50000E-002  3.35200E-002
                                .
                                .

'ELEMENTS'
CONNECT
   27453 T18IF 9 78 10 5890 5954 5889
   27454 T18IF 78 9 8 5954 5890 5888
   27458 T18IF 2 1 52 5887 5886 5937
                                .
                                .
   1 TE12L  3360 2500 2501 2483
   2 TE12L  4558 3639 3640 3644
   3 TE12L  5705 645 642 644
                                .
                                .
```

**Material properties' input**

```
'MATERI'
```

```
   1 NAME   CONCRETE
```
**(Use the elastic-ideal plastic relationship for concrete in compression)**

```
     YOUNG   3.94900E+010
     POISON  2.00000E-001
     TOTCRK ROTATE
     TENCRV HORDYK
     TENSTR  4.90000E+006
     GF1     2.08700E+002
     CRACKB  1.50000E-002
     COMSTR  7.18300E+007
     COMCRV CONSTA
```

```
   1 NAME   CONCRETE
```
**(Consider the lateral confinement effect)**

```
     YOUNG   3.94900E+010
     POISON  2.00000E-001
     TOTCRK ROTATE
     TENCRV HORDYK
     TENSTR  4.90000E+006
     GF1     2.08700E+002
     CRACKB  1.50000E-002
     COMSTR  7.18300E+007
     COMCRV THOREN
     CNFCRV VECCHI
```

```
   2 NAME   REBAR
     YOUNG   2.22000E+011
     POISON  3.00000E-001
     YIELD  VMISES
     HARDEN STRAIN
     HARDIA  5.50000E+008  0.00000E+000  6.30000E+008
1.25000E-001

   3 NAME   PLATE
     YOUNG   2.10000E+011
     POISON  3.00000E-001
     YIELD  VMISES
     HARDEN STRAIN
     HARDIA  4.90000E+008  0.00000E+000  6.30000E+008
1.14000E-001
```

```
   4 NAME   INTERFACE
     DSTIF       1.1E+13   1.2E+12
:Rost+bond , rostangrepp 0 mikrometer on fi 12 mm for 1.37MPA
and 17.77 MPA
      USRIFC   BOTH
      USRVAL  0   0.4    0.05    4.00E-03
                     0   7.183E+07    1.00  4.79E+6
              1.35E-04   7.183E+07    0.86  479
              2.80E-04   7.161E+07    0.78  0
              4.11E-04   7.126E+07    0.72  0
              6.21E-04   6.924E+07    0.65  0
              8.30E-04   6.745E+07    0.59  0
              1.07E-03   6.249E+07    0.56  0
              1.51E-03   5.438E+07    0.52  0
              1.90E-03   5.057E+07    0.52  0
              2.60E-03   4.611E+07    0.52  0
              4.71E-03   3.886E+07    0.52  0
              1.21E-02   4.856E+07    0.52  0
              1.50E+20   0.000E+00    0.52  0
: Vid tid 0 corrosion penetration is 0
                  0 0
                  1E6 0.0
                  14E9 2.0  6.00E-3  0E-6 7.0
      USRSTA  0.0  0.0  0.0  0.0  0.0  0.0  0.0
                1.10E+13   0.0 0.0 0.0 0.0 0.0
      USRIND  0 13 2
```

```
   4 NAME   INTERFACE
     DSTIF       1.1E+13   1.2E+12
     BONDSL      1
     SLPVAL      4.90000E+006   0.00006
```

**Geometry and Data properties' input (For the bond-slip model given by Lundgren)**

```
'GEOMET'
```

```
   1 NAME   CONCRETE
   2 NAME   REBAR
   3 NAME   PLATE
   4 NAME   INT1
     XAXIS   0.00000E+000  7.520000E-003  7.520000E-003
   5 NAME   INT2
     XAXIS   0.00000E+000  7.520000E-003  -7.50000E-003
   6 NAME   INT3
     XAXIS   0.00000E+000  -7.50000E-003  -7.50000E-003
   7 NAME   INT4
     XAXIS   0.00000E+000  -7.50000E-003  7.520000E-003
'DATA'
   1 NAME   CONCRETE
   2 NAME   REBAR
   3 NAME   PLATE
   4 NAME   INT1
   5 NAME   INT2
   6 NAME   INT3
   7 NAME   INT4
```

**Geometry and Data properties' input (For the bond-slip model given by Dörr)**

```
'GEOMET'
   1 NAME   CONCRETE
   2 NAME   REBAR
   3 NAME   PLATE
   4 NAME   INT1
   5 NAME   INT2
   6 NAME   INT3
   7 NAME   INT4
'DATA'
   1 NAME   CONCRETE
   2 NAME   REBAR
   3 NAME   PLATE
   4 NAME   INT1
   5 NAME   INT2
   6 NAME   INT3
   7 NAME   INT4
```

**Assignment of material, data and geometry**

```
MATERI
/ 1-26055 / 1
/ 26675-27452 / 2
/ 26056-26674 / 3
/ 27453 27454 27458 27460 27461 27464 27465 27467 27469 27471
27473 27476-27478 27481 27482 27485 27488 27490 27491 27494
27497-27499 27503 27504 27506 27508 27510-27512 27516 27518
27521 27523-27525 27527-27529 27531 27536 27538 27539 27542
27544-27547 27553-27555 27558 27560 27561 27563 27566-27568
27570 27573 27575 27577 27578 27581 27584 27585 27587 27590
27592 27593 27595 27598 27599 27601-27603 27608 27611-27613
27615 27617 27619 27620 27627-27631 27634 27636 27637 27642
27829 27838 27839 27844 27849 27850 27854 27855 27861 27863
27866 27867 27870-27872 27874 27877 27879 27883-27885 27888
27890 27891 27895-27897 27899 27902 27903 27906 27907 27911
27913 27914 27916 27917 27920 27921 27924-27926 27929 27930
```

27933 27936 27939-27941 27943 27944 27947 27952-27955 27960-
27963 27965 27966 27970-27972 27975 27976 27978 27983-27986
27988 27994-27996 27999 28002-28004 28007 28008 28011 28014-
28017 28019 28021 28024 28025 28027 28029 28030 28041 28051
28052 28056 28219 28220 28222-28224 28228 28233 28234 28237
28238 28242 28243 28246 28248 28249 28251 28253 28256 28259-
28261 28265-28267 28270 28272 28273 28275 28277 28278 28282
28283 28286 28288-28291 28295 28297 28301 28302 28304-28306
28309 28312 28313 28316 28318 28319 28321 28322 28326 28327
28329 28331 28334 28336 28338-28342 28347-28349 28354 28356
28357 28360 28361 28364 28366 28367 28370 28372 28374 28376
28378 28381 28383 28384 28390 28394 28395 28399 28402-28405
28783-28785 28791-28793 28797 28800 28803-28806 28817-28824
28826-28828 28831-28838 28848-28850 28854 28856 28857 28862-
28864 28866 28867 28870 28875-28877 28880 28881 28883 28884
28886 28887 28895-28899 28903 28907-28912 28915 28916 28919-
28924 28927 28928 28933 28934 28937-28939 28941 28942 28947
28948 28950 28956-28963 28965 28966 28976 28980 28984 28987
28989 28992 29003 29004 29186-29192 29201 29206-29209 29212
29213 29216 29217 29219 29220 29222 29232-29235 29237-29240
29242-29245 29248 29253 29254 29256 29257 29259 29260 29264-
29269 29271 29272 29277-29279 29286-29289 29296-29299 29301-
29304 29307 29309 29310 29312 29314-29317 29325-29327 29334
29335 29338-29340 29344 29345 29348-29355 29370 29371 29374
29513 29540 29541 29552-29556 29563 29565-29568 29572-29574
29579 29580 29585 29586 29589-29592 29594 29596 29602 29603
29608-29611 29613-29619 29624 29625 29630-29633 29635 29639-
29642 29645 29646 29649-29651 29654 29661-29664 29669-29672
29677-29685 29690 29691 29693 29698 29699 29701-29704 29708
29710 29711 29717 29718 29721-29723 29916-29918 29922-29924
29926 29927 29929 29930 29935-29944 29953 29957 29958 29967-
29975 29979-29981 29983 29986-29989 29993 29996 29997 29999-
30002 30006 30007 30010 30013 30016-30022 30028-30030
30032-30034 30041 30042 30045 30046 30053 30054 30057-30060
30063 30064 30068 30071-30074 30077 30079-30083 30092 30095-
30100 30103 30106 30109 30114 30118 30119 30129 30130 30305-
30311 30321 30322 30330-30333 30338 30339 30342 30343 30346
30349 30351-30359 30364 30369 30374 30375 30377-30380 30383
30386 30389-30391 30398 30401-30404 30408-30413 30418-30423
30428 30433 30434 30436 30439 30441 30446-30452 30456-30461
30464 30465 30469-30471 30474 30475 30484-30487 30503 30504
30658-30661 30685-30690 30692 30697-30699 30703-30706 30709-
30712 30715 30716 30721 30723 30725-30729 30732-30735 30740
30748-30751 30754-30757 30762 30764-30766 30771 30772 30775
30776 30780 30781 30783-30788 30793-30796 30801-30804 30814-
30817 30820 30822-30825 30828 30833-30835 30837 30840-30844
30847 30848 30852 30855-30857 30859 30862 30863 30866 30868
30870 30872 30874 30875 30879 30880 30883 30884 30886 30887
30889 30892 30893 30895 30896 30900-30902 30905 30907 30909
30913-30915 30917 30919 30920 30922 30926 30930 30932-30935
30937 30940 30941 30943 30948-30952 30956 30957 30959 30962
30964 30965 30969 30971 30972 30974 30976 30979 30980 30982
30983 30986 30988 30989 30991 30994 30996 30997 31000 31004-
31007 31009 31010 31014 31016 31018 31021-31026 31032 31033
31035 31038 31043 31230 31233 31235 31241 31251-31253 31256
31262 31264 31265 31268 31269 31273 31275 31276 31278 31280-

```
31282 31286 31287 31289 31292-31294 31298 31300 31301 31304
31305 31308-31310 31312 31315 31318 31319 31322 31323 31327
31328 31331 31332 31334 31335 31337 31338 31342 31345 31346
31348-31351 31356-31359 31364 31367-31369 31373 31374 31377
31379-31382 31387 31389-31393 31397 31398 31400 31401 31405
31406 31409 31410 31412 31413 31418 31420 31422 31423 31426
31428 31431 31432 31440 31453-31455 31616-31618 31621 31625
31629 31635 31636 31639-31641 31644 31645 31647 31650 31652
31654 31655 31657 31658 31662-31664 31668 31669 31671 31674
31676 31679-31681 31684 31685 31687 31692-31694 31696 31698-
31700 31703 31707 31708 31710 31711 31714 31715 31717 31720
31723-31725 31728 31730 31732 31733 31735 31737 31743-31746
31750-31753 31755 31758 31759 31762 31763 31765 31768 31771
31773 31775 31777 31779 31780 31782 31785 31791-31793 31798
31800 31801 31806 31807 / 4

DATA
/ 1-26055 / 1
/ 26675-27452 / 2
/ 26056-26674 / 3
/ 27453 27454 27458 27460 27461 27464 27465-27473(2) 27476-
27478 27481 27482-27488(3) 27490 27491-27497(3) 27498 27499
27503 27504-27510(2) 27511 27512 27516 27518 27521 27523-27525
27527-27529 27531 27536 27538 27539 27542 27544-27547 27553-
27555 27558 27560 27561 27563 27566-27568 27570 27573-27577(2)
27578-27584(3) 27585 27587 27590 27592 27593 27595 27598 27599
27601-27603 27608 27611-27613 27615-27619(2) 27620 27627-27631
27634 27636 27637 27642 27829 27838 27839-27849(5) 27850 27854
27855 27861 27863 27866 27867 27870-27872 27874 27877 27879
27883-27885 27888 27890 27891 27895-27897 27899 27902 27903
27906 27907 27911 27913 27914 27916 27917 27920 27921 27924-
27926 27929 27930-27939(3) 27940 27941 27943 27944 27947 7952-
27955 27960-27963 27965 27966 27970-27972 27975 27976 27978
27983-27986 27988 27994-27996 27999 28002-28004 28007 28008-
28014(3) 28015-28017 28019 28021 28024 28025-28029(2) 28030
28041 28051 28052 28056 28219 28220 28222-28224 28228 28233
28234 28237 28238 28242 28243 28246 28248 28249-28253(2) 28256
28259-28261 28265-28267 28270 28272 28273-28277(2) 28278 28282
28283 28286 28288-28291 28295 28297 28301 28302 28304-28306
28309 28312 28313 28316 28318 28319 28321 28322 28326 28327-
28331(2) 28334-28338(2) 28339-28342 28347-28349 28354 28356
28357 28360 28361 28364 28366 28367 28370-28378(2) 28381 28383
28384 28390 28394 28395 28399 28402-28405 / 4
/ 28783-28785 28791-28793 28797-28803(3) 28804-28806 28817-
28824 28826-28828 28831-28838 28848-28850 28854 28856 28857
28862-28864 28866 28867 28870 28875-28877 28880 28881 28883
28884 28886 28887 28895-28899 28903 28907-28912 28915 28916
28919-28924 28927 28928 28933 28934 28937-28939 28941 28942
28947 28948 28950 28956-28963 28965 28966 28976-28984(4) 28987
28989 28992 29003 29004 29186-29192 29201 29206-29209 29212
29213 29216 29217 29219 29220 29222 29232-29235 29237-29240
29242-29245 29248 29253 29254 29256 29257 29259 29260 29264-
29269 29271 29272 29277-29279 29286-29289 29296-29299 29301-
29304 29307 29309 29310-29314(2) 29315-29317 29325-29327 29334
29335 29338-29340 29344 29345 29348-29355 29370 29371 29374
29513 29540 29541 29552-29556 29563 29565-29568 29572-29574
```

```
29579 29580 29585 29586 29589-29592 29594 29596 29602 29603
29608-29611 29613-29619 29624 29625 29630-29633 29635 29639-
29642 29645 29646 29649-29651 29654 29661-29664 29669-29672
29677-29685 29690 29691 29693 29698 29699 29701-29704 29708
29710 29711 29717 29718 29721-29723 / 5
/ 29916-29918 29922-29924 29926 29927 29929 29930 29935-29944
29953 29957 29958 29967-29975 29979-29981 29983 29986-29989
29993 29996 29997 29999-30002 30006 30007-30016(3) 30017-30022
30028-30030 30032-30034 30041 30042 30045 30046 30053 30054
30057-30060 30063 30064 30068 30071-30074 30077 30079-30083
30092 30095-30100 30103-30109(3) 30114 30118 30119 30129
30130 30305-30311 30321 30322 30330-30333 30338 30339 30342
30343-30349(3)    30351-30359 30364-30374(5) 30375 30377-30380
30383-30389(3) 30390 30391 30398 30401-30404 30408-30413
30418-30423 30428 30433 30434 30436 30439 30441 30446-30452
30456-30461 30464 30465 30469-30471 30474 30475 30484-30487
30503 30504 30658-30661 30685-30690 30692 30697-30699 30703-
30706 30709-30712 30715 30716 30721-30725(2) 30726-30729
30732-30735 30740 30748-30751 30754-30757 30762 30764-30766
30771 30772 30775 30776 30780 30781 30783-30788 30793-30796
30801-30804 30814-30817 30820 30822-30825 30828 30833-30835
30837 30840-30844 30847 30848 30852 / 6
/ 30855-30857 30859 30862 30863 30866-30874(2) 30875 30879
30880 30883 30884 30886 30887 30889 30892 30893 30895 30896
30900-30902 30905-30909(2) 30913-30915 30917 30919 30920 0922-
30930(4) 30932-30935 30937 30940 30941 30943 30948-30952 30956
30957 30959 30962 30964 30965 30969 30971 30972-30976(2) 30979
30980 30982 30983 30986 30988 30989 30991 30994 30996 30997
31000 31004-31007 31009 31010 31014-31018(2) 31021-31026 31032
31033 31035 31038 31043 31230 31233 31235 31241 31251-31253
31256 31262 31264 31265 31268 31269 31273 31275 31276-31280(2)
31281 31282 31286 31287 31289 31292-31294 31298 31300 31301
31304 31305 31308-31310 31312-31318(3) 31319 31322 31323 31327
31328 31331 31332 31334 31335 31337 31338 31342 31345 31346
31348-31351 31356-31359 31364 31367-31369 31373 31374 31377
31379-31382 31387 31389-31393 31397 31398 31400 31401 31405
31406 31409 31410 31412 31413 31418-31422(2) 31423 31426 31428
31431 31432 31440 31453-31455 31616-31618 31621-31629(4) 31635
31636 31639-31641 31644 31645 31647 31650-31654(2) 31655 31657
31658 31662-31664 31668 31669 31671 31674 31676 31679-31681
31684 31685 31687 31692-31694 31696 31698-31700 31703 31707
31708 31710 31711 31714 31715 31717-31723(3) 31724 31725
31728-31732(2) 31733-31737(2) 31743-31746 31750-31753 31755
31758 31759 31762 31763 31765-31771(3) 31773-31779(2) 31780
31782 31785 31791-31793 31798 31800 31801 31806 31807 / 7

GEOMET
/ 1-26055 / 1
/ 26675-27452 / 2
/ 26056-26674 / 3
/ 27453 27454 27458 27460 27461 27464 27465-27473(2) 27476-
27478 27481 27482-27488(3) 27490 27491-27497(3) 27498 27499
27503 27504-27510(2) 27511 27512 27516 27518 27521 27523-27525
27527-27529 27531 27536 27538 27539 27542 27544-27547 27553-
27555 27558 27560 27561 27563 27566-27568 27570 27573-27577(2)
27578-27584(3) 27585 27587 27590 27592 27593 27595 27598 27599
```

```
27601-27603 27608 27611-27613 27615-27619(2) 27620 27627-27631
27634 27636 27637 27642 27829 27838 27839-27849(5) 27850 27854
27855 27861 27863 27866 27867 27870-27872 27874 27877 27879
27883-27885 27888 27890 27891 27895-27897 27899 27902 27903
27906 27907 27911 27913 27914 27916 27917 27920 27921 27924-
27926 27929 27930-27939(3) 27940 27941 27943 27944 27947 7952-
27955 27960-27963 27965 27966 27970-27972 27975 27976 27978
27983-27986 27988 27994-27996 27999 28002-28004 28007 28008-
28014(3) 28015-28017 28019 28021 28024 28025-28029(2) 28030
28041 28051 28052 28056 28219 28220 28222-28224 28228 28233
28234 28237 28238 28242 28243 28246 28248 28249-28253(2) 28256
28259-28261 28265-28267 28270 28272 28273-28277(2) 28278 28282
28283 28286 28288-28291 28295 28297 28301 28302 28304-28306
28309 28312 28313 28316 28318 28319 28321 28322 28326 28327-
28331(2) 28334-28338(2) 28339-28342 28347-28349 28354 28356
28357 28360 28361 28364 28366 28367 28370-28378(2) 28381 28383
28384 28390 28394 28395 28399 28402-28405 / 4
/ 28783-28785 28791-28793 28797-28803(3) 28804-28806 28817-
28824 28826-28828 28831-28838 28848-28850 28854 28856 28857
28862-28864 28866 28867 28870 28875-28877 28880 28881 28883
28884 28886 28887 28895-28899 28903 28907-28912 28915 28916
28919-28924 28927 28928 28933 28934 28937-28939 28941 28942
28947 28948 28950 28956-28963 28965 28966 28976-28984(4) 28987
28989 28992 29003 29004 29186-29192 29201 29206-29209 29212
29213 29216 29217 29219 29220 29222 29232-29235 29237-29240
29242-29245 29248 29253 29254 29256 29257 29259 29260 29264-
29269 29271 29272 29277-29279 29286-29289 29296-29299 29301-
29304 29307 29309 29310-29314(2) 29315-29317 29325-29327 29334
29335 29338-29340 29344 29345 29348-29355 29370 29371 29374
29513 29540 29541 29552-29556 29563 29565-29568 29572-29574
29579 29580 29585 29586 29589-29592 29594 29596 29602 29603
29608-29611 29613-29619 29624 29625 29630-29633 29635 29639-
29642 29645 29646 29649-29651 29654 29661-29664 29669-29672
29677-29685 29690 29691 29693 29698 29699 29701-29704 29708
29710 29711 29717 29718 29721-29723 / 5
/ 29916-29918 29922-29924 29926 29927 29929 29930 29935-29944
29953 29957 29958 29967-29975 29979-29981 29983 29986-29989
29993 29996 29997 29999-30002 30006 30007-30016(3) 30017-30022
30028-30030 30032-30034 30041 30042 30045 30046 30053 30054
30057-30060 30063 30064 30068 30071-30074 30077 30079-30083
30092 30095-30100 30103-30109(3) 30114 30118 30119 30129
30130 30305-30311 30321 30322 30330-30333 30338 30339 30342
30343-30349(3)    30351-30359 30364-30374(5) 30375 30377-30380
30383-30389(3) 30390 30391 30398 30401-30404 30408-30413
30418-30423 30428 30433 30434 30436 30439 30441 30446-30452
30456-30461 30464 30465 30469-30471 30474 30475 30484-30487
30503 30504 30658-30661 30685-30690 30692 30697-30699 30703-
30706 30709-30712 30715 30716 30721-30725(2) 30726-30729
30732-30735 30740 30748-30751 30754-30757 30762 30764-30766
30771 30772 30775 30776 30780 30781 30783-30788 30793-30796
30801-30804 30814-30817 30820 30822-30825 30828 30833-30835
30837 30840-30844 30847 30848 30852 / 6
/ 30855-30857 30859 30862 30863 30866-30874(2) 30875 30879
30880 30883 30884 30886 30887 30889 30892 30893 30895 30896
30900-30902 30905-30909(2) 30913-30915 30917 30919 30920 0922-
30930(4) 30932-30935 30937 30940 30941 30943 30948-30952 30956
```

```
30957 30959 30962 30964 30965 30969 30971 30972-30976(2) 30979
30980 30982 30983 30986 30988 30989 30991 30994 30996 30997
31000 31004-31007 31009 31010 31014-31018(2) 31021-31026 31032
31033 31035 31038 31043 31230 31233 31235 31241 31251-31253
31256 31262 31264 31265 31268 31269 31273 31275 31276-31280(2)
31281 31282 31286 31287 31289 31292-31294 31298 31300 31301
31304 31305 31308-31310 31312-31318(3) 31319 31322 31323 31327
31328 31331 31332 31334 31335 31337 31338 31342 31345 31346
31348-31351 31356-31359 31364 31367-31369 31373 31374 31377
31379-31382 31387 31389-31393 31397 31398 31400 31401 31405
31406 31409 31410 31412 31413 31418-31422(2) 31423 31426 31428
31431 31432 31440 31453-31455 31616-31618 31621-31629(4) 31635
31636 31639-31641 31644 31645 31647 31650-31654(2) 31655 31657
31658 31662-31664 31668 31669 31671 31674 31676 31679-31681
31684 31685 31687 31692-31694 31696 31698-31700 31703 31707
31708 31710 31711 31714 31715 31717-31723(3) 31724 31725
31728-31732(2) 31733-31737(2) 31743-31746 31750-31753 31755
31758 31759 31762 31763 31765-31771(3) 31773-31779(2) 31780
31782 31785 31791-31793 31798 31800 31801 31806 31807 / 7
```

### Definition of loads

```
'LOADS'
DEFORM
5731 TR 3 -1.00000E-003
DEFORM
5734 TR 3 -1.00000E-003
DEFORM
5737 TR 3 -1.00000E-003
DEFORM
5740 TR 3 -1.00000E-003
DEFORM
5743 TR 3 -1.00000E-003
DEFORM
5746 TR 3 -1.00000E-003
DEFORM
5749 TR 3 -1.00000E-003
DEFORM
5752 TR 3 -1.00000E-003
DEFORM
5755 TR 3 -1.00000E-003
DEFORM
5758 TR 3 -1.00000E-003
DEFORM
5761 TR 3 -1.00000E-003
DEFORM
5766 TR 3 -1.00000E-003
DEFORM
5769 TR 3 -1.00000E-003
DEFORM
5772 TR 3 -1.00000E-003
DEFORM
5775 TR 3 -1.00000E-003
DEFORM
5778 TR 3 -1.00000E-003
```

```
DEFORM
5781 TR 3 -1.00000E-003
DEFORM
5784 TR 3 -1.00000E-003
DEFORM
5787 TR 3 -1.00000E-003
DEFORM
5790 TR 3 -1.00000E-003
DEFORM
5793 TR 3 -1.00000E-003
DEFORM
5796 TR 3 -1.00000E-003
```

## Element groups

```
'GROUPS'
ELEMEN
  38 "Concrete" / 1-26055 /
  39 "Load plate1" / 26056-26209 /
  40 "Load plate2" / 26210-26364 /
  41 "Sup plate1" / 26365-26519 /
  42 "Sup plate2" / 26520-26674 /
  43 "Rebar1" / 26675-26933 /
  44 "Rebar2" / 26934-27192 /
  45 "Rebar3" / 27193-27452 /
  46 "Int1" / 27453 27454 27458 27460 27461 27464 27465-
27473(2) 27476-27478 27481 27482-27488(3) 27490 27491-27497(3)
27498 27499 27503 27504-27510(2) 27511 27512 27516 27518 27521
27523-27525 27527-27529 27531 27536 27538 27539 27542 27544-
27547 27553-27555 27558 27560 27561 27563 27566-27568 27570
27573-27577(2) 27578-27584(3) 27585 27587 27590 27592 27593
27595 27598 27599 27601-27603 27608 27611-27613 27615-27619(2)
27620 27627-27631 27634 27636 27637 27642 27829 27838 27839-
27849(5) 27850 27854 27855 27861 27863 27866 27867 27870-27872
27874 27877 27879 27883-27885 27888 27890 27891 27895-27897
27899 27902 27903 27906 27907 27911 27913 27914 27916 27917
27920 27921 27924-27926 27929 27930-27939(3) 27940 27941 27943
27944 27947 7952-27955 27960-27963 27965 27966 27970-27972
27975 27976 27978   27983-27986 27988 27994-27996 27999 28002-
28004 28007 28008-28014(3) 28015-28017 28019 28021 28024
28025-28029(2) 28030 28041 28051 28052 28056 28219 28220
28222-28224 28228 28233 28234 28237 28238 28242 28243 28246
28248 28249-28253(2) 28256 28259-28261 28265-28267 28270 28272
28273-28277(2) 28278 28282 28283 28286 28288-28291 28295 28297
28301 28302 28304-28306 28309 28312 28313 28316 28318 28319
28321 28322 28326 28327-28331(2) 28334-28338(2) 28339-28342
28347-28349 28354 28356 28357 28360 28361 28364 28366 28367
28370-28378(2) 28381 28383 28384 28390 28394 28395 28399
28402-28405 /
  47 "Int2" / 28783-28785 28791-28793 28797-28803(3) 28804-
28806 28817-28824 28826-28828 28831-28838 28848-28850 28854
28856 28857 28862-28864 28866 28867 28870 28875-28877 28880
28881 28883 28884 28886 28887 28895-28899 28903 28907-28912
28915 28916 28919-28924 28927 28928 28933 28934 28937-28939
28941 28942 28947 28948 28950 28956-28963 28965 28966 28976-
28984(4) 28987 28989 28992 29003 29004 29186-29192 29201
29206-29209 29212 29213 29216 29217 29219 29220 29222 29232-
```

```
29235 29237-29240     29242-29245 29248 29253 29254 29256
29257 29259 29260 29264-29269 29271 29272 29277-29279 29286-
29289 29296-29299 29301-29304 29307 29309 29310-29314(2)
29315-29317 29325-29327 29334 29335 29338-29340 29344 29345
29348-29355 29370 29371 29374 29513 29540 29541 29552-29556
29563 29565-29568 29572-29574 29579 29580 29585 29586 29589-
29592 29594 29596 29602 29603 29608-29611 29613-29619 29624
29625 29630-29633 29635 29639-29642 29645 29646 29649-29651
29654 29661-29664 29669-29672     29677-29685 29690 29691
29693 29698 29699 29701-29704 29708 29710 29711 29717 29718
29721-29723 /
  48 "Int3" / 29916-29918 29922-29924 29926 29927 29929 29930
29935-29944 29953 29957 29958 29967-29975 29979-29981 29983
29986-29989 29993 29996 29997 29999-30002 30006 30007-30016(3)
30017-30022 30028-30030 30032-30034 30041 30042 30045 30046
30053 30054 30057-30060 30063 30064 30068 30071-30074 30077
30079-30083 30092 30095-30100 30103-30109(3) 30114 30118 30119
30129   30130 30305-30311 30321 30322 30330-30333 30338 30339
30342 30343-30349(3)    30351-30359 30364-30374(5) 30375
30377-30380 30383-30389(3) 30390 30391 30398 30401-30404
30408-30413 30418-30423 30428 30433 30434 30436 30439 30441
30446-30452 30456-30461 30464 30465 30469-30471 30474 30475
30484-30487 30503 30504 30658-30661 30685-30690 30692 30697-
30699 30703-30706 30709-30712 30715 30716 30721-30725(2)
30726-30729 30732-30735 30740 30748-30751 30754-30757 30762
30764-30766 30771 30772 30775 30776 30780 30781 30783-30788
30793-30796 30801-30804 30814-30817 30820 30822-30825 30828
30833-30835 30837 30840-30844 30847 30848 30852 /
  49 "Int4" / 30855-30857 30859 30862 30863 30866-30874(2)
30875 30879 30880 30883 30884 30886 30887 30889 30892 30893
30895 30896 30900-30902 30905-30909(2) 30913-30915 30917 30919
30920 0922-30930(4) 30932-30935 30937 30940 30941 30943 30948-
30952 30956 30957 30959 30962 30964 30965 30969 30971 30972-
30976(2) 30979 30980 30982 30983 30986 30988 30989 30991 30994
30996 30997 31000 31004-31007 31009 31010 31014-31018(2)
31021-31026 31032 31033 31035 31038 31043 31230 31233 31235
31241 31251-31253 31256 31262 31264 31265 31268 31269 31273
31275 31276-31280(2) 31281 31282 31286 31287 31289 31292-31294
31298 31300 31301 31304 31305 31308-31310 31312-31318(3) 31319
31322 31323 31327 31328 31331 31332 31334 31335 31337 31338
31342 31345 31346 31348-31351 31356-31359 31364 31367-31369
31373 31374 31377 31379-31382 31387 31389-31393 31397 31398
31400 31401 31405 31406 31409 31410 31412 31413 31418-31422(2)
31423 31426 31428 31431 31432 31440 31453-31455 31616-31618
31621-31629(4) 31635 31636 31639-31641 31644 31645 31647
31650-31654(2) 31655 31657 31658 31662-31664 31668 31669 31671
31674 31676 31679-31681 31684 31685 31687 31692-31694 31696
31698-31700 31703 31707 31708 31710 31711 31714 31715 31717-
31723(3) 31724 31725   31728-31732(2) 31733-31737(2) 31743-
31746 31750-31753 31755 31758 31759 31762 31763 31765-31771(3)
31773-31779(2) 31780 31782 31785 31791-31793 31798 31800 31801
31806 31807 /
```

**Boundary conditions and constrains**

```
'SUPPOR'
/ 5731-5761(3) 5766-5796(3) 5801-5831(3) 5836-5866(3) / TR 3
'END'
```

# Appendix D: Command file (*. com file)

## 1. Command file for analyses with embedded reinforcement

```
*FILOS
 INITIA
*NONLIN
 BEGIN EXECUT
   LOAD  STEPS  EXPLIC  SIZES 0.05(60)
   BEGIN ITERAT
     BEGIN CONVER
       DISPLA  OFF
       ENERGY  TOLCON 0.001
       FORCE  OFF
     END CONVER
     MAXITE 500
   END ITERAT
 END EXECUT
 BEGIN OUTPUT
   FXPLUS
   FILE "embedded"
 END OUTPUT
*END
```

## 2. Command file for analyses with bond-slip model

```
*FILOS
 INITIA
*INPUT
*NONLIN
 BEGIN EXECUT
   LOAD  STEPS  EXPLIC  SIZES 0.05(60)
   BEGIN ITERAT
     BEGIN CONVER
       DISPLA  OFF
       BEGIN ENERGY
         CONTIN
         TOLCON 0.01
       END ENERGY
       FORCE  OFF
     END CONVER
     MAXITE 300
   END ITERAT
 END EXECUT
 BEGIN OUTPUT
   FXPLUS
   FILE "interface"
 END OUTPUT
*END
```